TECHNISCHE UNIVERSITÄT MÜNCHEN

Fakultät für Chemie

Professur für strukturelle Membranbiochemie

NMR studies on the disease-linked single-pass membrane proteins TREM2 and TNFα

Andrea Steiner, M. Sc.

Vollständiger Abdruck der von der Fakultät für Chemie der Technischen Universität München zur Erlangung des akademischen Grades

Doktor der Naturwissenschaften (Dr. rer. nat.)

genehmigten Dissertation.

Vorsitzender: Prof. Dr. Steffen J. Glaser

Prüfer der Dissertation:

1. Prof. Dr. Franz Hagn
2. Prof. Dr. Bernd Reif
3. Prof. Dr. Dr. h.c. Christian Haass

Die Dissertation wurde am 27.05.2020 bei der Technischen Universität München eingereicht und durch die Fakultät für Chemie am 30.06.2020 angenommen.

List of publications

I hereby declare that parts of this thesis have been submitted to scientific international journals or have been already published:

Steiner A., Schlepckow K., Brunner B., Steiner H., Haass C. & Hagn F. **Intramembrane cleavage of TREM2 is determined by its intrinsic structural dynamics**. *EMBO J* (in revision); Posted at bioRxiv-Preprint Server for Biology on November 30, 2019
Temporary doi: 10.1101/860007

Haeusler E., Fredriksson K., Goba I., Peters C., Raltchev K., Sperl L., Steiner A., Weinkauf S. & Hagn F. (2020). **Quantifying the insertion of membrane proteins into lipid bilayer nanodiscs using a fusion protein strategy**. *BBA Biomembranes*
doi: 10.1016/j.bbamem.2020.183190

Other contribution:

Zeng, B., Mou T., Doukov T., Steiner A., Yu W., Papasergi-Scott M., Tall G., Hagn F. & Sprang S. (2019). **Structure, Function, and Dynamics of the Gα Binding Domain of Ric-8A.** *Structure*
doi: 10.1016/j.str.2019.04.013

Abstract

Integral membrane proteins (IMPs) still remain challenging for structural studies due to their highly hydrophobic nature and their need for a suitable membrane mimetic. Continuous advances in x-ray crystallography, cryo-EM as well as solution and solid-state NMR improve structure determination attempts of IMPs, however, the class of single-transmembrane proteins (SPTMPs) does not especially profit from these advances for two major reasons: (i) the transmembrane domain is comparatively small and highly flexible and (ii) the respective extracellular domain (ECD) is usually destabilized by detergents in a non-reversible manner. This is why a divide-and-conquer strategy is still a common approach to target this protein class by means of separately studying the different domains. This thesis is focused on two main goals: first, structural investigations on the TREM2 transmembrane domain (TREM2-TMD) using solution NMR spectroscopy; second: drug NMR fragment-based screening for the discovery of novel small molecule inhibitors of the TNFα ECD.

TREM2 mutations are involved in Alzheimer's disease progression and especially interesting, regarding TREM2-TM is a disease-related K186N variant within the lipid bilayer which is unable to engage with its adaptor protein DAP12, thus abolishing signal transduction. Structural investigation using solution NMR in combination with a cell-based γ-secretase cleavage assay of the wild-type TM domain and a charge-removal variant dramatically highlight the crucial role of lysine residue at position 186. It is essential for formation of the signaling complex with DAP12 and leads to an unstructured and dynamic helix region in an unbound-state that allows for proper γ-secretase processing.

The second part of this thesis was centered around the discovery of novel small molecule inhibitors of TNFα which represents a highly interesting target due to its involvement in various auto-immune diseases. Using a fragment-based NMR screening approach, several initial hit compounds could be identified. Different methods were established to further evaluate the mode of action of these compounds, including FRET- and qPCR-based assays to determine

apparent K_D values and the kinetics of subunit exchange. Combining these methods with NMR chemical shift perturbation experiments, it was revealed that these fragments interact with the hydrophobic core of trimeric TNFα. The obtained data will pave the way for the stepwise optimization of the initial fragments and enable the design of an efficient small molecule.

Zusammenfassung

Integrale Membranproteine (IMPs) stellen immer noch eine Herausforderung für strukturbiologische Studien dar, allem voran aufgrund ihrer hydrophoben Natur und der Notwendigkeit eines passenden Membranmimetikums. Kontinuierliche Fortschritte im Bereich der Röntgenstrukturanalyse, des Cryo-EM als auch Lösungs- und Festkörper-NMR verbessern deutlich die Bestrebungen der Strukturbestimmung, allerdings profitiert die Klassen der Single-pass Transmembranproteine (SPTMPs) kaum von diesen Neuerungen, da (i) die Transmembrandomänen (TM) vergleichbar klein und hochdynamisch sind und (ii) die entsprechenden extrazellulären Domänen (ECD) für gewöhnlich irreversibel destabilisiert werden. Daher stellt im Zusammenhang mit dieser Proteinklasse die divide-and-conquer Strategie einen weit verbreiteten Ansatz dar, das heißt die Erforschung der einzelnen Domänen unabhängig voneinander. Diese Doktorarbeit fokussiert sich auf zwei Schwerpunkte: Zum einen auf Strukturuntersuchungen der TREM2-Transmembrandomäne mittels Lösungs-NMR Spektroskopie; Zum anderen auf ein NMR Screening von Verbindungen für die Entdeckung eines neuen small molecule Inhibitors der TNFα ECD.

TREM2-Mutationen begünstigen das Fortschreiten der Alzheimer-Krankheit und besonders interessant hierbei ist eine krankheitsbedingte K186N-Variante von TREM2-TM innerhalb der Lipiddoppelschicht, die nicht in der Lage ist, mit ihrem Adapterprotein DAP12 in Kontakt zu treten, wodurch die Signalübertragung verhindert wird. Strukturuntersuchungen unter Verwendung von Lösungs-NMR in Kombination mit einem zellbasierten γ-Sekretase-Spaltungsassay der Wildtyp-TM-Domäne und einer Ladungsvariante (hier: K186A) heben dramatisch die entscheidende Rolle des Lysin-Restes an Position 186 hervor. Dieser ist unerlässlich für die Bildung des Signalkomplexes mit Dap12 und führt im ungebundenen Zustand zu einer unstrukturierten und dynamischen Helixregion, die eine ordnungsgemäße Spaltung durch das Enzym γ-Sekretase innerhalb der Membran ermöglicht.

Der zweite Teil dieser Arbeit befasst sich mit der Entdeckung neuer small molecule Inhibitoren von TNFα, das aufgrund seiner Beteiligung an verschiedensten Autoimmunerkrankungen ein hochinteressantes Ziel darstellt. Unter Verwendung eines Fragment-basierten NMR-Screening-Ansatzes konnten mehrere Hit-Verbindungen identifiziert werden. Es wurden verschiedene Methoden etabliert, um die Wirkungsweise dieser Verbindungen weiter zu bewerten, einschließlich FRET- und qPCR-basierter Assays zur Bestimmung von K_D Werten und der Kinetik des Untereinheiten-Austauschs. Durch Kombination dieser Methoden mit chemical shift perturbation (CSP) Experimenten mittels NMR wurde gezeigt, dass diese Fragmente mit dem hydrophoben Kern von TNFα interagieren. Die erhaltenen Daten werden den Weg für die schrittweise Optimierung der Ausgangsfragmente ebnen und das Design eines effizienten small molecules ermöglichen.

1 INTRODUCTION

1.1 Structural biology of Membrane proteins

Membrane proteins (MPs) make up roughly 25% of the human proteome[1] and constitute more than 60% of current drug targets[2]. More than two thirds of small molecule drugs target proteins of the G-Protein coupled receptors (GPCR) superfamily therefore overrepresenting this class of integral membrane proteins (IMPs)[3]. Considering that only 2-3% of all experimentally determined structures in the PBD are IMPs[4] it becomes clear that there is still a plethora of IMPs to be structurally investigated. The scarcity of membrane protein structures is related to the fact that approximately 90% of deposited structures were solved by X-ray crystallography and that membrane proteins are notoriously difficult to crystallize. High-yield production of IMPs in order to obtain crystals amenable for X-ray crystallography is still a bottleneck. Additionally, IMPs usually assemble in a planar 2-dimensional membrane environment while crystals are inherently 3-dimensional, although a huge progress has made in developing lipid cubic phases to study membrane proteins[5-7]. Apart from x-ray crystallography, cryo-electron microscopy (cryo-EM) has become a powerful method to obtain near-atomic resolution structures of IMPs[8] and solid-state NMR spectroscopy is advancing with respect to structure determination in lipid bilayers[9].

1.2 Single-pass transmembrane proteins (SPTMPs)

Despite all progress made regarding structural biology methods for membrane protein structure determination, investigation of one especially important class of membrane proteins, namely single-pass transmembrane proteins (SPTMPs), is still lagging behind mostly due to their highly dynamic nature, which is why the approximately 20 structures up to date have almost exclusively been solved by solution NMR.

Single pass transmembrane proteins (SPTMPs) also called bitopic membrane proteins are characterized by a single α-Helix passing the lipid bilayer unidirectional connecting the extracellular domain (ECD) of the protein with its intracellular domain (ICD). About 1300 of these SPTMPs have been identified in the human genome (Pahl M.C. *et al.*, 2013). Depending on the location of the N-terminus the SPTMPs are classified as Type I or Type II meaning their N-terminus is directed towards the extracellular space (N_{out}) or towards the inside of the cell (N_{in}), respectively. Since the N-terminus of Type I - SPTMPs has to be transported through the lipid bilayer these proteins possess a N-terminal targeting peptide which is being cleaved off during membrane insertion.

SPTMPs are highly diverse regarding their functional repertoire, including cell-to-cell communication, enzymes, receptors and their regulators, trafficking and adhesion.

The majority of SPTMPs are located in the plasma membrane with receptors and enzymes being the most abundant functional classes. Bioinformatic studies of the human proteome suggest that approximately 60% of all membrane proteins with enzymatic function and 88% of all non-GPCR receptors are bitopic proteins[10].

The ECDs of transmembrane receptors are relatively large globular domains (with a median residue length of 380 amino acids) and therefore well suited to recognize large first messenger molecules such as cytokines, hormones and other SPTMPs (Pahl M.C. *et al.*, 2013). The ICDs on the other hand have been shown to be relatively short domains (with a median residue length of 56), highly disordered and usually rely on the recruitment of adaptor proteins to transmit the signal into the cytoplasm of the respective cell.

The transmembrane domain (TMD) meanwhile luckily evolved from the community's view being merely a membrane anchor. Bormann et al.[11] showed that glycophorin has the ability to dimerize exclusively via interactions between the two membrane embedded helices demonstrating that TMDs are crucial for receptor functionality. Cross-membrane signaling is probably enabled due to changes in conformation or oligomerization state of these TMDs.

The first structure of a membrane protein to be solved by solution NMR was Glycophorin A, a 40-residue peptide[12]. Experiments were conducted in dodecylphosphocholin (DPC) micelles and it was shown that the small spherical DPC micelle was suitable to preserve its dimeric state[12]. Approximately 15 years later, Mineev *et al*. refined the structure in a bicelle environment[13] and few years afterwards the crystal structure of the dimeric protein in lipidic cubic phase was published[14]. Glycophorin A demonstrates a high degree of conservation regarding its structure and oligomeric state in various membrane mimetics.

1.2.1 TM-TM interaction within the membrane

To date, approximately two dozen high-resolution structures of transmembrane helices have been published revealing distinct helix-helix interfaces in detail (Figure 1)[15].

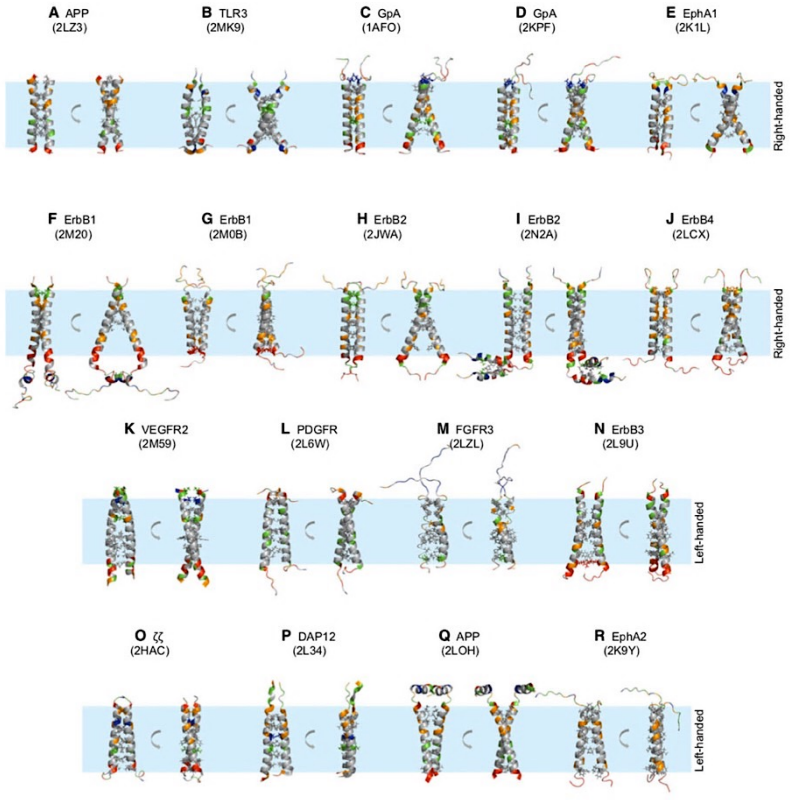

Figure 1: Currently available mammalian homodimer structures of WT SPTMP-TMDs. The pale blue box indicates the lipid bilayer. Residues involved in interaction are shown as sticks. Reprinted form reference [15]

The motif identified to induce dimerization of Glycophorin A was found to be GxxxG[16] which is highly conserved among SPTMPs with more than 50% of SPTMP-Helices bearing this motif[17]. Regardless of its high abundance, this motif is not necessarily involved in helix assembly as seen for DAP12 which is bearing a GxxxG motif but interaction with its binding partners is rather driven by salt bridge formation of ionizable residues[18]. Non-covalent associations of TM helices within the membrane are mediated by several motifs including van der Waals, hydrogen bonding, ionic, π-π or cation-π interactions[19-23].

Worth mentioning about ionic interactions within the membrane is the fact, the biological membrane has a low dielectric constant imposing protonation of carboxylic Glu and Asp moieties. Thus, Glu and Asp rather contain two polar side-chains like Gln and Asn, respectively[24,25].

1.2.2 Targeting transmembrane domains

Detergents usually destabilize the respective ECDs which is why a divide-and-conquer approach, by means of separately studying protein domains of SPTMPs is a commonly used approach. Usually the soluble domain is cleaved off and studied independently from its membrane anchor which has been done for members of the Bcl2 family of proteins[26], Tumor necrosis factor[27], transforming growth factor[28] and many more.

Limitations to this divide-and-conquer approach have extensively been studied for the epidermal growth factor receptor (EGFR)/ErbB family of receptors. Nearly all parts of the ErbB receptors, namely extracellular, juxtamembrane, transmembrane and kinase domains have structurally been solved and it was demonstrated that ErbB signaling is not just simply mediated by ligand-induced dimerization but that a complex interplay between the different domains is necessary to ensure receptor functionality and allosteric regulation[29]. Considering that it is evidently proven that pre-formed EGFR dimers are found at the surface even in absence of the EGF ligand[30,31] stresses that dimerization alone is not enough for receptor signaling but that

additional conformational changes and rearrangements are required for trans-membrane signal transduction (Figure 2). Introduction of a linker sequence between extracellular and transmembrane domain leads to receptor activation[32] probably due to a decoupling of the conformational regulation of the ECD and the transmembrane dimer formation.

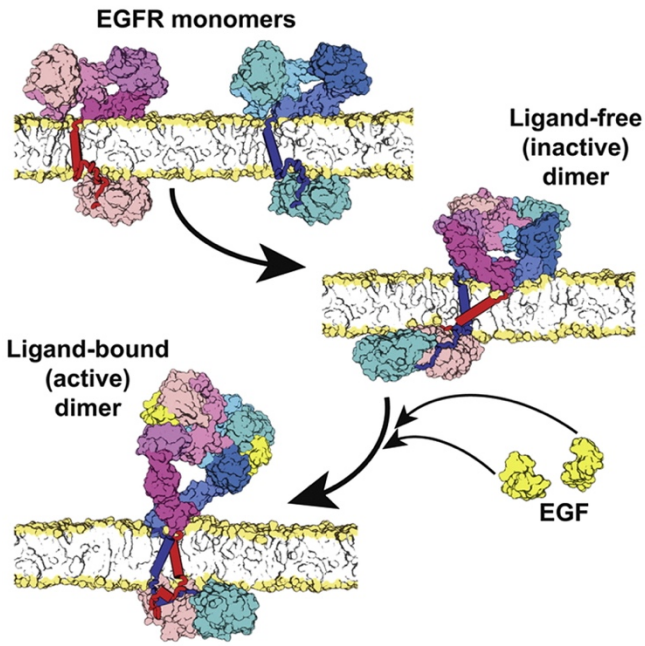

Figure 2: Model of EGFR activation: Pre-existing inactive EGFR dimers exist at the membrane showing C-terminally interacting TM domains. Upon ligand binding the interaction of the two helices shifts to their N-termini enabling the juxtamembrane dimer formation. Reprinted with permission from reference [32]

Jura *et al*. proposed a data-based model which includes ligand-based conformational changes of the extracellular domain leading to TM helix rotational positioning and dimer formation therefore providing the necessary orientation for the luminal juxtamembrane segments to dimerize, thus stabilizing the asymmetric kinase domain arrangement enabling auto-phosphorylation of the ErbB receptor tyrosine kinase (RTK)[29].

In fact, it was shown for oncogenic Neu (ErbB-2/Her2) RTK that valine 664 → glutamine mutation within its transmembrane segment induces uncontrolled dimerization and receptor activation[33,34] due to rotational positioning of the TM in a manner that enables helix interaction at the N-terminal site[35-37].

Given that there is increasing evidence of disease-related mutations within protein transmembrane domains[38-40] it might be worth thinking about turning the divide-and-conquer

approach around and to intensify studies of the respective TM domains since mutations in these domains are able, similar to their soluble counterparts, to either activate the protein in absence of a ligand binding event or to inhibit crucial protein assembly within the membrane.

Several studies showed already that peptide-based targeting of TM-TM interactions is feasible, e.g. it was demonstrated that ErbB dimerization was efficiently blocked using transmembrane peptides[41]. Using a different approach, namely computed helical anti-membrane protein (CHAMP) peptide, integrin signaling could be specifically activated[42]. Hebert et al. extended the TM-derived peptide approach on GPCRs and inhibited ß2-adrenergic receptor dimerization and activation with peptides derived from the sixth helix[43].

Targeting protein-protein interactions (PPIs) within the membrane might open a whole new field of structure-based drug design underlining the importance of membrane protein and TM domain structure determination.

1.3 Intramembrane proteolysis

Intramembrane proteases (IMPs) also called intramembrane-cleaving proteases (I-CLiPs) are enzymes located within the hydrophobic lipid bilayer catalyzing the hydrolytic peptide bond cleavage of transmembrane helices (TMHs). They can be classified into 4 mechanistic families: Metallo IMPs, serine IMPs (also known as rhomboid proteases), aspartyl IMPs and glutamyl IMPs. The most prominent member of the aspartyl protease family is γ-secretase or in particular its catalytical unit presenilin (PS) which was reported in parallel by three different research groups to be the enzymatic component of γ-secretase responsible for peptide bond hydrolysis[44-46]. Although, full enzymatic capacity was only recovered upon co-expression of all subunits of the γ-secretase complex[47], namely presenilin (PS), nicastrin (NCT), presenilin enhancer 2 (PEN-2) and anterior pharynx-defective 1 (APH-1) showing an apparent stoichiometry of 1:1:1:1[48,49]. The name presenilin derived from its involvement in formation of senile plaques in terms of Alzheimer's disease (AD) progression. Amyloid precursor protein (APP) is first shed

by α- or ß-secretase generating the C-terminal fragments C83[50] or C99[51], respectively. Subsequent γ-secretase cleavage of C99 results in amyloid ß peptides (Aß) with different lengths among them Aß42 and Aß43 being especially prone to aggregate and amyloid plaque formation[52-55]. Targeting γ-secretase for AD treatment causes severe side-effects most likely due to two different reasons: Firstly, APP is by far not the only substrate for the promiscuous γ-secretase complex and furthermore, the second class of aspartyl proteases, namely Signal peptide protease (SPP) and SPP-like (SPPL) proteases, shows high sensitivity to the same inhibitors. An important target of SPPL2a and SPPL2b worth mentioning in this context is TNFα[56].

In January and February 2019, the cryo-EM structures of γ-secretase in complex with Notch-1[57] and APP C-terminal fragment C83[58] (Figure 3, left) have been published, respectively, pathing the way for a deeper understanding of substrate recognition and cleavage.

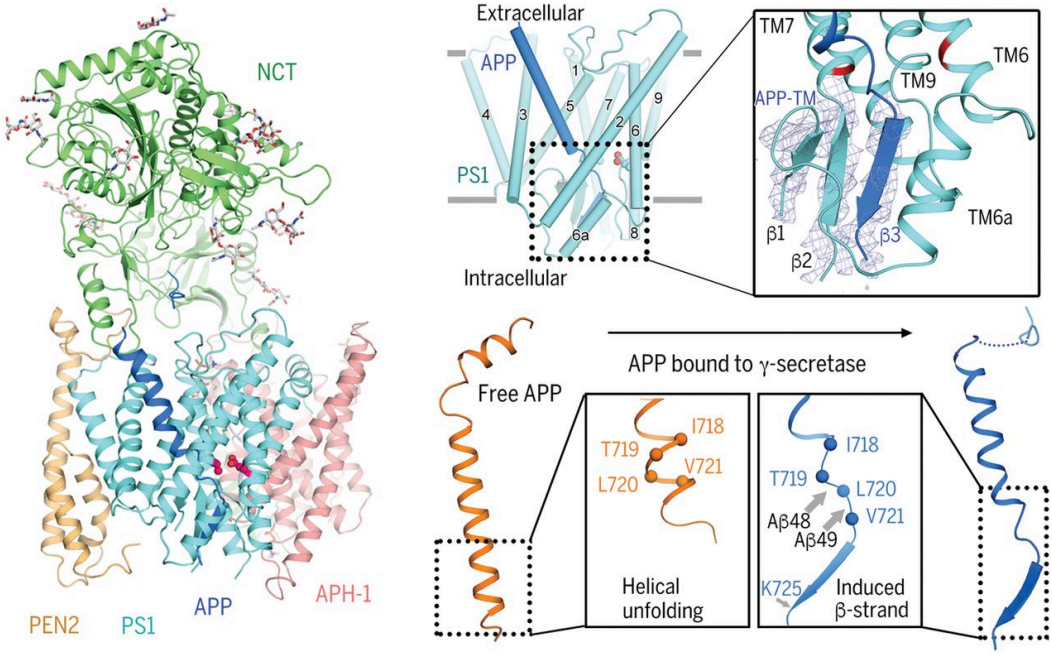

Figure 3: (Left) Cryo-EM structure of g-secretase in complex with APP fragment C83. (Right) Conformational changes of C83 upon binding include helical unfolding and a C-terminal ß-Sheet formation. The hybrid-ß-sheet with g-secretase is composed of a ß-strand of APP and two ß-strands of former Helix 6 of g-secretase (TM6). Reprinted with permission from reference [58]

APP C83 undergoes drastic conformational changes upon binding to γ-secretase. In comparison with its free-state, the C83 helix is unwound at the C-terminal end to expose the cleavage site (Figure3, lower panel on the right). The induced ß-strand of the substrate forms a hybrid ß-sheet with presenilin and transmembrane helix 6 (TM6) of presenilin flips towards the bound substrate forming hydrogen bonds with TM2[58] (Figure 3, upper panel on the right).

The Notch-1 helix undergoes similar structural changes upon binding exposing the cleavage site to presenilin[57]. Owing to a lack of sequence conservation among the γ-secretase substrates[59] it has long been unclear how γ-secretase selects its substrates. The complex structures of γ-secretase with APP and Notch-1 provide useful information for understanding the cleavage mechanism of γ-secretase in general and substrate cleavage in the context of diseases but there is still a need for further information to draw a more detailed picture about γ-secretase substrate selection and recognition, initial cleavage events, subsequent downstream cleavage events and release of the ICDs in the cytoplasmic space.

1.4 TREM2 – a protein linked to Alzheimer's disease

Triggering receptor expressed on myeloid cells 2 (TREM2) is a type I single pass transmembrane protein exclusively expressed on brain resident macrophages called microglia in the Central Nervous System (CNS)[60]. Upon removal of the membrane targeting peptide (aa 1-18) the mature protein, consisting of 212 amino acids (aa 19-230), is comprised of an extracellular domain (ECD) adopting an immunoglobulin V-like fold[60], a transmembrane helix and a cytoplasmic domain[61]. The ECD contains two disulfide bonds (Cys 36 ↔ Cys 110, Cys 51 ↔ Cys 60) and is post-translationally N-glycosylated at asparagine residues at positions 20 and 79[62,63].

Signal transduction via TREM2 induced by binding of extracellular ligands requires non-covalent association with its binding partner DNAX-activating protein of 12kDa (DAP12/TYROBP) or DAP10[64]. Assembly of the complex is mediated via a salt-bridge

formation within the hydrophobic environment of the lipid bilayer involving Lysine 186 (TREM2) and Aspartic acid 50 (DAP12). Mutation of either the positively or the negatively charged amino acid completely disrupts the interaction[18,65]. DAP12 is a disulfide-linked homodimer harboring two cytosolic immunoreceptor tyrosine-based activation motifs (ITAMs) which are phosphorylated by Src family kinases[66]. The phosphorylated tyrosine residues mediate the recruitment of the spleen tyrosine kinase (SYK) and by this trigger an intracellular signaling cascade[67]. The cellular response generated by the heterotrimeric signaling apparatus was reported to be manifold including regulation of phagocytosis as well as the promotion of cell survival and secretion of chemokines and cytokines[68].

Specific TREM2 ligands to initiate downstream signaling remain largely unknown but it was shown that the Ig V-like domain exposes a highly basic surface area which binds polyanionic ligands such as bacterial lipopolysaccharides[69] or zwitterionic phospholipids[63,70]. Furthermore, TREM2 seems to interact with ApoE[71-74] and amyloid-ß peptide (Aß)[75,76]. Aß is able to directly bind TREM2 and initiate downstream signaling via DAP12 *in vitro*. In addition, Aß oligomers demonstrated a higher affinity for TREM2 than the monomeric protein[75].

Upon signaling, the first step in proteolytic processing of TREM2 involves shedding of the ECD by A Disintegrin and metalloproteinase domain-containing protein 10 (ADAM10), the zinc-dependent sheddase responsible for processing of amyloid precursor protein (APP)[77], between histidine 157 and serine 158, releasing the soluble protein domain into the cerebrospinal fluid (CSF)[78-81]. Bound to DAP12, TREM2's remaining C-terminal fragment (TREM2-CTF) is protected from consecutive regulated intramembrane processing (RIP) while the unprotected signaling inactive TM helix is proteolytically degraded by γ-secretase inside the membrane[78].The intracellular domain (ICD) is released into the cytosol[78,82] and most likely translocates to the nucleus to induce target gene expression similar to γ-secretase substrates APP[83] and Notch[84], respectively.

1.5 K186N – A disease-related TREM2 transmembrane variant

Large genome-wide association studies (GWAS) revealed several TREM2 variants associated with an increased risk for developing Alzheimer's disease (AD)[85-87]. Most of these identified mutations are located in the ECD and most likely affect ligand binding and stability, as demonstrated for the R47H variant which displays slight conformational changes and a decreased thermal stability compared to the wild-type protein[62]. Another variant was found in the stalk region of TREM2, namely H157Y, showing an increased shedding activity[80,81].

Among the disease-linked mutations identified in these studies, the K186N variant should be highlighted. Located in the center of the hydrophobic bilayer lysine 186 is essential for complex formation with DAP12 and consequently homozygous mutations were found to be correlated with Polycystic lipomembranous osteodysplasia with sclerosing leukoencephalopathy (PLOSL) also known as "Nasu-Hakola disease" which is characterized by early-onset dementia and bone cysts leading to death during the 5th decade of life[88,89].

The signaling-deficient K186N variant TREM2 protein is able to be transported to the cell surface but accumulates there. It seemingly passes quality control in the ER while other missense variants are retained in the ER, namely Y38C, T66M, D86V and V126G[89].

A similar effect was shown for the T-cell receptor chains bearing basic residues in their transmembrane domains. Unassembled TCRα and TCRβ chains as well as the heterodimeric TCR are retained in the ER and get degraded[90,91] due to their exposed basic residues. In contrast, substitution to leucine residues led to efficient transport to the cell surface[92,93]. In complex with CD3γε the basic residues of TCR are shielded and degradation is inhibited[94].

DAP12 was initially discovered based on its homology with the TCR associated CD3 chains[95] which is why it seems plausible that DAP12 is not only crucial for efficient signal transduction of TREM2 but seems to be necessary for transport of TREM2 wild-type protein to the cell surface.

In 2010, Call *et al.*[18] solved the solution structure of the heterotrimeric complex of DAP12 in complex with another interaction partner, the natural killer cell-activating receptor NKG2C and showed that electrostatic interactions are necessary to form a signaling-competent complex.

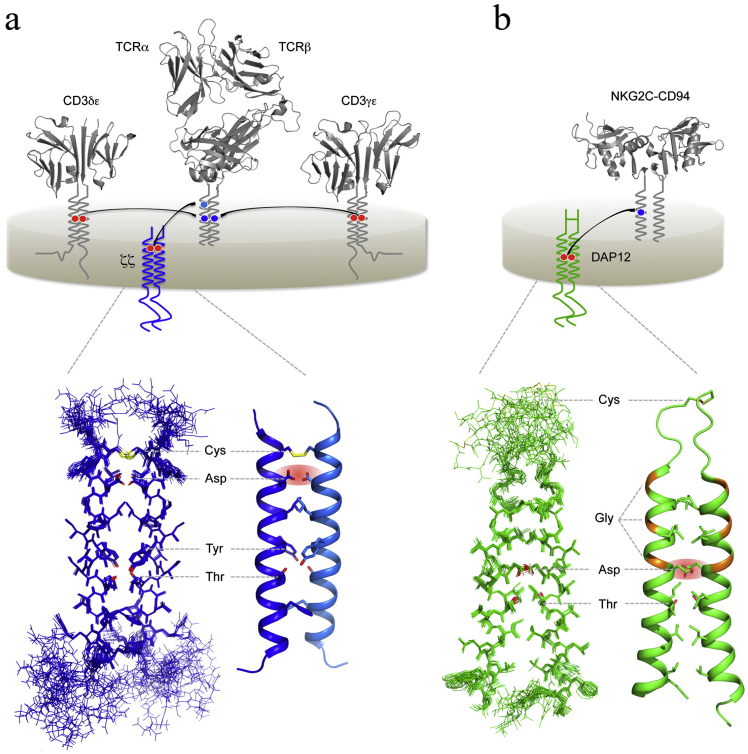

Figure 4: (a, top) Schematic diagram of the T cell receptor (TCR)-CD3 complex in the plasma membrane. TCRαβ heterodimer assembles with three different dimeric-signaling modules (CD3δε, CD3γε, and ζζ) through polar interactions within the hydrophobic lipid bilayer. In each assembly event, two acidic TM residues in the signaling module form a specific binding site for a single basic TM residue in the partner receptor. (a, bottom) Solution NMR structure of the human ζζTM dimer fragment embedded in DPC-SDS mixed detergent micelles (PDB ID 2HAC; [97]. (b, top) Schematic diagram of the natural killer (NK) cell-activating receptor complex NKG2C-CD94-DAP12. (b, bottom) Solution NMR structure of the human DAP12TM dimer fragment in TDPC-SDS mixed detergent micelles (PDB ID 2L34; [18]. Reprinted with permission from reference [100]

The interaction between DAP12 and NKG2C is mediated by a salt-bridge between the aspartate residue in DAP12 and the positively charged lysine residue of NKG2C (Figure 4, (b)) in combination with a critical threonine residue at the +4 position in DAP12, stabilizing Asp in a position that favors interaction with the lysine side-chain. A similar mechanism was also shown for DAP10 interaction with its arginine-bearing binding partners, e.g. NKG2D[96]. Although structurally similar to DAP12, the ζ-ζ dimer harbors two polar residues within the transmembrane domain however, it was shown that they are crucial for interhelical hydrogen bonding rather than interaction with the charged aspartate[97]. Nevertheless, complex assembly of the T-cell-receptor (TCR) with CD3 and ζ-ζ dimers, respectively, is based on the same

electrostatic principle: TCRα (R) interacts with a ζ-ζ dimer (D-D), while the TCRα (K) forms a complex with CD3δε (D-D) followed by interaction of TCRβ (K) with CD3γε (D-E)[98] (Figure 4 (a)).

Given that DAP12 alone has more than a dozen binding partners known to date[99] intramembrane complex formation via an electrostatic binding network represents a widely distributed mechanism for regulation of cell surface representation and signal transduction. Solution NMR spectroscopy has proven its superiority in order to study these dynamic molecular interactions occurring at the cell membrane[100] and using solution NMR techniques will continue to shed light on these systems in physiological and pathological context.

1.6 TNFα - a crucial pro-inflammatory cytokine

Tumor necrosis factor α (TNFα) is a type II single-pass transmembrane protein of 233 amino acid length[101]. TNFα ectodomain self-assembles into non-covalently linked trimers. The membrane-anchored precursor has a monomeric molecular mass of 26 kDa comprised of an ß-stranded extracellular domain (ECD, 57-233) bearing a disulfide bond between cysteine residues 145 and 177, a transmembrane domain (TMD, 36-56) and an intracellular domain (ICD, 1-35). Amino acid modifications include phosphorylation at cytoplasmic serine residues[102], myristoylation at lysine19 and lysine20[103] and an O-linked glycosylation at serine80[104]. Processing of TNFα includes release of the soluble domain (sTNFα, 77-233) via cleavage by metalloprotease TNFα converting enzyme (TACE/ADAM17) of the transmembrane-linked precursor (tmTNFα)[105]. This so-called shedding event happens between residues alanine 76 and valine 77. The remaining membrane-tethered fragment undergoes regulated intramembrane proteolysis (RIP) meaning stepwise degradation of the TMD portion and release of the ICD. The enzyme mediating this proteolysis reaction is the signal peptide peptidase like 2b (SPPl2b) protease, an intramembrane GxGD aspartyl protease, belonging to

the same family as γ-secretase[56,106]. SPPL2b releases TNFα-ICD into the cytosol which in turn triggers expression of interleukin-12 (IL-12) by activated dendritic cells[106].

Two receptors of TNFα, namely TNFR1 (55 kDa) and TNFR2 (75 kDa), mediate TNFα-induced signal transduction. They activate different signaling pathways and induce diverse biological effects of TNFα[107]. The proinflammatory effects are mainly associated with TNFR1 signaling while TNFR2 signaling leads to tissue homeostasis and immune modulation. Both receptors are also subjected to shedding by TACE thus converting them into natural TNFα inhibitors[108]. While TNFR1 binds the soluble and the membrane-bound form of TNFα, TNFR2 mainly interacts with the membrane-bound form[109].

1.7 Targeting TNFα in disease

The extracellular domain of TNFα is perhaps the most well studied protein in biochemistry. The crystal structure of the trimeric soluble domain has been solved already in 1989[27].

Overexpression of TNFα plays a central role in the pathogenesis of autoimmune inflammatory responses in rheumatoid arthritis (RA), inflammatory bowel disease (IBD), Crohn's disease (CD), and ankylosing spondylitis (AS)[110-112]. Consequently, anti-TNFα biologics have been developed for the treatment of inflammatory autoimmune diseases that are designed to block the biological function of TNFα ECD[113].

Five Biologics are currently approved for the treatment of TNFα induced inflammatory autoimmune diseases. The fully humanized antibody Adalimumab (Humira®, AbbVie) represents the top selling single brand recombinant biological worldwide with global sales of approximately 19.2 billion USD in 2019. Among the therapeutic antibodies Etanercept (Enbrel®, Pfizer) makes an exception, being a fusion protein of TNFα receptor 2 (TNFR2) soluble domain and the Fc portion of human IgG1.

In general, small molecules offer several advantages over biologics in particular production costs, oral administration and the ability to cross the blood-brain barrier. The last point is especially interesting in terms of targeting TNFα-mediated neuroinflammation. In 2005, a crystal structure of dimeric TNFα in complex with a novel small molecule inhibitor (SPD304) was discovered that is able to dissociate the trimeric form of TNFα, as shown by X-ray crystallography[114] (Figure 5, upper panel). Cell-based assays also confirmed its biological effects. In 2017, solution-NMR studies revealed that SPD304 enhances conformational

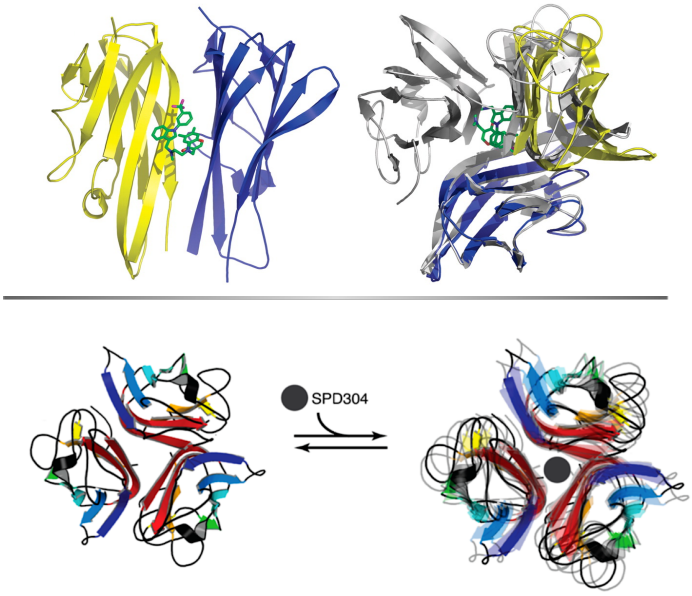

Figure 5: Influence of small molecule inhibition (SPD304) on TNFα. (a) X-ray crystallographic snapshot of SPD304 induced dimerization by small molecule driven exclusion of the third monomeric subunit. Reprinted with permission from reference [114]: He M.M. *et al*., Science (2005). (b) Solution NMR studies on SPD304 effects. In presence of SPD304, TNFα trimer shows increased dynamics. Reprinted with permission from reference [115]: Hofmann D. *et al.*, JACS (2018), Copyright (2017) American Chemical Society.

dynamics of the TNFα trimer and thereby hinders the interaction of TNFα and its receptor[115] (Figure 5, lower panel). SPD304 was unfortunately shown to be highly toxic but is currently optimized for clinical use[116,117].

Just recently, small molecules have been discovered that exert a stabilizing effect on asymmetric trimer conformations that naturally occur during subunit exchange. These molecules bind in the center of the TNFα core and seem to inhibit binding of TNFα to its receptor TNFR1 via allosteric effects[118].

Besides antibody-mediated neutralization and small molecule inhibition of excess TNFα, new concepts include preventing shedding of tmTNFα by antibody mediated blocking of the stalk region[119] or targeting the responsible receptors for signal transduction TNFR-1 and TNFR-2. For example, TNFR-2 agonist is able to promote expansion of immunosuppressive CD4+Foxp3+ regulatory T cells (Tregs) more potently than TNFα itself thus inhibiting autoimmune responses[120]. Selective inhibition of TNFR-1 on the other hand also effectively leads to proliferative expansion and activation of Tregs[121]. There is a plethora of different attempts to target pathological TNFα signaling (Figure 6) underlining the importance of TNFα or one of its receptors as drug targets.

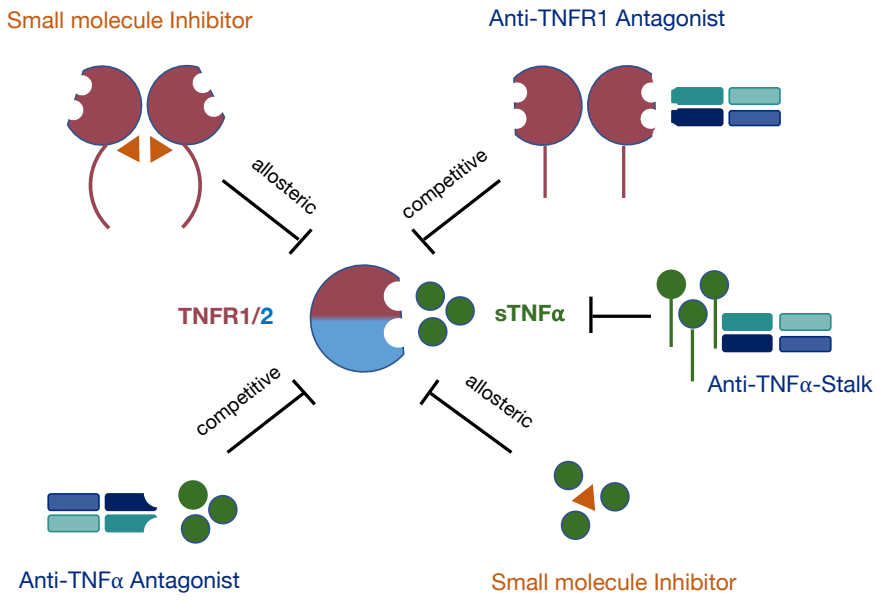

Figure 6: Targeting pathological TNFα signaling. Protein-Protein interactions can be targeted either in a competitive or allosteric manner. Small molecule inhibition of TNFα or its receptor TNF-R1 leads to allosteric changes of the binding interfaces. Competitive inhibition of TNF-R1, TNFα, or TNFα-Stalk region directly interferes with the binding region.

2 OBJECTIVES

The first main goal of this work was to gain insights into structural and dynamical features of γ-secretase substrate TREM2 transmembrane domain and to investigate charge-induced effects of lysine 186 using solution NMR spectroscopy. A flexible kink region, showing a lack of secondary structure and a decreased order parameter, in the C-terminal part of the wild-type protein was absent in the charge-neutralized DAP12-bound state as well as in the charge variant (here: K186A). This is pointing to a crucial function of lysine 186 not only regarding complex formation but also being responsible for inducing the flexible kink. Due to similarity between DAP-12-bound and K186A structures, K186A was used a mimic for the bound-state and used for investigation of lysine induced differences. Molecular dynamics simulations demonstrated that the lysine side-chain is aiming for the phosphate moieties in the lipid head group region causing the wild-type helix to tilt within the membrane. Paramagnetic relaxation enhancement (PRE) experiments confirmed that the helical stretch downstream of the kink region is in fact outside of the membrane anchored on the surface by two tryptophan residues. K186A on the other hand is a continuous and straight α-helix completely inserted within the membrane and consequently displayed an altered initial γ-secretase cleavage event compared to the wild-type protein where the initial ε-cleavage site was found to be within the dynamic kink region. Furthermore, studies were expanded including different charge variants, namely K186P and K186L into ^{1}H, ^{15}N-TROSY spectral comparison, γ-secretase cleavage analysis and stability measurements. K186P showed comparable results to the wild-type protein while K186L demonstrates high similarity to results obtained for the initial charge variant K186A underlining the fact that helix distortions leading to reduced stability and enhanced flexibility facilitate γ-secretase access and cleavage.

In order to gain access to all domains of TREM2, a protocol for production, refolding and purification of TREM2 ECD was established.

The second major goal was a screening of small molecules targeting TNFα ECD. This was done by applying an NMR-based fragment screening to identify putative hit compounds. Once those had been identified, assays were established and conducted to characterize their mode of action *in vitro*. Concentration-dependent loss of the tight trimeric assembly of TNFα ECD was surveyed using binding of extrinsic hydrophobic dyes to monitor the occurrence of exposed hydrophobic areas upon compound treatment. A FRET assay was conducted to determine the compound-specific influence on the monomeric subunit exchange rate. Finally, NMR titration experiments were used to derive apparent K_D values.

In addition, novel methods for the production of membrane-anchored full-length TNFα have been developed in order to investigate the structure and dynamics of this protein in a native membrane environment. This has been achieved by expression of full-length TNFα with the tail-anchored membrane protein chaperone Get3 as well as by using Sortase A mediated protein ligation of separately produced TNFα ECD and TM constructs.

Abbreviations

APS	ammonium persulfate
Aß40	amyloid ß peptide 40
CD3	Cluster of differentiation 3
cDNA	copy deoxyribonucleic acid
CSF	Cerebrospinal fluid
C-terminal	Carboxy-terminal
CTF	C-terminal fragment
DAP12	DNAX activating protein of 12 kDa
DNA	deoxyribonucleic acid
DNAse	deoxyribonuclease
dNTPs	deoxyribonucleotide
DMSO	Dimethylsulfoxide
DMPC	1,2-dimyristoyl-sn-glycero-3-phosphocholine
DMPG	1,2-Dimyristoyl-sn-glycero-3-phosphorylglycerol
DPC	Dodecylphosphocholine (Fos-Cholin 12)
DTT	Dithiothreitol
ECD	Extracellular domain
EDTA	ethylenediaminetetraacetic acid
ER	Endoplasmic reticulum
ESI	electrospray ionization
et al.	et alia
FPLC	fast protein liquid chromatography
HEPES	4-(2-hydroxyethyl)-1-piperazineethanesulfonic acid
His_6	Hexahistidine
ICD	Intracellular domain

IPTG	isopropylthiogalactoside
LB	lysogeny broth
MS	mass spectrometry
MW	molecular weight
N-terminal	Amino-terminal
PAGE	polyacrylamide gel electrophoresis
PCR	polymerase chain reaction
PDB	Protein Data Bank
POPC	1-palmitoyl-2-oleoyl-sn-glycero-3-phosphocholine
POPG	1-palmitoyl-2-oleoyl-sn-glycero-3-phosphoglycerol
SDS	Sodium dodecyl sulfate
SOC	super optimal broth with catabolite repression
SOR	Sortase A recognition motif
T_a	Annealing temperature
TCR	T-cell receptor
TEMED	tetramethylethylenediamine
TEV	tobacco etch virus
THR	Thrombin cleavage site
TNFα	Tumor necrosis factor α
TNF-R1/2	Tumor necrosis factor receptor 1/2
TREM2	Triggering factor expressed on myeloid cells 2
TRIS	tris(hydroxymethyl)aminomethane

3 MATERIAL & METHODS

3.1 MATERIAL

3.1.1 Chemicals

Standard laboratory chemicals used for buffer and solution preparation were purchased from the following providers unless stated otherwise: Acros Organics (USA), AppliChem (Germany), BioRad (Germany), Carl Roth (Germany), Cayman Chemical Company (USA), Cube Biotech (USA), Merck/Millipore (Germany), Roche (Germany), Sigma-Aldrich (Germany), Serva (Germany), VWR (Germany).

3.1.2 Expression plasmids and primer list

All plasmids listed here had been created within this PhD Thesis' practical work. The cDNA of TREM2 and TNFα were kindly provided by Dr. Kai Schlepckow (DZNE, LMU) and Prof. Regina Fluhrer (DZNE, LMU) respectively. The DAP12 construct was kindly provided by Prof. Ville Kaila (TUM).

All gene constructs have been inserted into a pET21a plasmid backbone harboring an ampicillin resistance marker. The respective amino acid protein sequences are listed in the appendix.

Table 1: List of expression plasmids with corresponding abbreviation of the expressed protein and sequence description

Name of expression plasmid	Abbreviation	Description
pET21a-His_6-GB1-THR-TNFα	TNFα ECD	Amino acids 69-233
pET21a-His_6-GB1-THRmut-TNFα	cTNFα	Amino acids 80-233, N-terminal cysteine
pET21a-His_6-GB1-THR-TNFαTM	TNFα-TM	Amino acids 28-62, Extended GS-Linker

pET21a-GB1-THR-TNFαTM-C-His_6	TNFαTM-C	Amino acids 28-85 + Cys
pET21a-GB1-THR-TNFαTM-SOR-His_6	TNFαTM-SOR	Amino acids 28-62 + LPETG (SOR)
pET21a-GB1-THR-TREM2-His_6	TREM2_19-141	Amino acids 19-141
pET21a-GB1-THR-TREM2-SOR-His_6	TREM2-SOR	Amino acids 19-141 + LPETG (SOR)
pET21a-GB1-THR-TREM2(R47H)-His_6	R47H	Amino acids 19-141, R47H mutation
pET21a-TREM2	TREM2 ECD	Amino acids 19-131
pET21a-His_6-GB1-THR-TREM2TM	TREM2-TM (WT)	Amino acids 161-206
pET21a-His_6-GB1-THR-TREM2TM(K186A)	K186A	Amino acids 161-206, K186A mutation
pET21a-His_6-GB1-THR-TREM2TM(K186N)	K186N	Amino acids 161-206, K186N mutation
pET21a-His_6-GB1-THR-TREM2TM(K186L)	K186L	Amino acids 161-206, K186L mutation
pET21a-His_6-GB1-THR-TREM2TM(K186P)	K186P	Amino acids 161-206, K186P mutation

Table 2: DNA Primer list with the corresponding sequence and a description of the cloning purpose

Primer name	**Primer sequence**	**Description**
TNFα-1	*TGGTTCCGCGTGGTTCTGGTGGTCT AATCAGCCCTCTGGCCCAG*	Amplification of TNFα ECD (69-233) for insertion into pET21a-His_6-GB1-THR
TNFα-2	*GCTTTGTTAGCAGCCGGATCTCATTA CAGGGCAATGATCCCAAAGTAGA*	
TNFα-THRcys-1	*CAACGACCCTGGTTCCGCGTTGTTC TTTCTCGAACCCCGAGTGAC*	

TNFα-THRcys-2	*GTCACTCGGGGTTCGAGAAGAACAA CGCGGAACCAGGGTCGTTG*	Mutation of Thrombin cleavage site motif from LVPRG to LVPRC
TNFαTMshort-1	*CCTGGTTCCGCGTGGTTCTGGTAGG CGGTGCTTGTTCCTCAG*	Amplification of TNFαTM (28-62)- for insertion into pET21a- His_6-GB1-THR
TNFαTMshort-2	*GCTTTGTTAGCAGCCGGATCTCACT CTTCCCTCTGGGGGCC*	
TNFαTMsSOR-1	*ATCGGCCCCCAGAGGGAAGAGTTG CCAGAAACAGGAGGTGCTGCTGCCA CCGCTGAGCAATAA*	Insertion of Sortase Recognition Motif into pET21a- His_6-GB1-THR-TNFαTMshort
TNFαTMsSOR-2	*TTATTGCTCAGCGGTGGCAGCAGCA CCTCCTGTTTCTGGCAACTCTTCCCT CTGGGGGCCGAT*	
TNFαTMlong-1	*CCTGGTTCCGCGTGGTTCTGGTAGC ACTGAAAGCATGATCCGG*	Amplification of TNFαTM (2-81)- for insertion into pET21a- His_6-GB1-THR
TNFαTMlong-2	*GCTTTGTTAGCAGCCGGATCTCAAG AAGATGATCTGACTGCCTGG*	
TREM2-1	*CGCGTGGTTCTGGTGGTTCTTCTCA CAACACCACAGTGTTCCAG*	Amplification of TREM2 ECD (19-140)-His_6 for insertion into pET21a-GB1-THR
TREM2-2	*GTGGTGGTGGTGATGATGATGATGT CCAGCATCCCGGTGATCC*	
TREM2_19-131-1	*GTGGAGGTGCTGGCAGACTGAG ATCCGGCTGCTAACAAAG*	Deletion of aa132-141+HisTag in pET21a-TREM2(19-141)-His_6 (Dr. Kai Schlepckow)
TREM2_19-131-2	*CTTTGTTAGCAGCCGGATCTCAG TCTGCCAGCACCTCCAC*	
TREM2TMshort-1	*CCTGGTTCCGCGTGGTTCTGGTAGG AGCCTCTTGGAAGGAGAAATC*	Amplification of TREM2TM (161-206) for insertion into pET21a-His_6-GB1-Thrombin
TREM2TMshort-2	*GCTTTGTTAGCAGCCGGATCTCAAT GTGTCCCTGGCTTCTGTCCATG*	
K186A-1	*CTGGCCTGCATCTTTCTCATCGCGA TTCTAGCAGCCAGCCAGC*	Single point mutations of His_6-GB1-Thrombin-TREM2TM(161-206)
K186A-2	*GCTGGCTGGCTGCTAGAATCGCGAT GAGAAAGATGCAGGCCAG*	
K186N-1	*GGCCTGCATCTTTCTCATCAACATTC TAGCAGCCAGCCAGCGCCC*	

K186N-2	*GGGCGCTGGCTGCTAGAATGTTGAT GAGAAAGATGCAGGCC*	
K186L-1	*CTGGCCTGCATCTTTCTCATCTTGAT TCTAGCAGCCAGCGCC*	
K186L-2	*GGCGCTGGCTGCTAGAATCAAGATG AGAAAGATGCAGGCCAG*	
K186P-1	*CTGGCCTGCATCTTTCTCATCCCGAT TCTAGCAGCCAGCGCC*	
K186P-2	*GGCGCTGGCTGCTAGAATCGGGAT GAGAAAGATGCAGGCCAG*	
TREM2TMlong-1	*CCTGGTTCCGCGTGGTTCTGGTCTC TGGTTCCCCGGGGAG*	Amplification of TREM2TM (141-230) for insertion into pET21a-His_6-GB1-Thrombin
TREM2TMlong-2	*GCTTTGTTAGCAGCCGGATCTCATC ACGTGTCTCTCAGCCCTG*	
DAP12-C33S-1	*GCGCAAGCGCAGAGCGACTCCAGC TGCAGCACCGTGAGC*	Mutation of cysteine 33 to serine
DAP12-C33S-2	*GCTCACGGTGCTGCAGCTGGAGTC GCTCTGCGCTTGCGC*	

3.1.3 Protein and DNA standard

Name	**Manufacturer**
Dual Color Protein Standard III	SERVA
DNA 1kbp	SERVA
DNA 100bp	SERVA

3.1.4 Bacterial strains and growth media

3.1.4.1 Bacterial strains

Table 3: List of bacterial strains with respective genotype and manufacturer

Name	**Genotype**	**Manufacturer**
NEB5α	*fhuA2 a(argF-lacZ)U169 phoA glnV44 a80a(lacZ)M15 gyrA96 recA1 relA1 endA1 thi-1 hsdR17*	New England Biolabs (NEB)

XL10-Gold®	*TetrD(mcrA)183 D(mcrCB-hsdSMR-mrr)173 endA1 supE44 thi-1 recA1 gyrA96 relA1 lac Hte [F´ proAB lacIqZDM15 Tn10 (Tetr) Amy Camr]*	Agilent
BL21 (DE3)	*fhuA2 [lon] ompT gal (λ DE3) [dcm] ΔhsdS λ DE3 = λ sBamHIo ΔEcoRI-B int::(lacI::PlacUV5::T7 gene1) i21 Δnin5*	New England Biolabs (NEB)
BL21 (DE3) - RIPL	*ompT hsdS(r $^{-}$ m $^{-}$) dcm^{+} Tet^{r} gal λ(DE3) endA Hte [argU proL BB Cam^{r}] [argU ileY leuW Strep/Spec^{r}]*	Agilent

3.1.4.2 Bacterial growth media

Table 4: List of bacterial growth media and their composition

LB medium	Peptone	1 % (w/v)
	Yeast extract	0.5 % (w/v)
	NaCl	1 % (w/v)
	(Agar)	2 % (w/v)
SOC medium	Peptone	2 % (w/v)
	Yeast extract	0.5 % (w/v)
	Glucose	20 mM
	MgSO4	10 mM
	NaCl	10 mM
	KCl	2.5 mM
M9 minimal media	Na_2HPO_4	6 g/L
	KH_2PO_4	3 g/L
	NaCl	0.5 g/L
	NH_4Cl	0.5 g/L
	$MgSO_4$ (1 M)	2 mL/L
	$CaCl_2$ (0.5 M)	0.2 mL/L
		0.2 % (w/v)

	Glucose (20 % (w/v))	1 mL
	Biotin (1 mg/mL)	1 mL
	Thiamin (1 mg/mL	1 mL
	Trace elements (1000x)	

3.2 METHODS

3.2.1 Molecular Cloning

All initial gene constructs were generated using restriction-free approach from Unger et al.[122]. All further gene truncations/extensions or introduction of single point mutations were done using the QuikChange Lightning Site-directed Mutagenesis Kit (Agilent).

3.2.1.1 Restriction free cloning

Table 5: PCR reaction mixture for 1st PCR: Megaprimer generation

10x reaction buffer	5 µL
10 mM dNTPs	1 µL
Template DNA	25-50 ng
Forward primer (10µM)	1.3 µL
Reverse primer (10µM)	1.3 µL
***Pfu* Polymerase**	1 µL
ddH_2O	Add to 50 µL

Table 6: PCR reaction thermocycler program for 1st PCR: Megaprimer generation

95°C	2 minutes	
95°C	20 seconds	30x
62°C	20 seconds	
68°C	2 minutes	

68°C	5 minutes	
10°C	Hold	

Table 7: PCR reaction mixture for 2nd PCR: whole plasmid synthesis

10x QCL buffer	2.5 µL
solution	0.75 µL
10 mM dNTPs	0.5 µL
Target vector	25-50 ng
Purified megaprimer (1.PCR)	10x molar excess to target vector
QCL enzyme	0.5 µL
ddH_2O	Add to 25 µL

Table 8: PCR reaction thermocycler program for 2nd PCR: whole plasmid synthesis

95°C	2 minutes	
95°C	30 seconds	25x
62°C	30 seconds	
68°C	5 minutes	
68°C	10 minutes	
10°C	Hold	

3.2.1.2 DNA isolation agarose gel (clean-Up)

Purification of DNA was routinely performed using 1% (w/v) agarose gels and 1x TBE as running buffer. Addition of Roti-Stain to the gel mixture enables visualization of DNA bands without the need for ethidium bromide. After electrophoretic separation (120V, approx. 60 minutes) Wizard® SV Gel and PCR Clean-Up System was used for extraction of DNA from agarose gels.

Table 9: Dye and buffer composition for agarose gel electrophoresis

6x DNA loading dye	10 mM Tris-HCl (pH 7.6)
	60 mM EDTA
	0.1% bromophenol blue
	0.1% xylene cyanol FF
	50% glycerol
1x TBE (Tris/boric acid, EDTA)	89 mM Tris
	89 mM boric acid
	2 mM EDTA
	Fill up to 1L

3.2.1.3 Site-directed mutagenesis for introduction of single point mutations

Table 10: PCR reaction mixture for site-directed mutagenesis

10x QCL buffer	2.5 µL
Quick solution	0.75 µL
10 mM dNTPs	0.5 µL
QC primer 1	0.65 µL
QC primer 2	0.65 µL
QCL enzyme	0.5 µL
ddH_2O	Add to 25 µL

Table 11: PCR reaction thermocycler program for introduction of point mutations

95°C	2 minutes	
95°C	30 seconds	25x
62°C	30 seconds	
68°C	5 minutes	
68°C	10 minutes	
10°C	Hold	

3.2.2 Transformation and DNA amplification

3 µL of the respective PCR product was transformed into 50 µL of NEB5α cells. The thawed cells were incubated with the DNA on ice for 30 minutes. After heat shock for 30 seconds at 42°C SOC medium (200 µL) was added. The cell suspension was incubated for 1 hour at 37°C in the shaker (120 rpm). Cells were plated afterwards on selective agar plates and kept overnight at 37°C. DNA plasmid isolation from selected single colonies was done using the Wizard® Plus SV Minipreps DNA Purification System (Promega) and sent for sequencing to GATC or later on to Genewiz.

3.2.3 Recombinant protein production

Sequenced plasmids were transformed into *E. coli* BL21 (DE3) or BL21(DE3)-RIPL cells for protein expression. The pre-culture was used in a ratio of 1:40 for inoculation of the main culture. Induction took place at an optical density (OD) of 0.7 by addition of 1mM IPTG. Protein expression was carried out for 3-4 hours at 37°C or overnight at 20°C. Cells were harvested for 20 minutes at 6000 rpm and cell pellets frozen at -80°C until further usage.

3.2.4 Isotope labelling

Isotope labelling was achieved by including several adaption steps until final induction in M9 minimal medium. Starting with a 5 mL LB in H_2O (+ 2 % (w/v) glucose and antibiotic) culture cells were sedimented at 2000 x g for 5 minutes and transferred to 5 mL LB in D_2O (+ 2% (w/v) glucose and antibiotic). After 24 hours at 37°C shaking cells were again sedimented and transferred to 5 mL M9/D_2O (+2% glucose, antibiotic). In the evening the final volume was adjusted to 50 mL M9/ D_2O (taken from the main culture medium). Expression and harvest were carried out as mentioned in section 3.3.

3.2.5 SDS-PAGE

Detection of protein was routinely performed using SDS-PAGE analysis.

3.2.5.1 Gel Casting Recipe (13 gels)

Table 12: Pipetting scheme for casting SDS gels

Separating gel	
H_2O	28 mL
Acrylamide	30 mL
1.5 M Tris, pH 8.8	20 mL
10 % (w/v) SDS	0.8 mL
10 % (w/v) APS	0.8 mL
TEMED	0.08 mL

Stacking gel	
H_2O	29.3 mL
Acrylamide	7.5 mL
0.5 M Tris, pH 6.8	12.5 mL
10 % (w/v) SDS	0.5 mL
10 % (w/v) APS	0.5 mL
TEMED	0.05 mL

3.2.5.2 SDS-PAGE – Buffers and solutions

Table 13: Buffer/Loading dye composition and staining solution for SDS PAGE analysis

10 x SDS Buffer	30 g Tris
	10 g SDS
	144 g Glycin
2 x Lämmli (Protein Loading Dye)	65.8 mM Tris-HCl, pH 6.8

	26.3% (w/v) glycerol 2.1% SDS 0.01% bromophenol blue
PageBlue™ Protein Staining Solution	Thermo Fisher Scientifc

Electrophoretic separation of proteins was assessed by applying a constant current of 50 mA for 30 minutes. The SDS gel was first boiled once with water and then covered with PageBlue™ Protein Staining Solution. After shaking for 20-30 minutes the stain was removed and replaced with water. For better contrast the gel was left in water for some hours or overnight.

3.2.6 Chromatographic Methods and buffers

All chromatographic purification columns and column resin was purchased from GE Healthcare. FPLC purifications were carried out at an ÄKTA™ pure 25 protein purification chromatography system (GE Healthcare) operating at 4°C.

Table 14: List of chromatography columns and mode of purification

Name of column	Abbreviation	Type of chromatography
Nickel Sepharose excel histidine-tagged protein purification resin	NiNTA	Nickel affinity
Illustra NAP-5/-25	NAP5/25	Desalting
HiTrap Q FF 5mL	Q FF	Anion exchange
HiTrap SP FF 5 mL	SP FF	Cation exchange
Superdex 75 10/300	S75a	Size exclusion
Superdex Increase 200 10/300	S200a	Size exclusion
Superdex 75 16/60 HiLoad	S75p	Size exclusion
Superdex 200 16/60 HiLoad	S200p	Size exclusion

All Buffers for FPLC purification were filtered (2 μM pore size), degassed and equilibrated at 4°C before using at the ÄKTA™ purification system.

Table 15: Buffer composition for chromatographic protein purifications

Name of Buffer	Composition
Buffer A	20 mM Tris, pH 8.0, 100 mM NaCl, 0.5 mM EDTA
Buffer B	Buffer A + 10 mM imidazole
Buffer C	Buffer A + 400 mM imidazole
Buffer D	20 mM NaPi, 50 mM NaCl, 0.5 mM EDTA
Buffer E	25 mM HEPES, pH 8.8, 0.5 mM EDTA
Buffer F	25 mM HEPES, pH 8.8, 1 M NaCl, 0.5 mM EDTA
Buffer G	50 mM Tris, pH 8.5, 6 M Guanidine hydrochloride, 2 mM DTT

In terms of purification of all transmembrane constructs the buffer compositions are the same with the only difference being 0.1% DPC detergent present. The corresponding buffers will be marked with an asterisk meaning 0.1% DPC included, e.g. **Buffer A***.

3.2.7 Protein purification

3.2.7.1 Cell lysis

Frozen cell pellets were thawed on ice after addition of approx. 10 mL Buffer A / 1 g of cell pellet. In order to prevent proteolysis 1 tablet of cOmplete™, EDTA-free Protease Inhibitor Cocktail (Sigma) was added. The homogenized cell suspension was supplemented with lysozyme (a tip of spatula) and stirred on ice for 20-30 minutes before addition of 1 µL of DNase I (Roche) / 10 mL of cell suspension (DNase I stock: 10 U / 1 µL) and 5 mM $MgCl_2$ as co-factor. Final cell disruption was performed using ultrasonic treatment for 30 min on ice (1 sec pulse, 2 sec pauses; 30% amplitude). The following purification steps differed depending on the respective protein construct:

3.2.7.2 TNFα ECD

Upon cell disruption the whole cell lysate was spun down at 18000 rpm (39000 x g) in a Sorvall Lynx 2000 Centrifuge using a fixed angle T29-8x50 rotor for 20 minutes and the supernatant (SN) was loaded onto the equilibrated Ni-NTA resin (Buffer A) for subsequent affinity

chromatography of his-tagged TNFα ECD. After incubation of the SN with the Ni-NTA resin on a shaking plate, the resin was allowed to sediment before performing the affinity purification in a *gravity flow* mode. Upon washing of the bound protein with Buffer B the protein was eluted using Buffer C. The eluate was concentrated in a 10kDa Cut-Off Amicon Centrifugal Filter Unit (Merck) and directly applied to a Superdex 75 pg size exclusion chromatography column. Thrombin was added to the protein pool to cleave off the GB1 fusion protein and a second S75p was applied next day to efficiently separate GB1 and TNFα. For long-term storage the purified protein was flash frozen in liquid nitrogen and kept at -80°C.

3.2.7.3 Thiol-reactive labelling of TNFα carrying an N-terminal cysteine

Mutation of the Thrombin cleavage site from LVPRG to LVPRC according to Liu *et al.*[123] enables generation of an N-terminal cysteine for thiol reactive coupling reactions. The His_6-GB1-THRmut-TNFα construct was purified as described in section 3.2.5.2. with the only exception being 5 mM ß-mercaptoethanol (ßME) used throughout the whole purification to avoid disulfide formation of the introduced cysteine residue. Prior to the thiol reactive coupling to fluorescence dyes ßME was exchanged to inert TCEP with a final concentration of 1 mM using a desalting column and Buffer A. Either Fluoresceinisothiocyanate (5-IAF, Invitrogen; Figure 7 (left)) in DMF or Tetramethylrhodamine-5-maleimide (TMR5M, Chemodex; Figure 7 (right)) in DMSO was used for coupling with a 10x molar excess compared to the cTNFα concentration. The reaction was quenched after 2 hours of incubation at 37°C (heavy stirring)

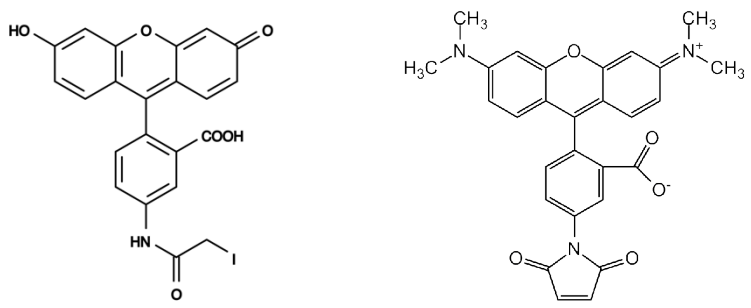

Figure 7: Chemical structures of fluorescent dyes 5-IAF (left) and 5-TAMRA (right) used for cysteine-specific coupling to TNFα ECD in terms of a FRET-based compound screen

by addition of 5x molar excess of DTT (compared to Dye) for additional 30 minutes. Removal of unbound Dye was done by desalting column followed by size exclusion chromatography.

3.2.7.4 TREM2 ECD

TREM2 ECD was expressed in *E. coli* BL21(DE3)-RIPL and was purified from inclusion bodies. Upon cell lysis the whole cell lysate was spun down, but the supernatant discarded. The remaining inclusion body pellet was directly dissolved in Buffer G. Shaking for 3 hours at RT or overnight at 4°C solubilized the protein fraction of the pellet. After a final centrifugation step to get rid of the remaining *E. coli* membrane lipids the clear GuHCl supernatant was decanted into a sterile 50 mL Falcon. The protein concentration was measured and diluted with Buffer G to a final concentration of 5 mg/mL for refolding. The final refolding buffer was taken from Sudom *et al*.[63]:

2 M urea, 50 mM Tris-HCl, 20% glycerol, 160 mM L- arginine, 3 mM cysteine and 1mM cystamine at pH 8.9

Instead of L-cysteine and cystamine, reduced and oxidized glutathione can be used as well at the same concentrations.

The protein solution was dropwise added to the refolding buffer while stirring in a ratio of 1:20. Stirring was continued for 48 more hours and the refolding solution was dialyzed against 25 mM HEPES pH 8.8, 0.5 mM EDTA and 25 µL Thrombin (Stock: 1U/µL) were added into the dialysis membrane. Afterwards a SP FF was performed and fractions containing the desired protein were pooled.

3.2.7.5 Transmembrane Helices (TNFα-TM, TREM2-TM)

Upon cell disruption 1.5 % (w/v) of DPC was added as a powder and left for shaking for about 1.5 hours at 4°C. Following incubation, sodium chloride concentration was added to a final concentration of 1 M and shaken for another 30 minutes. The mixture was centrifuged at 18000 rpm (39000 x g) in a Sorvall Lynx 2000 Centrifuge using a fixed angle T29-8x50 rotor for 20

minutes and the supernatant was transferred to an equilibrated NiNTA resin (Buffer A*). Bound protein was washed with 5 CV Buffer B* and the eluate (3 CV Buffer C*) was concentrated using a 30 kDa Cut-Off spin concentrator. The final purification step was a S200p size exclusion chromatography. Depending on the subsequent use of the protein, GB1 either remained on the TM helix or was cleaved off at this point by addition of 25 U of thrombin.

3.2.8 Determination of protein concentration

Protein solution were routinely analyzed at a NanoPhotometer® (Implen) and the specific wavelength of 280 nm. Calculation of protein concentration was performed using the extinction coefficient and the molecular weight given by the ProtParam web server (https://web.expasy.org/protparam/).

Table 16: List of extinction coefficients and molecular weights of all constructs

Protein	**+ / - GB1**	**Extinction coefficient [M^{-1} cm^{-1}]**	**Molecular weight [Da]**
TNFα ECD	+ GB1	35995 (oxidized)	27733.2
	- GB1	21555 (oxidized)	18404.9
TREM2 ECD (19-131)	~~GB1~~	25230 (oxidized)	12647.4
TNFα-TM	+ GB1	14565 (reduced)	13773.5
	- GB1	125 (reduced)	4910.8
TREM2-TM	+ GB1	25440 (reduced)	14495.4
	- GB1	11000 (reduced)	5167.2

3.2.9 Circular dichroism (CD) spectroscopy

Estimation of secondary structure content and the loss of secondary structure upon thermal or chemical unfolding was performed in a Jasco J-815 CD spectrometer using a 1 mm quartz cuvette. Maximum sample volume was 300 µL with a sample concentration of approx. 20 µM. Secondary structure spectra were recorded using a wavelength scan between 260 and 190 nm and the respective structure-specific minimum was taken for unfolding experiments. Thermal unfolding was achieved by heating the sample at the respective wavelength from 20 °C to 100 °C with a heating rate of 1 °C per minute while chemical unfolding was measured at a constant temperature of 20 °C at varying denaturant concentrations.

Table 17: Buffer compositions for different modes of protein unfolding using CD spectroscopy

Mode of Unfolding	Dilution Buffer
Thermal	20 mM NaPi, pH 7.0
Chemical (Urea)	20 mM Tris, pH 8, 0-8 M urea (0.5 M steps)
	+ 0.1 % DPC for TM constructs
Chemical (GuHCl)	20 mM Tris, pH 8, 0-8 M GuHCl (0.5 M steps)
	+ 0.1 % DPC for TM constructs

Conversion of raw ellipticity to mean residue molar ellipticity was done using the following formula where n is the number of peptide bonds:

$$\theta[deg \times cm^2 \times dmol^{-1}] = \frac{\theta[deg \times cm^2 \times dmol^{-1}]}{pathlength[mm] \times c_{Protein}[\mu M] \times n}$$

The fractional helicity (FH), representing the content of α-helical secondary structure, was calculated using the experimental mean residue weight (MRW) ellipticity at λ = 222 nm (θ^{exp}) and the corresponding values for the fully helical or fully unfolded conformation (θ^{h} and θ^{u} = -36000 and -3000 deg cm^2 dmol^{-1}, respectively) with the following equation:

$$FH = \frac{\theta_{\lambda}^{exp} - \theta_{\lambda}^{u}}{\theta_{\lambda}^{h} - \theta_{\lambda}^{u}}$$ [124].

Data analysis was done using Excel (calculation) and OriginPro (visualization).

3.2.10 Spectrofluorometer

Measurements were conducted at a Jasco FP-8300 Spectrofluorometer using a 10 mm quartz cuvette with a sample volume of 1mL and an integrated stirrer.

Investigation of subunit exchange of trimeric TNFα ECD was surveyed by FRET similar to a protocol reported by van Schie *et al.*[125]. 100 nM IAF-TNFα samples were mixed with a 10x molar excess of TMRM-TNFα and donor quenching was detected at 523 nm (emission maximum of IAF-TNFα) upon excitation at 450 nm (minimal co-excitation of TMRM-TNFα). The same experiments were performed including Hit-compounds which have been identified as putative binders in a fragment-based NMR screening with a final concentration of 1 mM. Monomeric subunit exchange was recorded at 37°C for 16 hours while shaking at 500 rpm.

3.2.11 Thermal Shift Assay (TSA)

Observation of the initial fluorescence that goes along with exposed hydrophobic protein areas and binding of the SYPRO Orange hydrophobic dye was conducted in terms of compound binding to TNFα ECD.

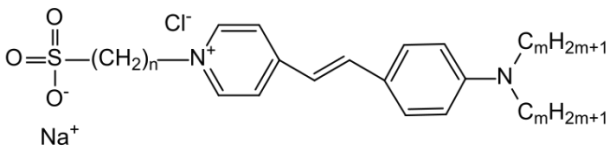

Figure 8: Chemical structure of SyproOrange Dye used for detection of exposed hydrophobic protein areas in terms of compound screening

Concentration dependent interaction of the respective compound with TNFα ECD was measured in a 96-well plate format. The protein concentration was 10 µM in 20 µL. Compound

concentrations ranged from 2 mM down to 12.5 μM (usually 1:2 dilution series). Negative controls included same compound concentrations without TNFα ECD. The commercial Sypro Orange dye was diluted 1:100 and 2.5 μL of the dilution was added to each well.

3.2.12 Dynamic Light Scattering (DLS)

Determination of protein / particle size distribution was performed in a DynaPro NanoStar instrument (Wyatt). Protein concentrations ranged from 10-20 μM in a 60 μL sample volume. Prior measurement the sample was spun down at maxim speed in a room temperature table top centrifuge to remove any particles that might interfere with accurate determination. The sample was transferred into a disposable plastic cuvette and inserted in the instrument. Measurements were recorded either at 25 °C or 37 °C. Microsoft Excel was used for data analysis while visualization was done with OriginPro.

3.2.13 Nanodisc assembly and determination of oligomeric state

Assembly of lipid nanodiscs and concomitant incorporation of the transmembrane domains was performed similar to published protocols[126,127].

Table 18: Reaction components for exemplary Nanodisc assembly

Component	Final Concentration	Ratio
His_6-GB1-TM domain	~ 40 μM	1
MSP1D1ΔH5	160 μM	4 (1)
DMPC/DMPG (75/25)	6.4 mM	160 (40)
or		
POPC/PG (75/25)	3.2 mM	80 (20)

The assembly components are mixed and brought to the calculated volume by adding Buffer A. After incubation for 1 hour at room temperature the assembly was transferred into a 20 kDa

Cut-Off dialysis membrane and dialyzed against 5 L of Buffer A overnight at room temperature. The dialyzed assembly was purified via NiNTA thereby removing the empty Nanodiscs and capturing the His_6 tag bearing loaded Nanodiscs. In order to select nicely homogenic Nanodiscs a S200a was performed and the peak fraction was pooled and concentrated up to 1 mL for the following Thrombin digest. After complete Thrombin digestion the assembled nanodiscs were again injected onto a S200a. The nanodisc peak was pooled and used for biophysical and structural experiments. Furthermore, the ratio of the peak areas of corresponding to the nanodiscs and cleaved GB1, respectively, could be used to calculate the ratio of inserted helices per nanodisc according to a protocol reported by Haeusler *et al*.[128].

3.2.14 Sortase A coupling

Sortase A forms a stabile peptide bond between two proteins or protein domains. The recognition motif of Sortase A is LPXTG on the C-terminus of one protein and the reaction consists of cleavage between the threonine and glycine residue, leading to the formation of a thioester intermediate between the enzyme and the N-terminal part harboring the recognition motif. This intermediate is attacked by a sterically accessible N-terminal glycine residue in the C-terminal protein fragment in a nucleophilic manner, leading to the formation of a peptide bond between both fragments and release of the enzyme.

In order to create full length TNFα-FL the Sortase A motif LPETG was therefore fused to the C-terminus of the transmembrane domain GB1-TNFαTM-SOR-His_6. The N-terminal glycine is created via Thrombin cleavage (LVPR|**G**) at the soluble domain of TNFα (G-TNFα), respectively. Upon reaction the His_6-tag gets cleaved leading to full-length protein without remaining His_6-tag. Removal of the short G-X_n-His6 peptides which would be reactive themselves was achieved by performing the reaction in Slide-A-Lyzer™ dialysis cups (10 MWCO). In order to keep the harmful effect of detergent on TNFα ECD low,

GB1-TNFαTM-SOR-His_6 was properly diluted to yield a final DPC concentration between 0.07 % and 0.1 % in the reaction mixture. A Ca^{2+}-independent Sortase A enzyme was introduced in order to minimize the effect of calcium-mediated cleavage of TNFα ECD. This enzyme carries 7 mutations (P94R/E105K/E108A/D160N/D165A/K190E/K196T) which reduces calcium dependency while still ensuring efficient catalysis of the coupling reaction[129]. The expression plasmid was kindly provided by Maximilian Fottner (AG Lang, TUM) and purified according to conditions published elsewhere[130].

To ensure saturation of G-TNFα, 2-fold excess of GB1-TNFαTM-SOR-His_6 was used. A standard reaction mixture was composed of 50 µM G-TNFα, 100 µM GB1-TNFαTM-SOR-His_6, 5 µM Sortase A and 5 mM ß-mercaptoethanol. After incubation at RT for 1 hour, the reaction mixture was transferred to a NiNTA chromatography purification followed by size exclusion chromatography.

3.2.15 Determination of γ-secretase cleavage site

All experiments according to method section 3.2.16 were kindly performed by Dr. Kai Schlepckow (DZNE, LMU München).

3.2.15.1 Generation and maintenance of stably transfected HEK293 Flp-In cell lines

In order to determine the initial ε-cleavage site within the human TREM2TM, a construct was generated that essentially follows the construct design as previously described for neuregulin 1 type III [131]. In brief, the TREM2 signal peptide at the N terminus was followed by a FLAG tag, an IM linker sequence, the TREM2 CTF (residues 158-230), a GG linker, a HA tag, and a PP motif for ICD stabilization. The corresponding DNA was purchased from IDT and inserted into the pcDNA5/FRT/TO vector via HindIII (New England BioLabs) and XhoI (ThermoFisher Scientific) restriction sites. The K186A mutant (AAG>GCG) was generated by site-directed mutagenesis employing PfuTurbo DNA polymerase (Agilent Technologies). All constructs

were verified by DNA sequencing (Eurofins Genomics). Transfection of HEK293 Flp-In cells (ThermoFisher Scientific) with the wildtype and mutant constructs was performed using lipofectamine 2000 according to the manufacturer's recommendations (ThermoFisher Scientific). Successful transfectants were selected using 100 µg/ml hygromycin B (ThermoFisher Scientific) and stably transfected cell lines were generated as pools. Culturing of stable cell lines was performed as previously described [79].

3.2.15.2 In vitro γ-secretase cleavage assay

The *in vitro* γ-secretase assay to generate TREM2 ICDs was essentially performed as previously reported [132]. Total protein concentrations of cell homogenates of the TREM2 CTF wild-type and mutant cell lines were determined using the BCA assay (Interchim) in order to properly adjust the volume of the buffer (150 mM sodium citrate pH 6.4, 1 mM EDTA, protease inhibitor mix (Sigma)) used for the assay. To allow generation of the ICD of TREM2, samples were incubated at 37°C overnight and inhibition of γ-secretase mediated ICD formation was performed using 1 µM L-685,458 (Sigma, L1790). In the last step, soluble (S100) and insoluble (P100) fractions were separated by ultracentrifugation (55,000 rpm; 60 min).

3.2.15.3 Determination of ε-cleavage sites by IP/MS

Soluble fractions as derived from the *in vitro* γ-secretase assay were subjected to peptide alkylation as previously described [131] to generate monomeric peptide. In the following, the 6-fold volume of IP/MS buffer (0.1 % n-octyl glucoside, 10 mM Tris–HCl, pH 8.0, 5 mM EDTA, and 140 mM NaCl) was added and samples were pre-cleared for 1 hour using protein G sepharose (GE Healthcare, 17-0618-01). Immunoprecipitation was carried out overnight at 4 °C using anti-HA agarose beads (Sigma, A2095). On the next day beads were washed three times with IP/MS buffer and two times with water. After the last washing step water was carefully sucked off and beads were stored at -20 °C until MS analysis. MALDI MS determination of γ-secretase cleavage sites was performed as previously reported[80,131,133].

3.2.16 Molecular Dynamics (MD) Simulations

TREM2-TM was inserted into a hexagonal box of 1-palmitoyl-2-oleoyl-glycero-3-phosphocholine (POPC) and 1-palmitoyl-2-oleoyl-glycero-3-phosphoglycerol (POPG) lipid bilayer (3:1 ratio) using the CHARMM-GUI web server (http:/www.charmm-gui.org)[134] in presence of 0.15 M KCl. Equilibration of the system was done at 310 K in two phases with 3 cycles each. The force constants to fix the position of the protein and membrane were gradually reduced in each cycle. In the first phase, a timestep of 1 fs and a simulation time of 50 ps in each cycle were used whereas in the second phase a timestep of 2 fs and a simulation time of 200 ps for each cycle were used. Total equilibration time was 750 ps. MD simulations of up to 150 ns duration were carried out with the isothermal-isobaric ensembles at 310 K with the program NAMD[135] in the absence of a transmembrane potential. Long-range electrostatic interactions were described using the particle-mesh Ewald method[136]. A smoothing function was applied to truncate short-range electrostatic interactions. Analysis and visualization of the obtained trajectories was done with VMD[137].

3.2.17 NMR Spectroscopy

All NMR experiments were recorded at cryoprobe equipped 600 MHz, 800 MHz, 900 MHz and 950 MHz proton frequency Bruker Avance III spectrometers. Data acquisition and processing was performed using TopSpin® 3.7 software. NMRFAM-SPARKY[138] was used for Data analysis and visualization.

3.2.17.1 Transverse relaxation-optimized spectroscopy (TROSY)

Transverse relaxation-optimized spectroscopy (TROSY)[139] is tackling the problem of fast relaxation during the pulse program and data acquisition which comes along with increasing size of the protein, meaning the bigger the protein, the shorter T_2 and the broader the lines in the spectrum. TROSY is selecting for the slow relaxing resonance line at the expense of partial

loss of the potential signal but therefore increasing the signal-to-noise ratio and thus the sensitivity substantially on account of the greater peak height of the sharp (slow relaxing) line. Considering a system of two scalar coupled spins, *I* and *S*, and a scalar coupling constant of J_{IS} transverse (T_2) relaxation of this system is dominated by dipole-dipole (DD) interaction of *I* and *S* as well as chemical shift anisotropy (CSA) of each individual spin. Cross correlation between DD and CSA results in two lines of a doublet spin having different linewidths because e.g. the ^{15}N nucleus in an N-H group is relaxed by two mechanisms: the dipolar interaction with the proton and the CSA of 15N itself. Both relaxation mechanisms, DD and CSA, are not independent but cause interfering relaxation and this interference can be destructive or constructive. The mode of interference is dependent on the spin state of spin *I* resulting in two lines of spin S with different widths and vice versa. Thus, in a two-state spin system four signals can be observed. In conventional HSQC spectra the two lines are usually collapsed by decoupling resulting in a line whose width is the average of the two lines of the doublet in each dimension. TROSY on the other hand retains the peak splitting due to heteronuclear coupling and selects for the slowest relaxation properties (destructive interference) for both nuclei. This TROSY effect is especially pronounced for the ^{1}H-^{15}N pair in large molecules at high fields (>700 MHz) since the CSA relaxation increases with higher magnetic field strength for both nuclei, ^{1}H and ^{15}N. The optimal TROSY effect can be obtained at field strengths of 23.5 T corresponding to a frequency of 1 GHz. The TROSY experimental pulse sequence resembles the HSQC pulse sequence but differs in three important aspects:

(i) The 180° pulse to the I spin in the middle of t_1 is removed therefore the spin state of the proton is not inverted during this period. The magnetization follows either the 1-2 or 3-4 transition and both transitions do not mix.

(ii) During t_2 evolution period there is no nitrogen decoupling implemented thus the spin state of nitrogen does not get inverted during acquisition. The proton magnetization still follows 1-3 or 2-4 transition.

(iii) The phase cycle is designed in a way that only one single coherence path is kept, namely 3-4 during t_1 and 2-4 during t_2. The signals from the other three paths are cancelled out.

At the end of the sequence the magnetization is back on *I*, where it is observed.

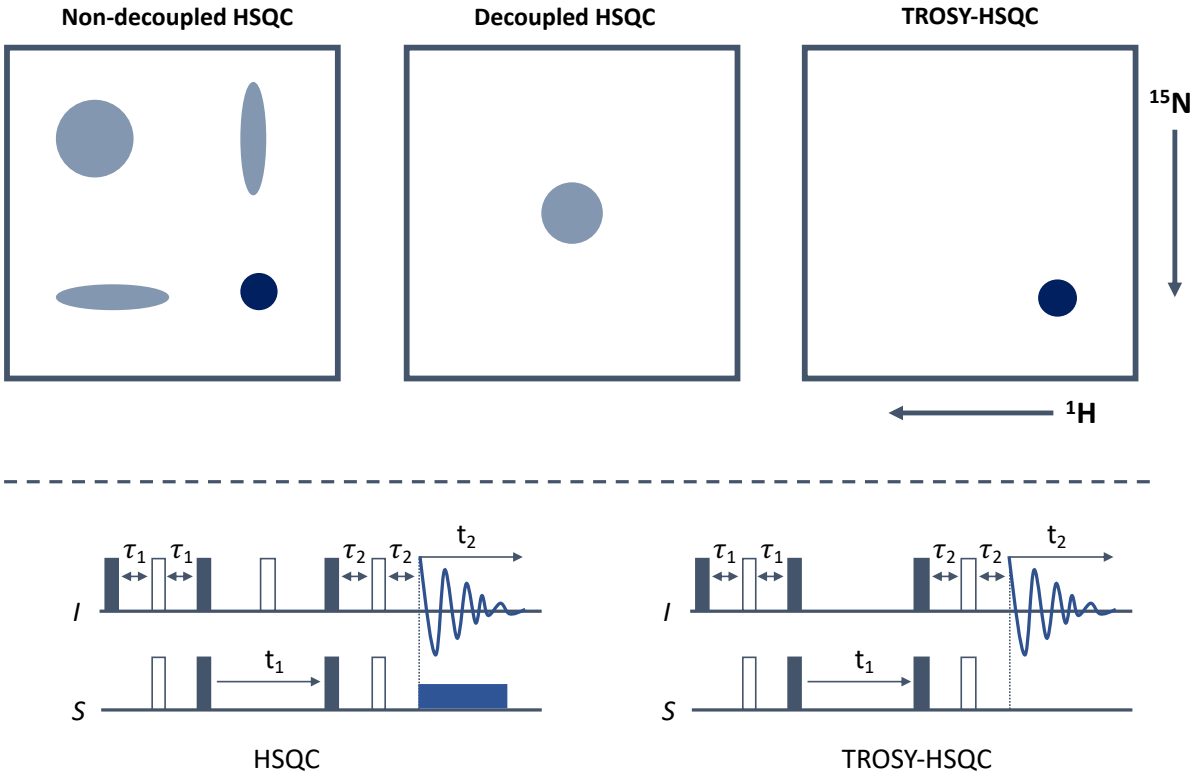

Figure 9: Representation of the TROSY effect. TROSY is a modified HSQC pulse sequence leading to selection of the slow relaxing component (sharpest line) in every dimension. This effect is especially important for larger proteins at high frequencies. After reference [139]

3.2.17.2 NMR structure determination

Sequence-specific resonance assignment is the first step in the protocol for protein structure determination by NMR spectroscopy[140]. Implementation of TROSY in triple resonance experiments results in several-fold improved sensitivity for U-^{2}H, ^{13}C, ^{15}N-labeled protein samples. These experiments include long delays during which ^{13}C and ^{15}N magnetization evolves in the transverse plane. Fast transverse relaxation during these delays and during ^{1}H acquisition limits the application of triple-resonance experiments to larger molecule and thus

benefits from the TROSY effect by minimizing transverse relaxation of ^{15}N during evolution and of ^{1}HN during detection, respectively. The HNCA experiment was one of the earliest 3D experiments modified using the TROSY principle. The magnetization in the HNCA experiment is transferred from the ^{1}H to ^{15}N and then via N-Cα J-coupling to the $^{13}Cα$ and then back again to ^{15}N and ^{1}H for detection. The amide nitrogen is coupled to the Cα of its own residue as well as to the Cα of the preceding one which is why both Cαs are visible in the spectrum. Due to stronger coupling to the directly bonded Cα this peak is the more intensive one. Thus, the HNCA experiment alone already makes a sequential assignment possible however, other 3D experiments might help to either confirm or complement the assignment.

In addition, nuclear overhauser effect spectroscopy (NOESY) gives rise to homonuclear 1H-1H NOEs along the heteronuclear dimension which yields in distant restraints crucial for structure calculations.

For obtaining backbone resonance assignments and NOE distance restraints, TROSY-based 3D-triple resonance experiments[141] and a 3D-^{15}N-edited-[^{1}H,^{1}H]-NOESY experiment were recorded in a non-uniform-sampled (NUS) manner[142]. Non-uniform sampling allows for experimental time reduction by omitting a significant part of the data acquired by reducing the number of points recorded in every indirect dimension. The time-domain data will be collected at non-fixed intervals and schedules were prepared using Poisson-gap sampling[143]. Poisson gap sampling shows a low probability of creating large gaps between the sampled points which is favored regarding reconstruction of the data set. Mathematical reconstruction of NUS data is necessary since some of the data is skipped and Fourier transformation (FT) is not ideal anymore. 3D-NUS spectra were reconstructed using the iterative soft threshold (IST) method[144]. The IST reconstruction procedure begins with FT of a sparse data set where according to the Poisson gap sampling schedule not measured grid points are set to zero. The resulting frequency domain spectrum contains noise-like artifacts which are however, caused by the non-uniform sampling schedule. The tallest peak identified is chosen to select a threshold

whose value is slightly below the maximum of this peak. All data above this threshold value are moved to a second spectrum. The remaining spectrum with the tallest signal truncated is now reverse Fourier transformed into the time-domain spectrum. This cycle is iterated until the remaining spectrum is basically empty. Processing of the reconstructed spectrum is done using NMRPipe[145]. Spectral analysis was done with SPARKY4 (Goddard and Kneller, UCSF) and NMRFAM-SPARKY[138]. Backbone angles for structure calculations were predicted from chemical shift information using the program TALOS+[146] and verified by specific NOE contacts. Structure calculations were done with Xplor-NIH[147] using standard protocols. The 20 structures with the lowest total energies were used to obtain structural statistics of the ensemble. Ramachandran map analysis was performed with the RAMPAGE webserver[148].

3.2.17.3 Paramagnetic relaxation enhancement (PRE) experiments

Paramagnetic relaxation enhancement (PRE) experiments were performed in order to determine the location of the TM domains within the DPC detergent micelle. Therefore, the free radical compound 16-doxyl-stearic acid (16-DSA) was used. Protein regions that are located inside the micelle and therefore in close contact to the radical experience line broadening, which in turn can be monitored by a signal decrease. Recovery of the signal intensity by quenching the radical with ascorbic acid makes it possible to calculate the intensity ratio of the protein signals in a reduced (radical quenched) and oxidized (radical active) state and plot it against the residue number.

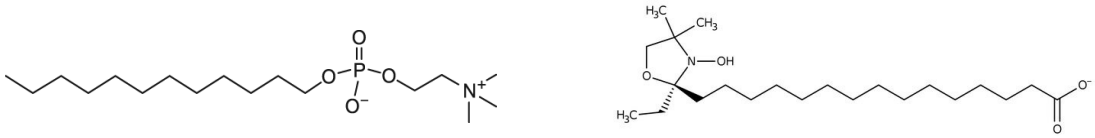

Figure 10: Chemical structures of DPC (Fos-Cholin-12) and paramagnetic label 16-doxyl stearic acid (16-DSA)

Purified and ^{2}H, ^{15}N-labeled TREM2-TM and K186A protein samples in 20 mM NaPi, 50 mM NaCl, 0.5 mM EDTA, 200 mM DPC were mixed with the paramagnetic label 16-doxyl stearic acid (16-DSA) dissolved in the same buffer. The final 16-DSA concentration was 4 mM which results in approximately one 16-DSA molecule per DPC micelle (DPC aggregation number:

~50). The resulting ratio of protein to 16-DSA was 1:4. 2D-[^{1}H,^{15}N]-TROSY spectra were recorded with a recycle delay of 2 seconds with 96 complex points in the indirect ^{15}N dimension and 32 scans per increment. The free radical in the spin labeled fatty acid leads to distance-dependent line broadening of the amide resonances in the protein. The same experimental parameters were used for a reference experiment after the addition of 40 mM ascorbic acid (from a 1M stock in 20 mM NaPi, pH 6.5, 50 mM NaCl and 0.5 mM EDTA), which is quenching the free radical in the spin label. Signal intensity ratios of the amide resonances in the corresponding spectra can be calculated using the individual peak height values in the oxidized case (I_{ox}), i.e. containing a radical, and the reduced spectrum (I_{red}), i.e. after reduction of the free radical by ascorbic acid. The resulting values range between 0 and 1 indicating either close or no proximity to the spin labeled fatty acid hydrocarbon chain, respectively.

3.2.17.4 Investigation of protein backbone dynamics

Protein dynamics is an important factor relating to protein structure, stability and function[149]. NMR dynamic investigations probe site-specific motions by measuring transverse (T_2) and longitudinal relaxation (T_1) rates and heteronuclear NOE. These experiments measure protein motions on the nano- to picosecond timescale and provide useful information of the internal dynamics of the protein. To determine the site-specific fast motion of the protein backbone, more specifically the ^{15}N dynamics of the ^{1}H-^{15}N bond[150,151], T_1, T_2 and $\{^{1}H\}$, ^{15}N - heteronuclear NOE were extracted by measuring the peak intensities in a series of 2D-[^{1}H, ^{15}N]-TROSY spectra as a function of varying relaxation delay.

T_1 and T_2 relaxation rates as well as $\{^{1}H\}$-^{15}N-heteronuclear NOEs have been recorded in a fully interleaved manner at two magnetic field strengths (600 and 950 MHz proton frequency). For T_1 rates, 14 relaxation delays ranging from 100 ms to 1.8 s have been used, including three duplicates for error estimation. For the determination of T_2 rates 14 delays ranging from 16 to 192 ms were used. Heteronuclear NOE was measured with and without proton saturation (2s saturation time). For all 2D spectra, 1024 and 96 complex points in the ^{1}H and the ^{15}N

dimension were recorded, respectively. Order parameters of TREM2-TM have been obtained with the software Relax[152-154] in fully automated fitting mode using relaxation data at two static magnetic fields.

3.2.17.5 Saturation Transfer Difference (STD) - NMR

STD-NMR is a simple and fast ligand-based NMR method to monitor binding to a protein[155]. Ligand screening and characterization of ligand binding can be performed without the need for isotopically labelled receptor protein since this method is focusing on the ligand signals only. It is based on the Nuclear-Overhauser effect (NOE) and the observation of ligand proton resonances. In principle, two spectra are recorded: the off-resonance spectrum (I_0) and the on-resonance spectrum (I_{sat}). Subtracting the off-resonance from the on-resonance spectrum (I_0-I_{sat}) will give rise to the difference or STD spectrum (Figure 11).

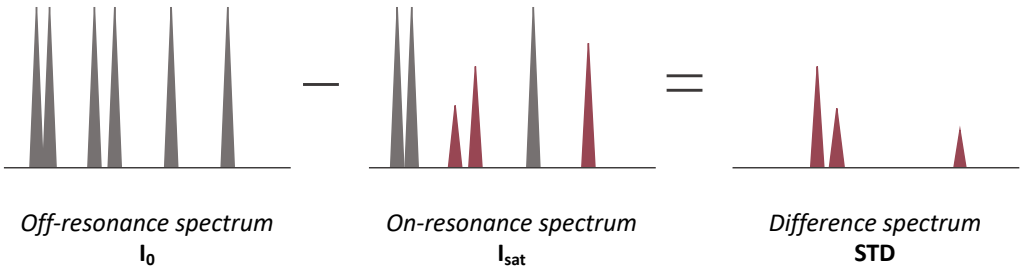

Figure 11: Mechanistic model of Saturation Transfer Difference (STD) – NMR. The off-resonance spectrum is recorded at a frequency set far away from any protein signal. The on-resonance spectrum is obtained via selective saturation of the protein which leads to decreased ligand signals through magnetization transfer. The corresponding STD spectrum shows solely the former bound ligand signals. After Viegas A. et al., J Chem Educ (2011)

The off-resonance spectrum is the reference spectrum recorded at an irradiation frequency set far away from any protein or ligand signal. The second spectrum is recorded at a selective frequency for the protein signal. Spin diffusion causes saturation of the protein via intra-molecular NOEs which are transferred to a bound ligand via inter-molecular NOEs. Fast exchange of the ligand causes accumulation of saturated ligand molecules in the solution during saturation time of the experiment since T1 relaxation (relaxation rate R1=1/T1) of fast tumbling small molecules is smaller than the kinetic exchange rate (k_{ex} >> R1). The signal of the saturated ligand will decrease, and this can be detected in the on-resonance spectrum. By subtracting the on-resonance spectrum from the off-resonance spectrum only the signals originating from those

parts of the ligand that are in contact with the protein will be visible with intensities of each proton that reflect the former proximity of the ligand to the protein. All other ligand signals are cancelled out since the two spectra don't differ.

3.2.18 NMR data driven docking

Docking of the complex between TREM2-TM and DAP12 was done with the HADDOCK2.2 webserver[156] using the herein determined structure of TREM2-TM in its complex with DAP12 and the structure of DAP12 in complex with the transmembrane helical region of NKG2C[18]. The core residues, in particular D50, that form the complex interface within DAP12 with NKG2C were defined as active (monomer1: V47, D50, T54, A58, V61; monomer2: V42, L43, I46, G49, L53, I57, A60), whereas surface neighbors were defined as inactive residues. For TREM2-TMH, the residues that showed large chemical shift perturbations in the NMR titration with unlabeled DAP12 were defined as active, and in particular the charged K186 residue (L176, L179, A180, F183, K186, I187, A189, A190, S191, L193, W194, A195, A197). After the calculations, the obtained structural clusters were selected based on the correct orientation of the binding partners and the overall docking score.

The generation of the structural model of the complex between γ-secretase and TREM2-TM was done by using the γ-secretase-Notch cryo-EM structure[57] as a template and by replacing the amino acid sequence of Notch by the TREM2 sequence in the program Chimera[157]. The exact position of the TREM2-TM sequence in the binding groove of γ-secretase was defined with the experimentally determined cleavage site for the wild-type and the K186A case.

4 RESULTS

4.1 Biophysical studies on TREM2 transmembrane domain

4.1.1 Expression and purification of TREM2-TM and DAP12-TM in DPC

All transmembrane domains, namely TREM2-TM WT, K186A and DAP12-TM show clearly visible expression bands as exemplified here for TREM2-TM WT expression analysis of whole cell lysates (Figure 12, (a)). Application of detergent solubilized whole cell lysate to Nickel affinity chromatography leads to intense protein bands in the elution fraction (Figure 12, (b, c)) and subsequent size exclusion chromatography (S200p) results in highly pure GB1-fusion proteins (Figure 12, (d, e)). Thrombin cleavage was complete after overnight incubation at room temperature.

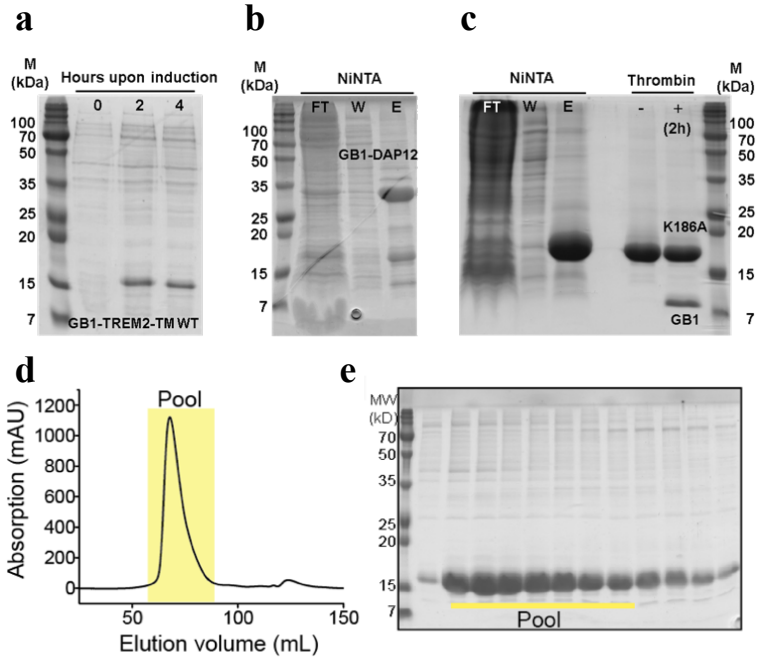

Figure 12: Expression and purification of TM constructs. (a) Expression test in *E. coli* BL21 (DE3) cells exemplified for TREM2-TM WT. Appearance of a 15 kDa band after 2 hours of expression proves successful expression (b) NiNTA affinity chromatography exemplified for GB1-DAP12_C33S. (c) NiNTA and start of Thrombin cleavage of K186A. Thrombin cleavage was performed overnight to yield complete digest (d) Size exclusion chromatogram (S200p) of TREM2TM WT in 0.1% DPC (e) SDS-PAGE analysis of SEC peak fractions. The yellow box in the SEC chromatogram and the line below the respective fractions indicates the pooled fractions.

4.1.2 Determination of the oligomeric state of TREM2-TM WT / K186A

Investigation of the oligomeric state in lipid Nanodiscs was performed as described in section 3.2.14. Figure 13, (a) shows the S200a size exclusion chromatogram of loaded nanodiscs before and after thrombin digest. The corresponding SDS Page analysis (Figure 13, (b)) demonstrates clearly that MSP1D1ΔH5 and GB1-TREM2-TM elute in the same S200a peak fractions and that consecutive thrombin digest was complete, shown by the disappearance of the GB1-TREM2-TM band and appearance of a clear GB1 band. The helix itself is too small and cannot be detected. Calculation of the apparent oligomeric behavior yielded 1.7 WT-helices/Nanodisc (Figure 13, (c)) and 2.3 K186A-helices/Nanodiscs (Figure 13, (d)) suggesting that even with a 2 times excess Nanodiscs WT adopts rather a dimeric conformation while K186A seems to form higher oligomers in agreement with the tendency of Alzheimer's disease-related K186N variant to accumulate in the membrane[88].

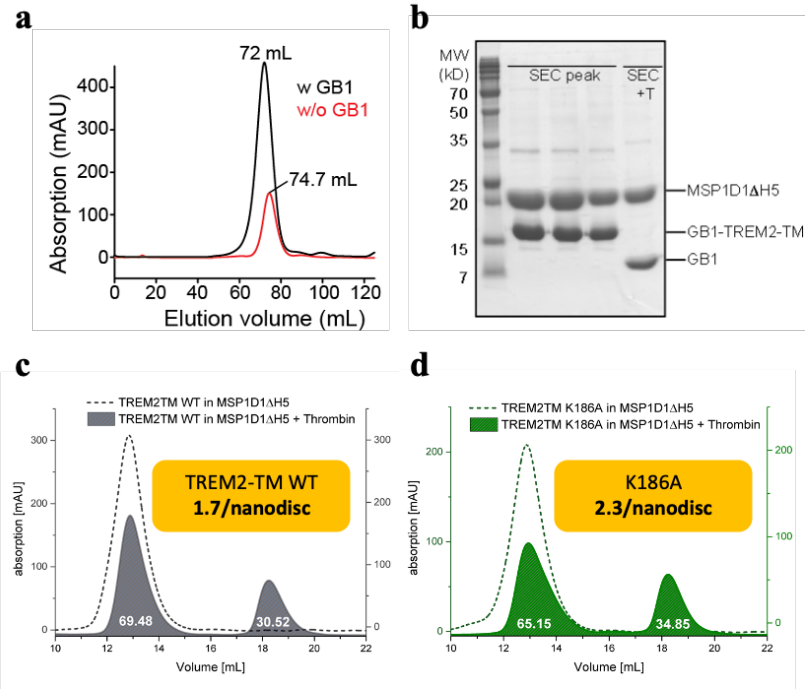

Figure 13: Determination of the oligomeric state of TREM2TM WT and K186A in Nanodiscs. (a) Size exclusion profile of loaded Nanodiscs before and after Thrombin digest. (b) SDS PAGE analysis of loaded Nanodiscs and consecutive Thrombin digest. (c,d) Size exclusion profiles for determination of the oligomeric state; Indicated is the calculated ratio of helices per nanodisc (orange square)

4.1.3 NMR structure determination of TREM2-TM WT

Backbone resonance assignments for U-^{2}H, ^{13}C, ^{15}N, -labeled TREM2-TM WT (aa 161-206) was obtained in 200mM DPC for 88% of all on-proline residues (Figure 14, (a)). The content of secondary structure was estimated using ^{13}Cα and ^{13}Cβ chemical shifts and yielded an α-helix ranging from S174 to W198 (Figure 14, (c)). Compared to the Uniprot annotation (Entry: Q9NZC2) of an TREM2-TM segment ranging from I175 to A195 the α-helical content structurally determined here is longer. Helical content of approximately 55% is in nice agreement with the results obtained by CD spectroscopy of 57% helical structure of

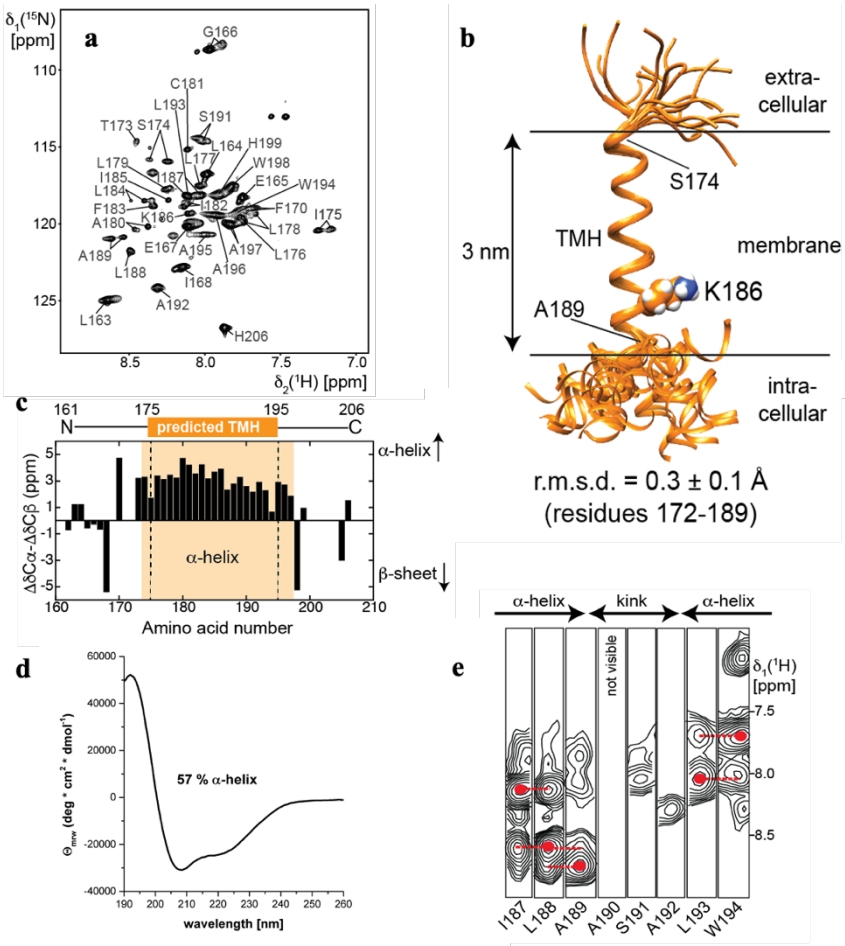

Figure 14: Solution NMR structure of wild-type TREM2-TM in DPC micelles. (a) 2D-[^{1}H, ^{15}N]-TROSY spectrum of ^{2}H,^{13}C,^{15}N-labeled TREM2-TM at 37 °C. Assigned resonances are labeled. (b) Final NMR-derived structural bundle of the 20 lowest-energy structures of TREM2 shows that the C-terminal end of the transmembrane helix can adopt various positions relative to the well-defined TMH. (c) Secondary chemical shifts plotted against the residue number indicates an α-helical region between residues 174 and 197. The used TREM2-TM construct along with the predicted transmembrane helix content (aa 175-195) is also indicated. (d) Circular dichroism (CD) spectrum of TREM2-TM in DPC micelles indicates an α-helical secondary structure content of ~57%. (e) 3D-^{15}N-edited NOESY spectra show that the transmembrane helix is interrupted at residues 190-192. Dashed red lines indicate sequential amide NOE contacts that are characteristic for an α-helical secondary structure.

TREM2-TM (Figure 14 (d)). However, evaluation of the magnitude of $^{13}C\alpha$ and $^{13}C\beta$ chemical shifts showed that the C-terminal part of TREM2-TM demonstrates a lower α-helical propensity, therefore the 3-dimensional structure was determined (Figure 14, (b)) and intrahelical contacts surveyed using NOE-based NMR spectroscopy (Figure 14, (e)). The typical pattern of cross-peaks that arise from neighboring amide protons breaks between residues A189 and L193 confirming a lack of secondary structure and enhanced dynamics. This unstructured kink region leads to a variable orientation of the short C-terminal helix stretch with respect to the N-terminal α-helix.

To exclude a structural effect of the small spherical detergent micelle, TREM2TM was inserted into di-myristoyl-glycero-phosphocholine/di-myristoyl-glycero-phosphoglycerol (DMPC/PG, 3:1) phospholipid nanodiscs assembled with MSP1D1ΔH5 and the resonances assigned in a planar lipid environment (Figure 15, (a)). Comparison of 2D-[^{1}H,^{15}N]-TROSY spectra of TREM2TM WT in DPC and DMPC/PG nanodiscs just showed minor differences most likely due to slight changes in the electronic environment of DPC micelle compared to lipid nanodiscs. The structure determined in this planar lipid bilayer environment shows the same secondary α-helical content and missing NOE contacts between A189 and L193 Figure 15, (b, c)).

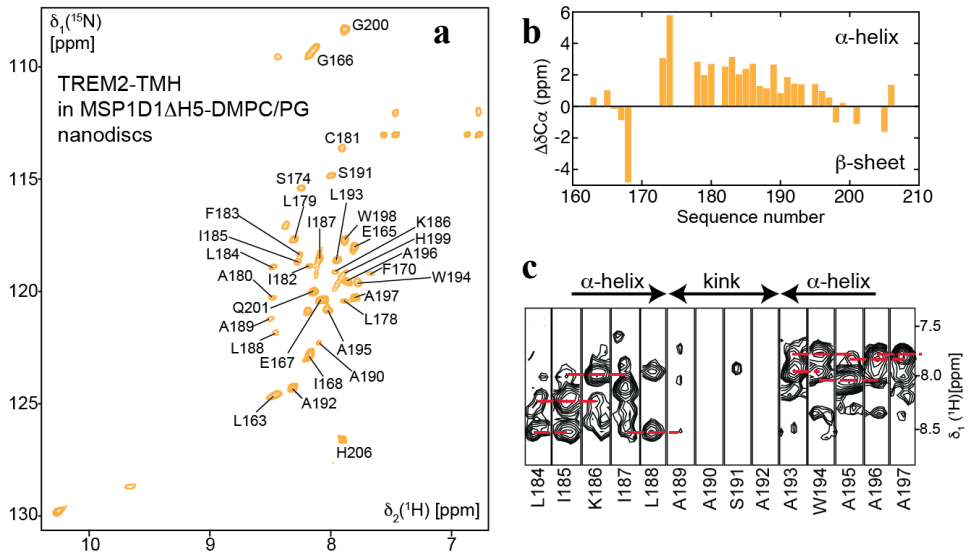

Figure 15: (a) NMR resonance assignment of TREM2 TM WT in MSP1D1ΔH5-DMPC/PG nanodiscs (b) secondary structure analysis using $^{13}C\alpha$ and $^{13}C\beta$ chemical shifts. (c) NOESY analysis of intra-helical backbone contacts.

4.1.4 Structural analyses of K186A and DAP12-bound TREM2-TM WT

Based on the assumption that lysine 186 is a key factor that determines the structure and dynamics of TREM2-TM WT due to its unfavored location in the hydrophobic lipid environment, structural effects by either charge removal (K186A) or complex formation with adaptor protein DAP12 was investigated using NMR spectroscopy.

Complex formation with DAP12 leads to a markedly altered 2D-TROSY spectrum of TREM2-TM especially in its C-terminal end including the unstructured kink region (Figure 16, (b, upper panel)). Determination of the solution structure of isotopically labelled TREM2-TM in complex with DAP12 resulted in a continuous α-helix ranging from S174 to W198 without unstructured

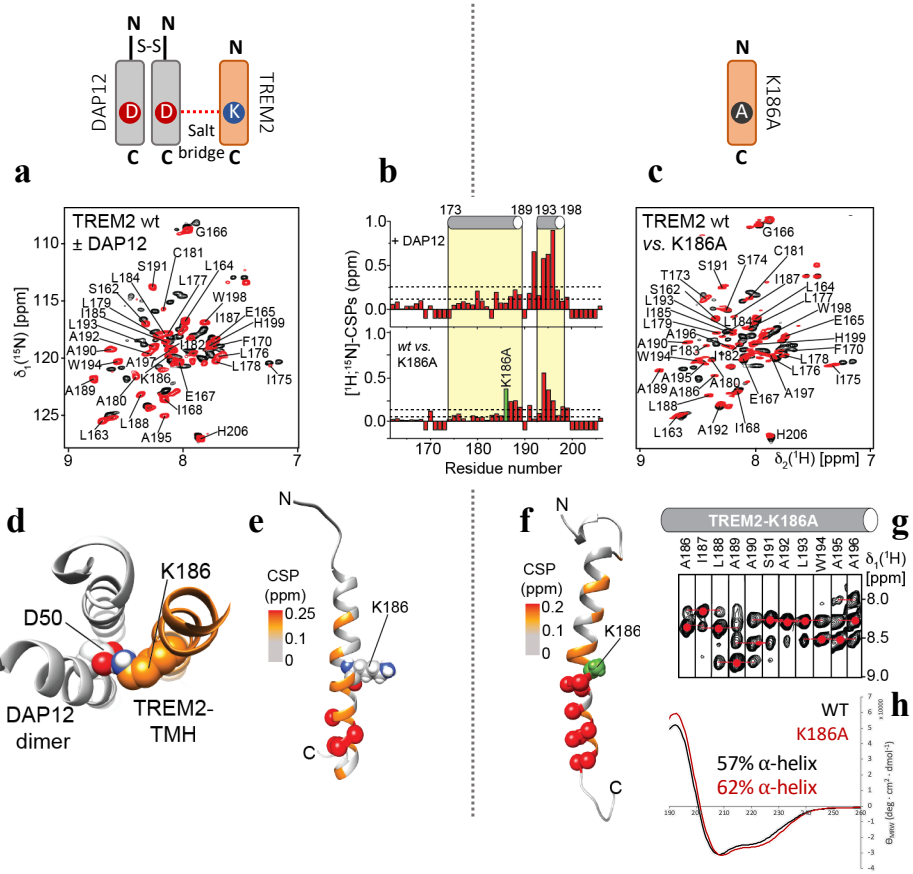

Figure 16: Overlay of 2D-[^{1}H,^{15}N]-TROSY spectra of ^{2}H,^{15}N-labeled TREM2-TMH in DPC micelles (black) and in complex with (a) unlabeled DAP12 (red) or (c) TREM2-TMH lacking its positively charged lysine residue (K186A, red). (b) Chemical shift perturbations (CSP) between the two spectra in panels (a) or (c). (e) NOE-derived lowest-energy structure of TREM2-TMH in complex with disulfide-bridged dimeric DAP12 shows one continuous α-helix. (d) The experimental structure of TREM2-TMH was docked to a previously determined structure of DAP12 in complex with NKG2C [18]. The positive charge in K186 is engaged in a salt bridge with D50 of DAP12. (f) Removal of the positive charge (K186A) leads to a very similar structure of the TREM2-TMH as in its complex with DAP12. The CSP values color coded onto the NOE-derived structures in each case (g) A continuous α-helical secondary structure in the kink region (aa 189-192) was probed by sequential amide NOE contacts in TREM2-K186A-TMH. Red dots indicate the chemical shift of intra-residual (i) amide resonance and red broken lines the inter-residual connectivity (i±1). (h) For TREM2-K186A-TMH a ~5% increase in α-helical secondary structure can be detected by CD spectroscopy.

kink region (Figure 16, (e)). Based on the solution-NMR complex structure of DAP12 with NKG2C[18] a structural model of TREM2-TM in complex with DAP12 was obtained using NMR-data driven docking calculations in the HADDOCK webserver[156] (Figure 16, (d)). Visualization of the complex structure with the best HADDOCK Score and the correct parallel orientation of the two proteins demonstrates the salt bridge between K186 (TREM2-TM) and D50 (DAP12) and therefore the helix stabilization via charge neutralization.

Considering the significance of lysine 186, the next logical step was the design of a charge mutant, namely K186A, that might serve as a mimic for the neutralized DAP12-bound state. In fact, spectral comparison of wild-type TREM2-TM with K186A and in complex with DAP12, respectively, displayed nearly identical chemical shift perturbation pattern throughout the protein sequence (Figure 16, (b, lower panel)). NOE-based structure determination of K186A demonstrates a continuous α-helix ranging again from S174 to W198 (Figure 16, (g, f)). In agreement with a stabilized and therefore extended α-helix, CD spectroscopy shows a higher helical content of K186A compared to wild-type protein (Figure 16, (h)). Addition of wild-type DAP12 to K186A charge variant did not lead to chemical shift changes in the $^{1}H,^{15}N$-TROSY spectrum (Figure 17, (c)) similar to addition of DAP12 D50A charge variant to TREM2-TM WT (Figure 17, (b)) confirming the crucial interaction of lysine K186 and D50 for complex formation.

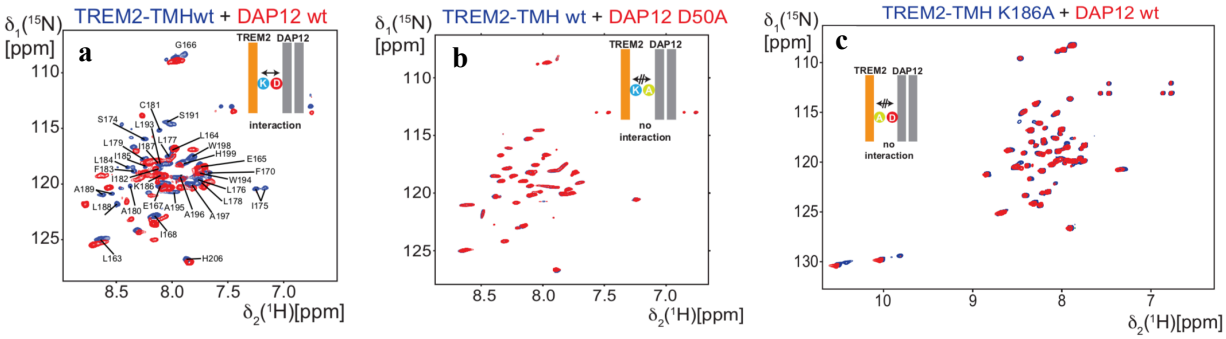

Figure 17: $^{1}H,^{15}N$-TROSYspectral overlays of (a) TREM2-TM WT and wild-type DAP12, (b) TREM2-TM WT and DAP12 charge variant (D50A) and (c) K186A variant and wild-type DAP12. Removal of either lysine 186 (TREM2) or aspartate 50 (DAP12) leads to disruption of complex assembly.

4.1.5 NMR studies and molecular dynamics simulations on TM-Helix flexibility

Conformational flexibility which is a key parameter in substrate recognition in intramembrane proteolysis was investigated in the nanosecond to picosecond timescale for TREM2-TM WT and K186A. T_1, T_2 and $\{^1H\},^{15}N$-heteronuclear NOE experiments were therefore recorded at 600MHz and 950MHz proton frequencies, respectively. The resulting generalized order parameter S^2 ranges from 0 to 1 indicating unrestricted (0) or completely rigid dynamics (1). The pattern of S^2 values obtained for both constructs is in nice agreement with the different structures, respectively. TREM2-TM WT displays S^2 values of around 0.9 for the structured first half of the helix, values of approximately 0.6 for the unstructured kink region and 0.7 for the C-terminal helix (Figure 18, (a)). Thus, the N-terminal helix is highly rigid, whereas the kink region shows increased flexibility and the C-terminal helix slightly increased rigidity again. In contrast to the wild-type pattern, K186A shows an order parameter of ~0.9 (Figure 18, (b)), meaning high rigidity, along its structured part (174-195) which fits nicely to the experimentally determined continuous α-helix.

To gain more insights into the molecular mechanism, molecular dynamics simulations of TREM2-TM WT and K186A inserted into a POPC/PG lipid bilayer system were performed with a starting structure of a linear helix geometry taken from the calculated NMR ensemble, respectively. The simulation indicates that the lysine 186 side-chain is attracted by the phosphate moieties of the phospholipid headgroup region which results in a tilted geometry of the helix with respect to the membrane axis (Figure 18, (c)). The kink in the structure is therefore due to the electrostatic attraction of lysine 186 and the phosphate groups pushing the C-terminal helix outside the membrane which finally forces the kinked structure. In the timeframe of the simulation however, the kink was not observed since longer simulation times would have been needed. But MD simulations provided useful information about the initial contact formation between K186 and lipid headgroups which would finally result in the experimentally determined kink for TREM2-TM WT. Due to removal of the charge, the MD

trajectory for K186A shows juts minor tilting (Figure 18, (d)). The K186A helix is stably inserted in the membrane.

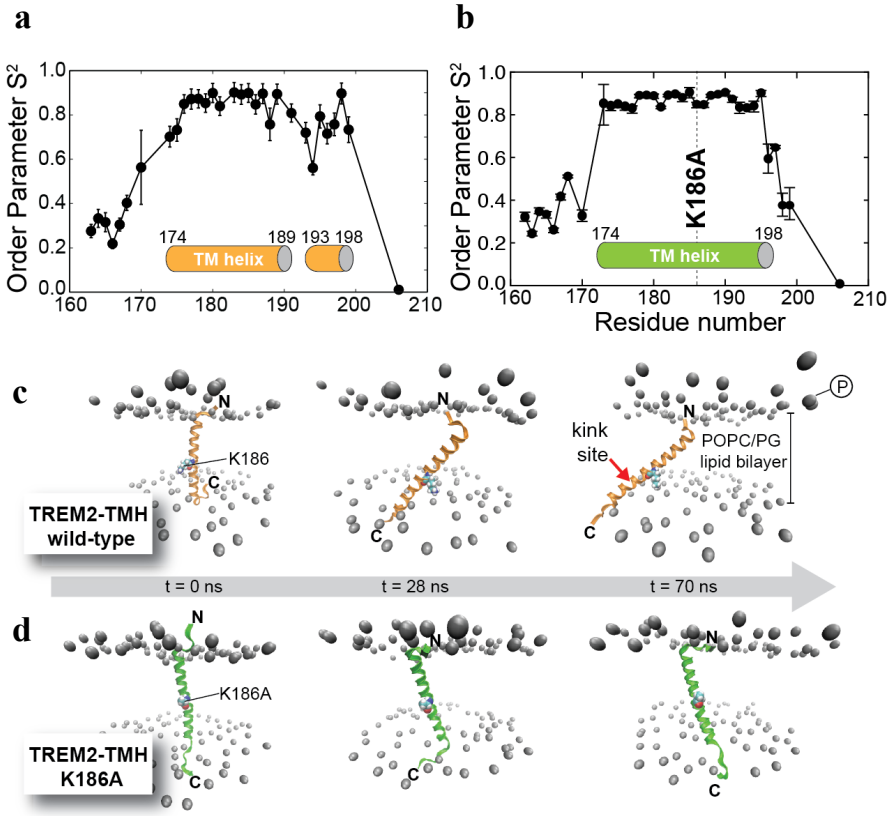

Figure 18: Dynamics of TREM2-TM and K186A variant (a,b) Generalized order parameter S^2 for backbone amide resonances derived from NMR relaxation experiments with wild-type TREM2-TM (a) and the K186A variant (b), indicative of motions in the nanosecond to picosecond time scale. S^2 can adopt values between 1 (rigid) and 0 (unrestricted motion). (c,d) Molecular dynamics simulations of TREM2-TM wt (c) and K186A (d) in a POPC/POPG (3:1) bilayer provide information on the stability of helix insertion into a lipid bilayer membrane.

Since molecular dynamics simulations were performed in a POPC/PG bilayer system, a possible influence of membrane thickness on TREM2-TM WT structure was experimentally investigated by NMR. Therefore, nanodiscs were assembled with palmitoyl-oleyl-glycero-phosphocholine/palmitoyl-oleyl-glycero-phosphoglycerol (POPC/PG, 3:1) thus increasing the thickness of the membrane compared to DMPC/PG. Spectral comparison of 2D-[^{1}H,^{15}N]-TROSY spectra of wild-type TREM2-TM in DPC and DMPC/PG (Figure 19, (a)) and DMPC/PG and POPC/PG (Figure 19, (b)) are almost identical demonstrated by small CSPs (Figure 19, (c, d)), proving that TREM2-TM structure in DPC micelles already presents the

biologically active conformation and transfer to a planar lipid bilayer or increasing the membrane thickness does not alter the experimentally determined structure in DPC.

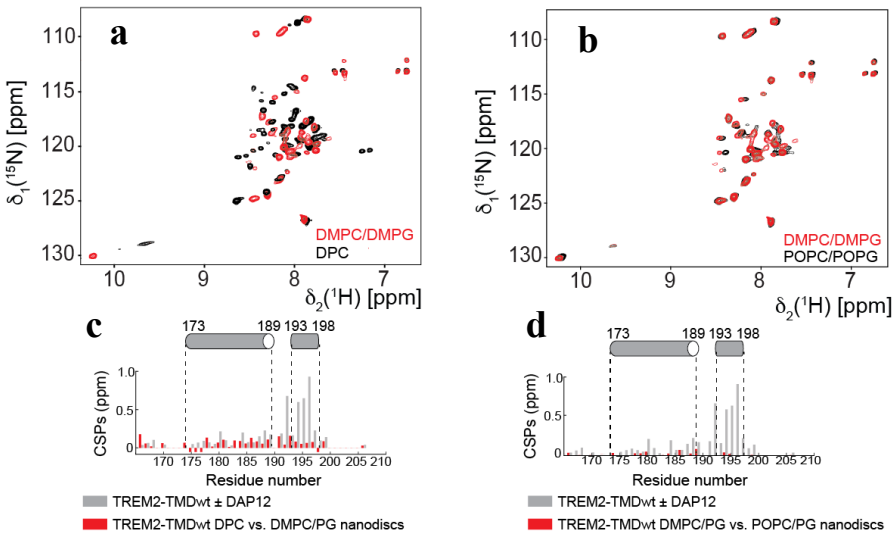

Figure 19: TREM2-TMH in different membrane mimetics. (a,b) $^{1}H,^{15}N$-TROSY spectral comparisons of (a) TREM2-TMH in DPC vs. DMPC/PG nanodiscs and (b) TREM2-TMH in DMPC/PG vs. POPC/PG nanodiscs. (c,d) Chemical shift perturbation analysis of the respective membrane mimetic (red) in comparison with pronounced CSPs caused by addition of binding partner DAP12 (grey)

4.1.6 Positioning of TREM2-TM in the membrane

4.1.6.1 PRE experiments and NOE analysis in a DPC micelle environment

Paramagnetic relaxation experiments (PRE) were performed in order to experimentally prove that the C-terminal helix of TREM2-TM is indeed located outside of the hydrophobic membrane region. Insertion of the paramagnetic label 16-doxylstearic acid (16-DSA) in the DPC detergent micelle leads to a signal intensity decrease which is pronounced for close by residues. The signal can be recovered by radical quenching using ascorbic acid. TREM2-TM WT shows markedly reduced intensity ratio for the transmembrane region (174-189) but values increase for the kink region and the C-terminal helix suggesting that while the N-terminal helix lies within the micelle, the unstructured kink region and the C-terminal helix are located outside of the hydrophobic environment (Figure 20, (a, orange)). By contrast to the wild-type results and in line with previous results, the K186A helix is stably inserted demonstrated by an overall

increased intensity ratio for the entire helical structure (173-196) (Figure 20, (a, green)). A graphical representation of results obtained by PRE experiments is shown in Figure 20, (b).

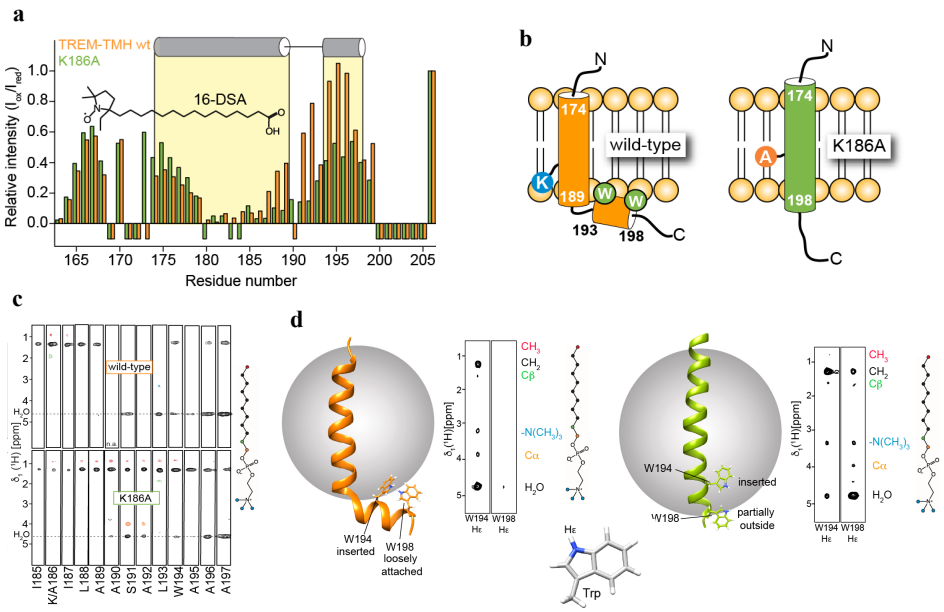

Figure 20: Membrane positioning of TREM2-TM WT and the K186A variant. (a) Paramagnetic relaxation enhancement (PRE) with a free-radical-modified stearic fatty acid in DPC micelles. Low values indicate location inside whereas values close to one suggest a location outside the detergent micelle. Orange bars: TREM2-TM WT, green bars: K186A variant. The N-terminal residues of TREM2-TMH-wt are located deeper inside the micelles as in the K186A case, whereas the C-terminal end is positioned at the outside for wild-type and inside for the K186A variant. Negative bars indicate missing assignments. (b) Model representation of membrane location according to PRE-data analysis. (c) NOE-cross peaks between backbone amides of TREM2-TM WT (top) or the K186A variant (bottom) and selected regions of DPC (see color coding of the structure of the DPC molecule on the right). The K186A variant shows strong contacts to the hydrophobic aliphatic regions of the detergent throughout the transmembrane helix whereas no such contacts can be seen at the kink site of the wild-type helix, indicating a location outside of the micelle for this part. (d) Model of the position of TREM2-TM WT and K186A within the membrane. The amino acids in the kink region are exposed to the solvent in the wild-type case but buried in the membrane for the K186A variant.

In order to confirm these results, NOE contacts of backbone amide resonances to selected regions of the DPC molecule were analyzed (Figure 20, (c)). The N-terminal helix of the wild-type protein shows NOE contacts to the hydrocarbon region of DPC, whereas these contacts are missing in the kink region and can just faintly be seen for the C-terminal helix. Additionally, residues in the kink region display pronounced water exchange peaks, indicating solvent accessibility and reduced hydrogen bonding in this area. K186A demonstrates a continuous NOE contact pattern to methyl and methylene groups for the entire transmembrane helix. For visualization purposes a model of membrane positioning of both proteins was constructed on the basis of results obtained from PRE and NOE contact analyses (Figure 20, (d)). Wild-type TREM2-TM contains a transmembrane region (174-189), followed by a solvent accessible kink

region and a C-terminal α-helical stretch on the surface of the membrane. Two tryptophan residues (W194 and W198) are located on the same side of the C-terminal helix and serve as anchors for surface attachment. K186A helix is completely inserted with both tryptophan side-chains buried within the micelle.

4.1.6.2 NOE analysis in lipid nanodiscs

In order to confirm the results obtained in a DPC micelle environment, membrane positioning of wild-type TREM2-TM was further investigated in lipid nanodiscs by analysis of NOE contacts of backbone amide resonances to selected regions of DMPC/PG lipid molecules (Figure 21, (a, b)). In nice agreement with the previously described membrane location, TREM2-TM displays faint contacts for the kink region followed by upcoming contacts to the lipid headgroup region of the C-terminal helix stretch. In addition, water exchange signals can be seen for this region confirming a location of the C-terminal helix on the membrane surface. Figure 21, (c) shows the model of TREM2-TM in lipid bilayer constructed based on NOE analysis.

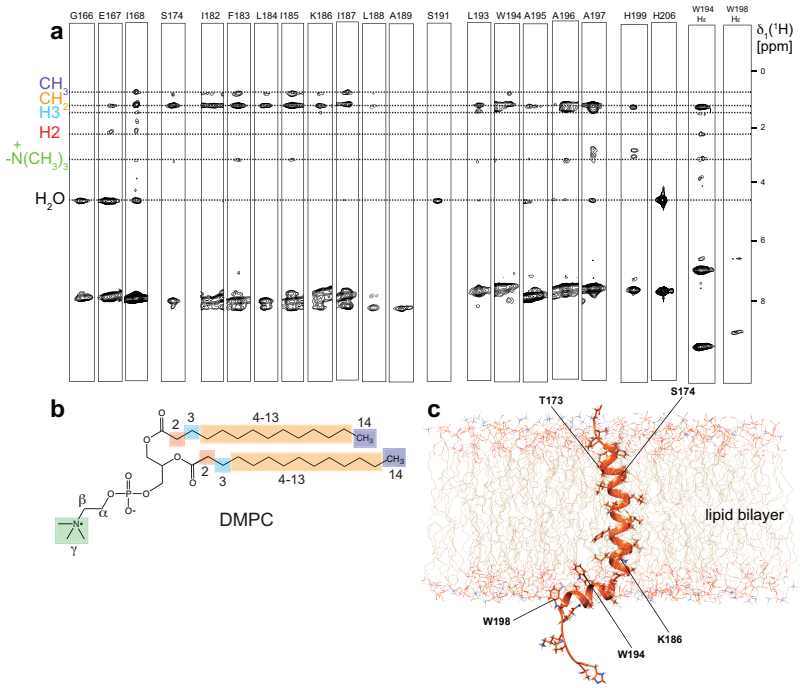

Figure 21: NOE analysis of TREM2-TM in lipid nanodiscs. (a) NOE pattern of TREM2-TM to selected regions of the DMPC lipid molecule. (b) Chemical structure of DMPC molecule with indicated moieties used for contact analysis. (c) Graphical representation of the NOE analysis. TREM2-TM N-terminal helix lies within the hydrophobic bilayer while the kink region and the succeeding C-terminal helix stretch show interaction with the lipid headgroup region.

4.1.6.3 Hydrogen deuterium exchange (HDX) in DPC and nanodiscs

Hydrogen deuterium exchange was measured in order to complement NOE-derived contacts to H_2O/DPC and H_2O/DMPC/PG, respectively. Reference spectra of TREM2-TM WT in DPC micelles and nanodiscs as well as K186A in micelles were therefore recorded, exchanged to D_2O and immediately recorded again. Rapid exchange of ^1H to ^2H leads to signal loss which was analyzed by ^1H,^{15}N-TROSY spectral comparison. In agreement with PRE and NOE results, wild-type TREM2-TM shows a higher accessibility to water especially at its C-terminus which is being pushed out mediated by the interaction of lysine 186 and phospholipid headgroups. This effect is similarly pronounced for TREM2-TM WT in DPC and lipid nanodiscs, respectively (Figure 22, (a, b)). By contrast, K186A is less affected by D_2O exchange and signals are retained throughout the continuous α-helix from leucine 176 to alanine 196 (Figure 22, (c)).

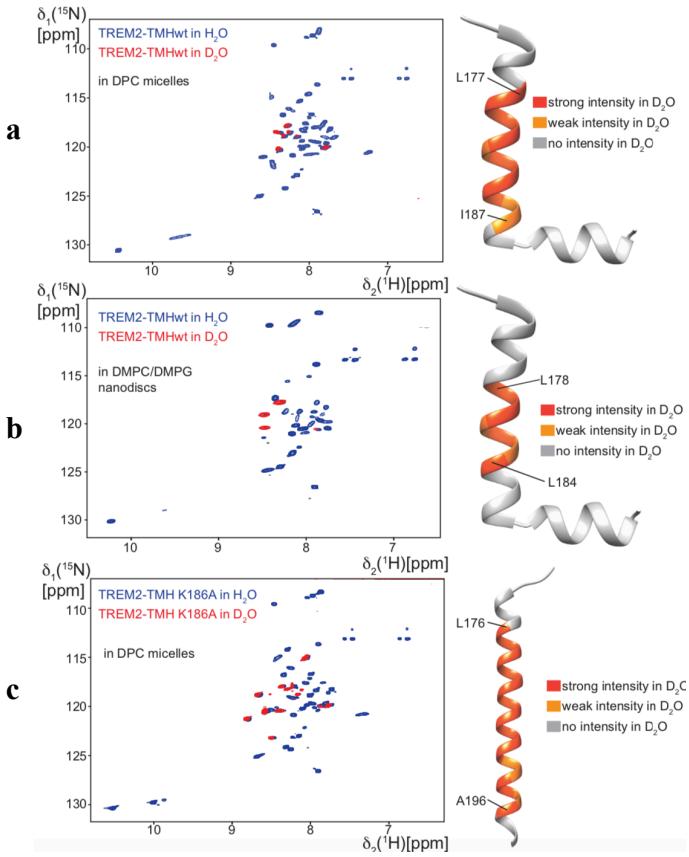

Figure 22: Hydrogen-deuterium exchange (HDX) probed by NMR for (a) TREM2-TM WT in DPC micelles, (b) TREM2-TM WT in lipid nanodiscs and (c) K186A variant in DPC micelles. Irrespective of the membrane mimetic, wild-type TREM2-TM is highly exchanging with D_2O leading to signal loss for solvent accessible regions. Corresponding mapping onto the determined structure confirms solvent exposed positioning of the C-terminal helix stretch. K186A is stable inserted and retains the membrane embedded signals of its continuous α-helix

4.1.7 Investigation of different charge-removal variants (K186L, K186P, K186N)

In order to investigate the effect of different amino acid substitutions at position 186, the wild-type lysine residue was mutated to hydrophobic leucine (K186L), helix destabilizing proline (K186P) and polar disease-related asparagine (K186N). All charge variants showed a comparable wild-type expression yield and pure protein bands after S200p size exclusion chromatography (Figure 23, (a, b)). Comparison of helical content (Figure 23 (c)) using CD

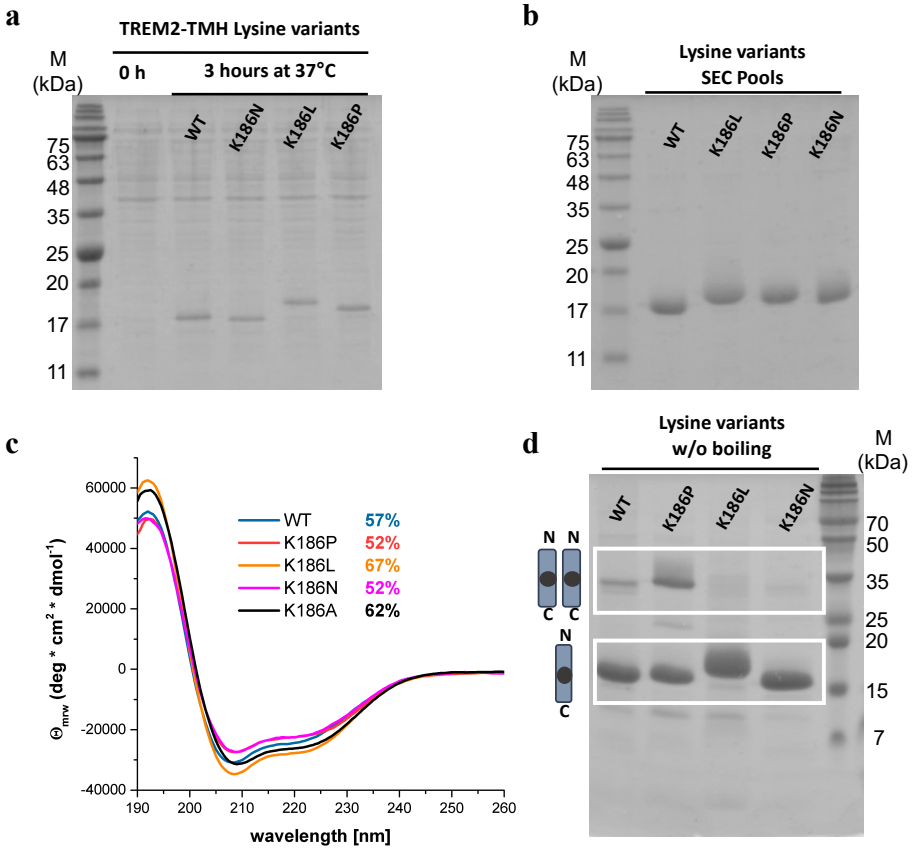

Figure 23: TREM2-TMH lysine variants. (a) Expression of lysine variants K186N, K186L and K186P in E. coli BL21(DE3). (b) Pooled S200p SEC fractions for the respective construct. (c) CD spectra of wild-type TREM2-TM and all lysine variants. Indicated is the calculated helical content of all constructs. (d) SDS-PAGE of final NMR samples without boiling. WT and K186P show a distinct dimer band, while K186L and K186N seem to be dominantly monomeric.

spectroscopy shows that K186P and K186N show a slightly lower helicity with respect to TREM2-TM WT while K186L displays a comparable helical content to K186A. Omitting the heating step before loading the samples onto an SDS Gel demonstrates that TREM2-TM WT and K186P show distinct dimer bands by contrast to K186L and K186N, which are predominantly monomeric (Figure 23 (d)).

Looking at the chemical stability of all TREM2-TM constructs measured by chemical unfolding experiments using CD spectroscopy and GuHCl as denaturant (Figure 24), it is apparent that kinked wild-type TREM2-TM and helix-destabilized K186P variant demonstrate a lower chemical stability which results in a measurable transition point at bout 7 M GuHCl concentration at a wavelength of 222 nm. In comparison, K186A and K186L don't show any spectral differences after addition of 8 M GuHCl and asparagine variant K186N just shows a slight decrease in secondary structure at 222 nm, suggesting that the introduced polar side-chain might destabilize the helix to some extent.

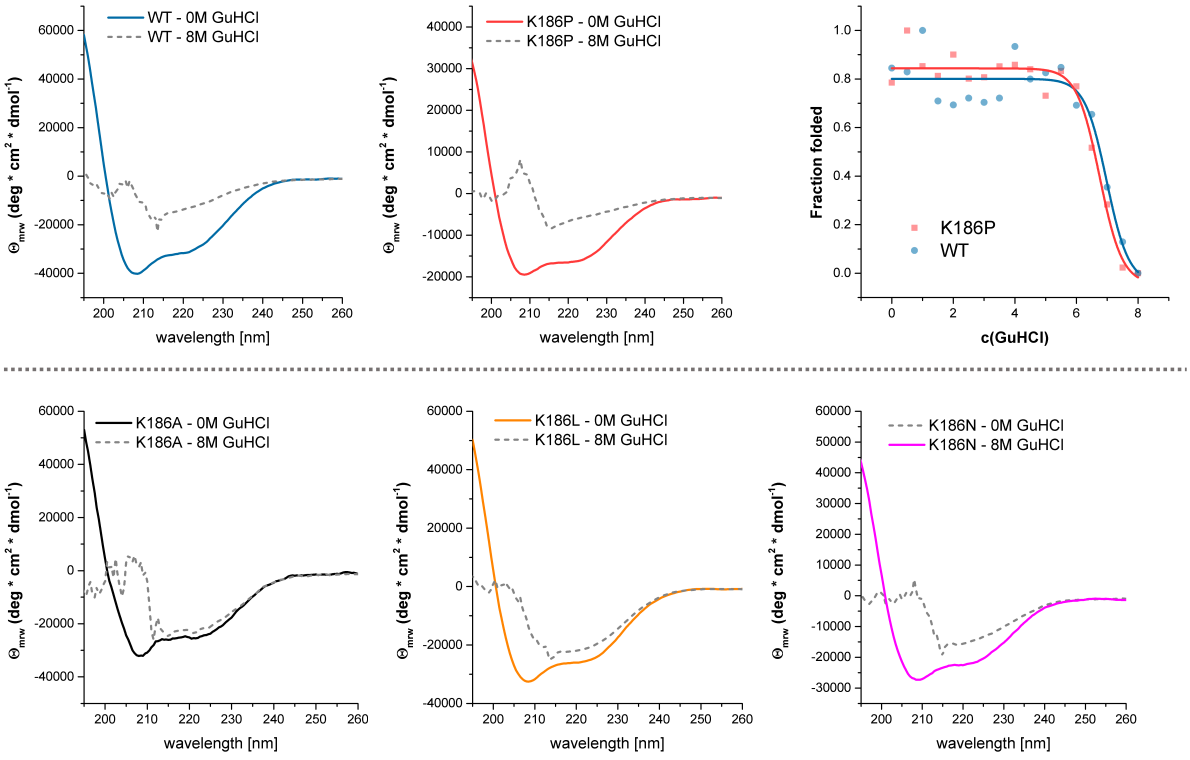

Figure 24: Chemical Unfolding of TREM2-TM constructs using CD spectroscopy and GuHCl as denaturant. Only kinked TREM2-TM WT and destabilized K186P show measurable transition points at approximately 7 M of GuHCl concentration.

All newly introduced lysine variants were subjected to an ^{1}H, ^{15}N-TROSY comparison with K186A. The ^{1}H, ^{15}N-TROSY spectra of K186A and K186L nicely overlay showing just minor chemical shift perturbations (Figure 25 (a)), thus extending the side-chain length but keeping the hydrophobic nature of the respective amino acid led to comparable structural changes with respect to wild-type TREM2-TM of K186A and K186L. Introduction of proline at the same position caused significant CSPs of proline-adjacent residues in a range of +/-5 to proline 186

(Figure 25 (c)). The proline substitution induces helix bending, thus leading to a kink in helix geometry[158,159]. This helix distortion leads to a decreased helical content (Figure 23 (c)) which is comparable to wild-type TREM2-TM. Slow interconversion between the cis/trans peptidyl-prolyl bond in addition to a kink-induced increase in dynamics leads to the existence of different species of K186P displayed by extensive peak splitting for a single signal. Although proline causes a kinked helix geometry, ^{1}H, ^{15}N-TROSY spectral overlay of K186P and K186A demonstrates that amino acids L193-W198 don't experience larger CSPs suggesting that the helical stretch which is outside of the membrane in case of wild-type TREM2-TM still lies within the bilayer for both K186A and K186P. Replacement of lysine 186 with disease-related asparagine (K186N) leads to pronounced CSPs in two areas, firstly downstream of asparagine 186, I187 and A189/A190 experience chemical shift changes due to the polar amino acid and secondly, in a region upstream of N186 including L178, A180 and C181 (Figure 25 (b)). The polar asparagine side-chain might be engaged in intrahelical or even interhelical contacts that would cause the spectral changes observed in comparison to K186A.

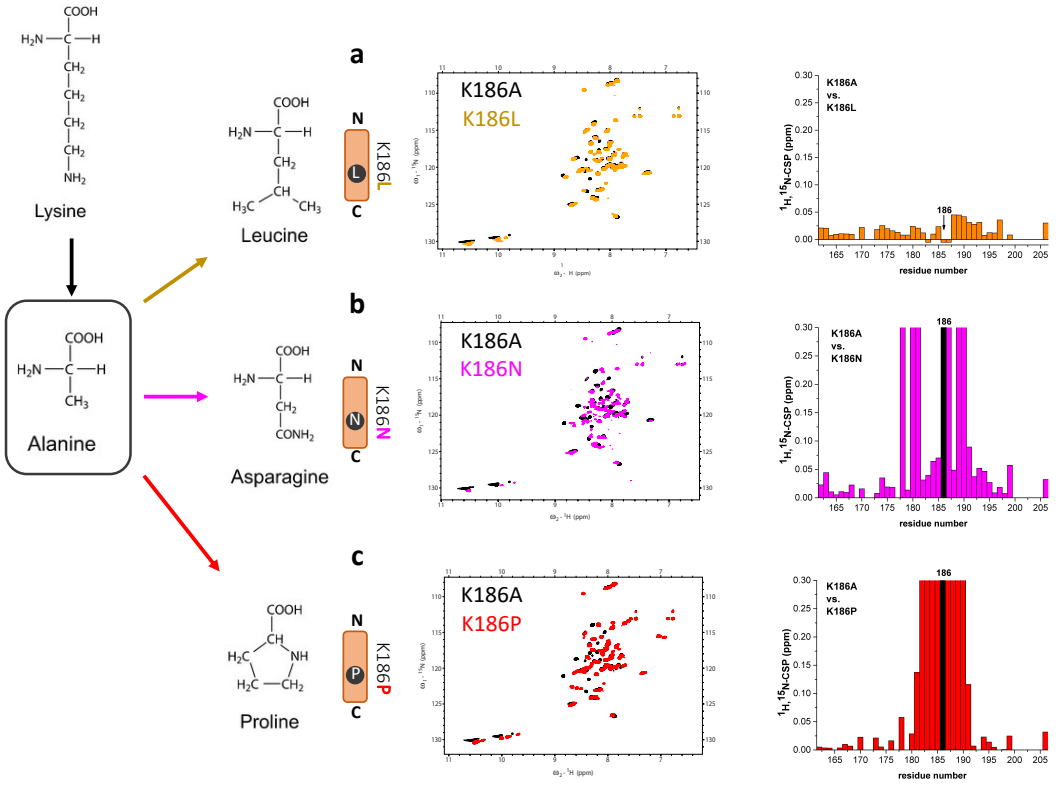

Figure 25: Spectral comparison and chemical shift perturbation analysis of lysine variants (a) K186L, (b) K186N and (c) K186P with respect to K186A.

4.1.8 Intramembrane cleavage

Determination of the initial γ-secretase cleavage site was performed in order to answer the question if intrinsic structural dynamics is a key feature which defines substrate cleavability. The intracellular domain (ICD) of TREM2 is released via this ε-cleavage into the cytosol, thus *in vitro* detection of the ICD fragment and mass-spectrometric (MS) analysis enables determination of the exact cleavage site. Isolated membranes of HEK293 cells stably expressing the TREM2 CTF were incubated for 16 hours to allow *de novo* formation of the TREM2 ICD in the presence and absence of the γ-secretase inhibitor L-685,458[160] at 37 °C. Immunoprecipitation of the soluble fraction using an anti-HA antibody revealed γ-secretase dependent generation of the TREM2 ICD. Immunoprecipitated ICDs were subjected to mass spectrometry as described previously[131]. MS analysis revealed major and minor peaks for the different constructs which were absent at 4 °C and reduced upon treatment with L-685,458 (Figure 26). The major ε-cleavage site of wild type TREM2-TM after A192 correlates well with the observed enhanced dynamics between amino acids 189 and 193. The cleavage sites determined for the proline variant (K186P) are located in a similar area, namely after S191 and L193 which fits nicely to the proline-introduced helix distortion enabling γ-secretase cleavage. Interestingly, the K186A mutation, which strongly stabilizes the α-helical structure of TREM2-TM, abolishes cleavage after amino acid 192 and shifts the ε-cleavage to a new site after amino acid 195 and to a lower extent to 193. The same major cleavage site after A195 was determined for K186L. Given that lysine and proline at position 186 break the helix inducing a kink whereas alanine and leucin at the same position confer helical continuity, MS results additionally underline the assumption that structurally dynamic regions appear to be preferred sites for substrate cleavage by γ-secretase in case of TREM2.

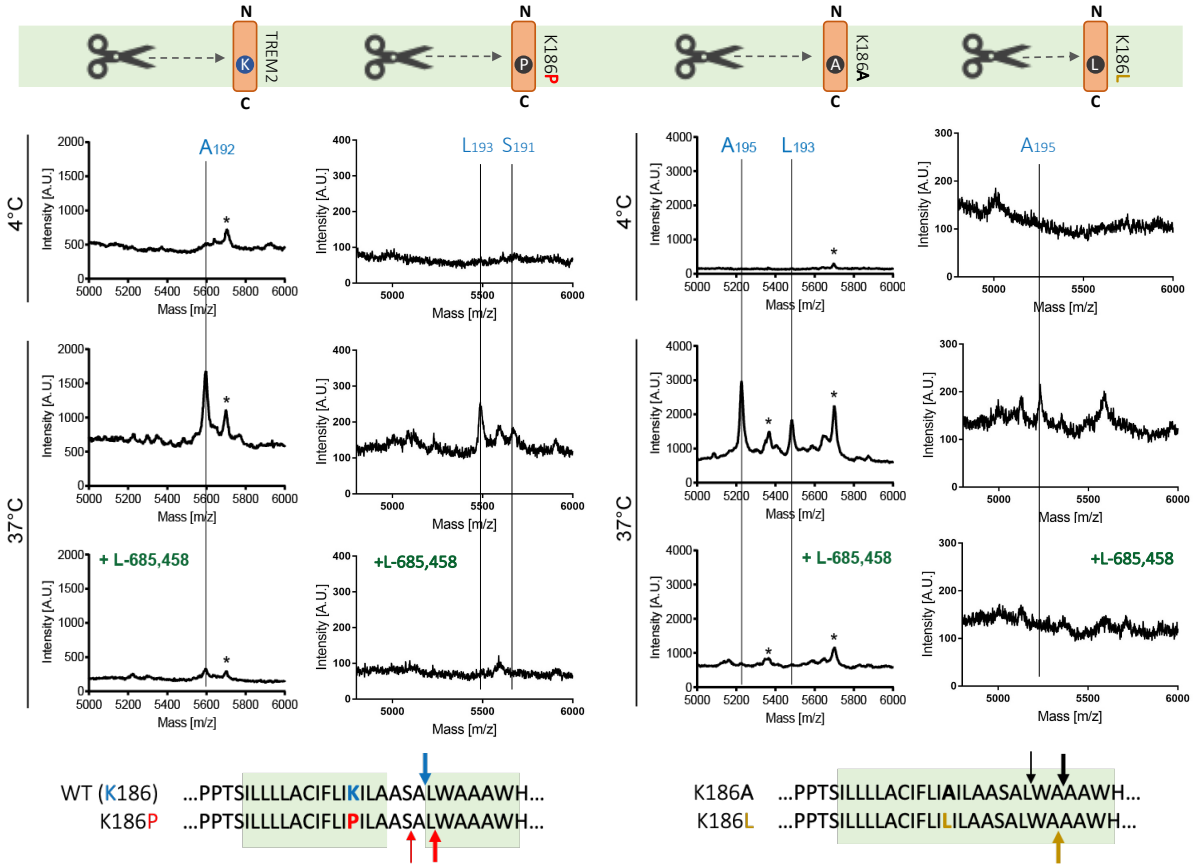

Figure 26: γ-secretase cleavage assay and mass spectrometric analysis for wild-type TREM2-TM, K186P, K186A and K186L. Detected masses were assigned to the protein sequence and minor (small arrow) and major (bold arrow) cleavage sites are indicated for the different constructs. WT and K186P show a comparable cleavage pattern as well as K186A and K186L, respectively.

4.2 Biophysical characterization of TREM2-ECD

4.2.1 Expression and purification

The extracellular domain of TREM2 was challenging to express. First trials with regular *E. coli* BL21 (DE3) yielded in low protein amount not suitable for NMR. Analysis of the protein's amino acid sequence showed that approx. 25% of the primary sequence comprises of arginine, isoleucine, proline and leucine so all following expressions were carried out in the codon plus *E. coli* BL21 (DE3)-RIPL strain. The expression yield increased drastically but investigation of the cell fractions demonstrated that TREM2 ECD was expressed into the insoluble inclusion body (IB) fraction. The initially used construct was bearing a GB1-tag at the N-terminus and an uncleavable His_6-tag on the C-terminus. Regarding first refolding attempts GB1 turned out

to be problematic since the refolding solution stayed clear suggesting that GB1 might keep even incorrectly folded TREM2 in solution. GB1 could be cleaved off efficiently leading to precipitation of the probably incorrectly folded TREM2 at this point. But it appeared that GB1 might bind to TREM2 since thorough washing of NiNTA-bound TREM2 didn't remove GB1 which was still present in the following SEC. Sudom *et al.*[63] published the crystal structure of TREM2 using a construct which is N-terminally shortened compared to the construct used here. A shorter construct was therefore cloned missing 10 amino acids on the N-terminus. The His_6-tag was deleted as well in agreement with the crystal structure construct.

The new construct – TREM2(19-131) – showed a slightly worse expression yield compared to the construct carrying the GB1. But purification of the inclusion body pellet yielded enough protein for subsequent refolding. Refolding was carried out for 48 hours and formation of disulfide bonds was surveyed using non-reducing SDS-PAGE analysis (Figure 27).

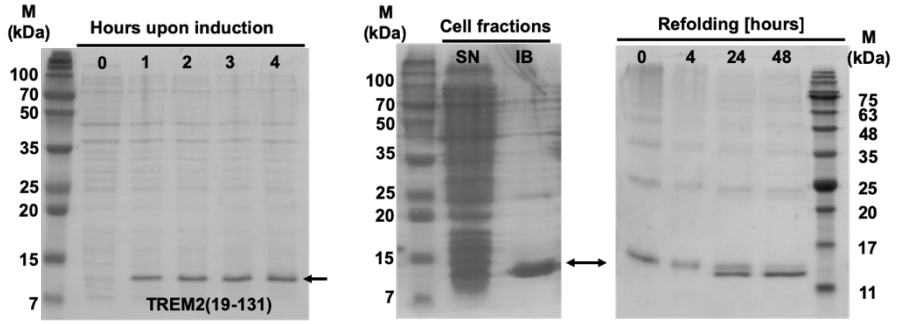

Figure 27: Expression, Purification and Time course of refolding of TREM2. (*Left*) Clearly visible expression band of TREM2(19-131) upon induction in BL21(DE3)-RIPL. (*Middle*) Inclusion body (IB) pellet fraction contains TREM2. (*Right*) Non-reducing SDS-PAGE proves disulfide-bond formation, the globular-packed species runs faster (lower molecular weight band)

Following refolding, an ion exchange chromatography was applied to select for correctly folded TREM2 ECD (Figure 28). The protein peak at about 25% Buffer F (approx. 250mM NaCl) shows TREM2 ECD. Unfortunately, protein precipitation was detected during the attempt to concentrate TREM2 ECD peak fractions, therefore the sample was flash frozen supplemented with 200 mM L-arginine and 10 % glycerol in order to increase stability and to enhance cryo

protection, respectively. After one freeze and thaw cycle, there was no secondary structure detectable anymore using CD spectroscopy.

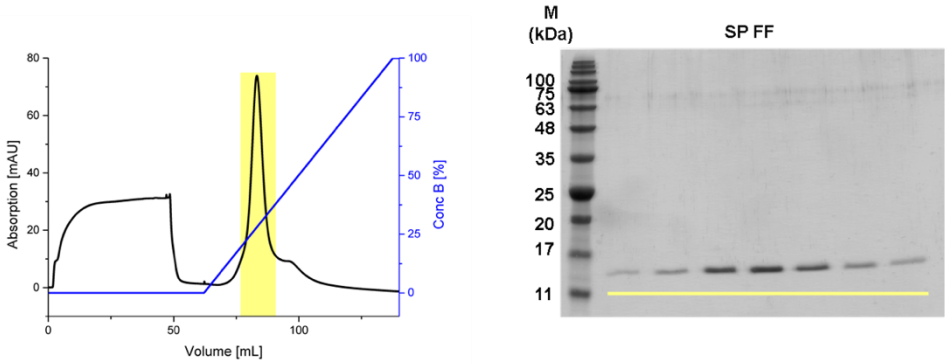

Figure 28: Cation exchange chromatography (SP FF) of TREM2(19-131) upon refolding (*left*). Corresponding SDS PAGE analysis of highlighted fractions (*right*).

4.3 Biophysical characterization of TNFα-ECD

4.3.1 Expression and purification

GB1-TNFα expresses in high yield in *E. coli* BL21 (DE3), clearly demonstrated by the appearance of a band at around 28 kDa in the expression test SDS gel picture (Figure 29, (a)). Application of the soluble (supernatant, SN) fraction upon cell disruption to NiNTA resin followed by size exclusion chromatography yields in highly pure fusion protein (Figure 29, (b,c)). Removal of His_6-GB1 (fusion tag) via thrombin digest is complete after overnight incubation at 4 °C (Figure 29, (d)) and subsequent reverse NiNTA or size exclusion chromatography leads to pure TNFα protein with approximate yields of ~70 mg/L (in LB), ~50 mg/L ($^2H^{15}N$) and ~35 mg/L ($^2H^{15}N^{13}C$).

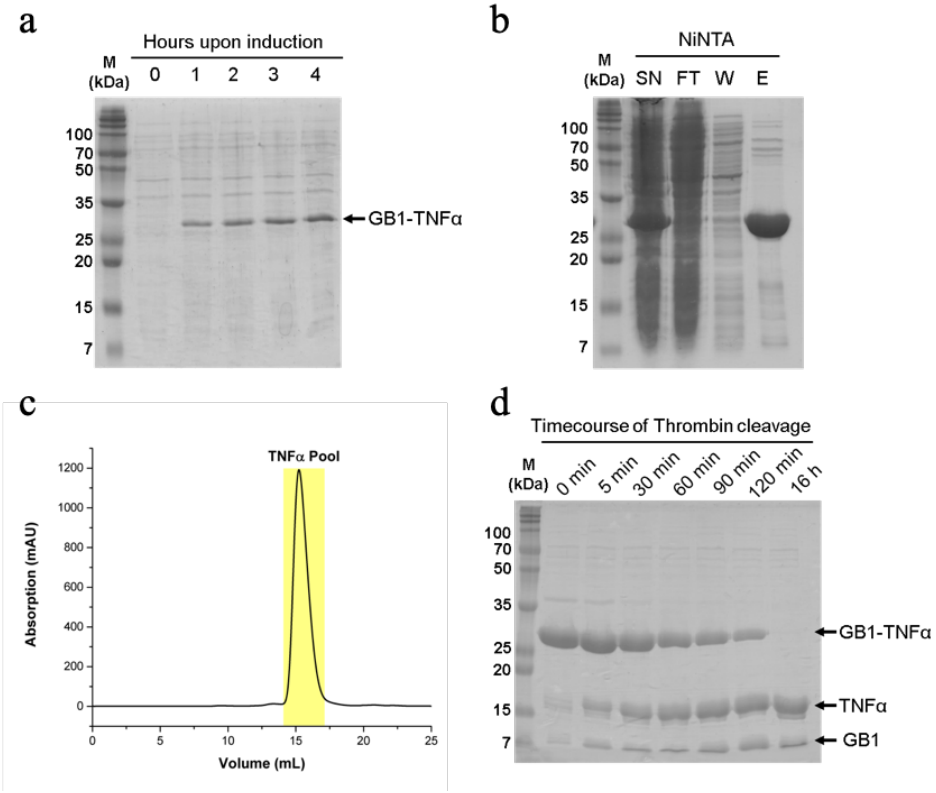

Figure 29: (a) Expression of GB1-TNFα in *E. coli* BL21(DE3). (b) Nickel affinity chromatography of cleared supernatant. GB1-TNFα can be found in the elution fraction (E) at a molecular weight of approx. 28 kDa. (c) Size exclusion chromatography of GB1-TNFα.Pooled peak fractions are highlighted (c) Thrombin digest of pooled SEC pool is complete after overnight incubation at 4°C.

4.3.2 Spontaneous cleavage N-terminally of serine 80

TNFα was found to undergo metal-catalyzed, site-specific peptide bond cleavage. This spontaneous cleavage event is restricted to prior enzymatic liberation of the solubility enhancer GB1. Thrombin digestion makes the N-terminus accessible and prone to this unwanted cleavage event. Usually TNFα is highly concentrated, therefore the molecular weight difference is not easily detectable in the SDS-PAGE analysis (Figure 30, (a)). Higher resolution of the used SDS gel makes the difference obvious (Figure 30, (b)) and ESI-MS analysis of the TNFα double band shows two distinct masses (Figure 30, (c)). The higher mass of 18395.0 Da corresponds to the wanted species namely the TNFα carrying the N-terminal glycine (G-TNFα) upon thrombin digest while the lower mass of 17087.4 Da represents the cleavage product which is 12 amino acids shorter thus corresponds to a cleavage N-terminally of serine 80 (middle serine in a triple serine motif) which is usually protected via post-translational O-glycosylation.

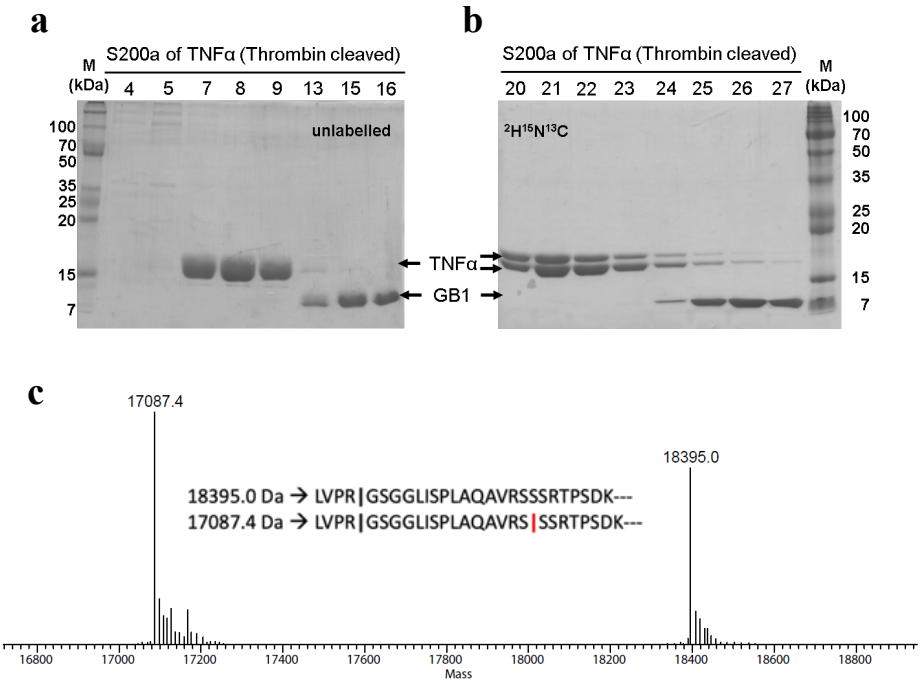

Figure 30: Spontaneous cleavage N-terminally of serine 80. (a) SDS-PAGE analysis of Thrombin cleaved unlabeled TNFα. (b) SDS-PAGE analysis of thrombin cleaved ^{2}H, ^{15}N, ^{13}C-labeled TNFα. Higher gel resolution shows double band for TNFα fractions. (c) ESI-MS analysis of TNFα demonstrates two masses: wanted G-TNFα corresponds to the higher mass of 18395.0 Da while the second detected mass of 17087.4 Da corresponds to a 12 amino acid shorter TNFα cleavage product

Different divalent cations that could act as Lewis acid thus causing spontaneous cleavage were screened for their ability to generate the lower mass product. Thrombin digest of TNFα was therefore performed either in presence of 5 mM EDTA (Figure 31, line 1) or with 10 mM respective cation added. Cobalt, magnesium, calcium and nickel, respectively, caused complete cleavage (Figure 31, line 2-5) and generation of the lower mass product while zinc and copper only partially created the unwanted species (Figure 31, line 6+7) upon overnight incubation at room temperature. It seems that performing the thrombin digest in presence of 5 mM EDTA mostly prevents the unwanted cleavage event.

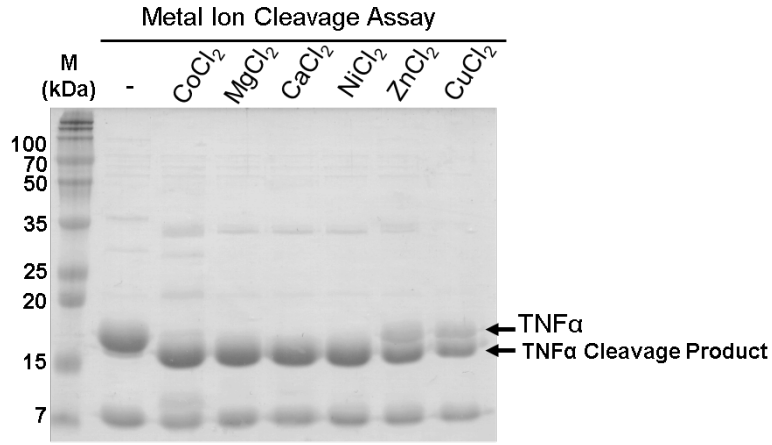

Figure 31: Metal ion-based cleavage assay of TNFα. Thrombin cleavage of TNFα in presence of 5mM EDTA led to generation of the wanted species. Incubation of 10mM divalent cation respectively shows occurrence of the observed cleavage product.

4.3.3 Oligomeric state and stability

Purified TNFα elutes as a stable homo trimer in the SEC. The elution volumes of ~10 mL (S75a) or ~16 mL (S200a) can be used to determine the apparent molecular weight using the respective calibration curves of the columns. The homogeneous single peak population has an apparent MW of 65 kDa on the S200a column and 52 kDa on the S75a column and therefore fits perfectly to the trimeric TNFα homo oligomer (Figure 32).

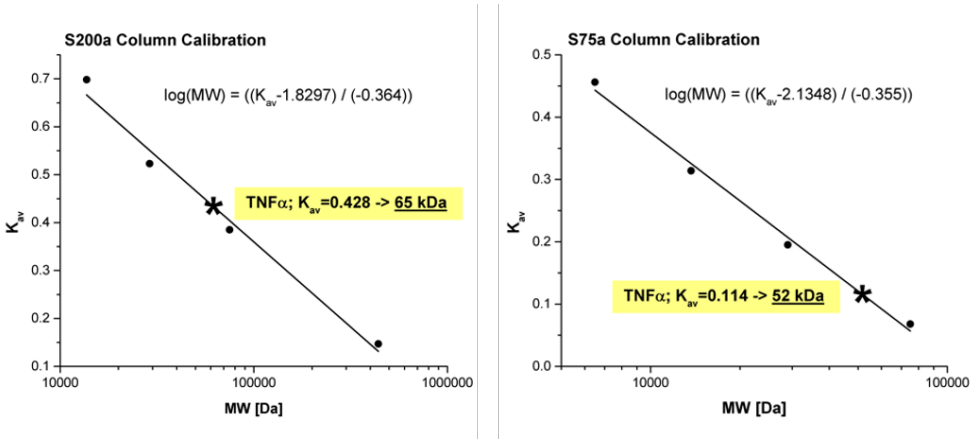

Figure 32: Determination of the apparent molecular weight of TNFα using the size exclusion column specific calibration curves

Thermal denaturation of 20 µM TNFα using circular dichroism spectroscopy shows a melting temperature of approx. 74 °C (Figure 33, (b)). Chemical denaturation with guanidine hydrochloride (GuHCl) demonstrates a sigmoidal curve with a transition point at about 3 M of denaturant concentration (Figure 33, (c)).

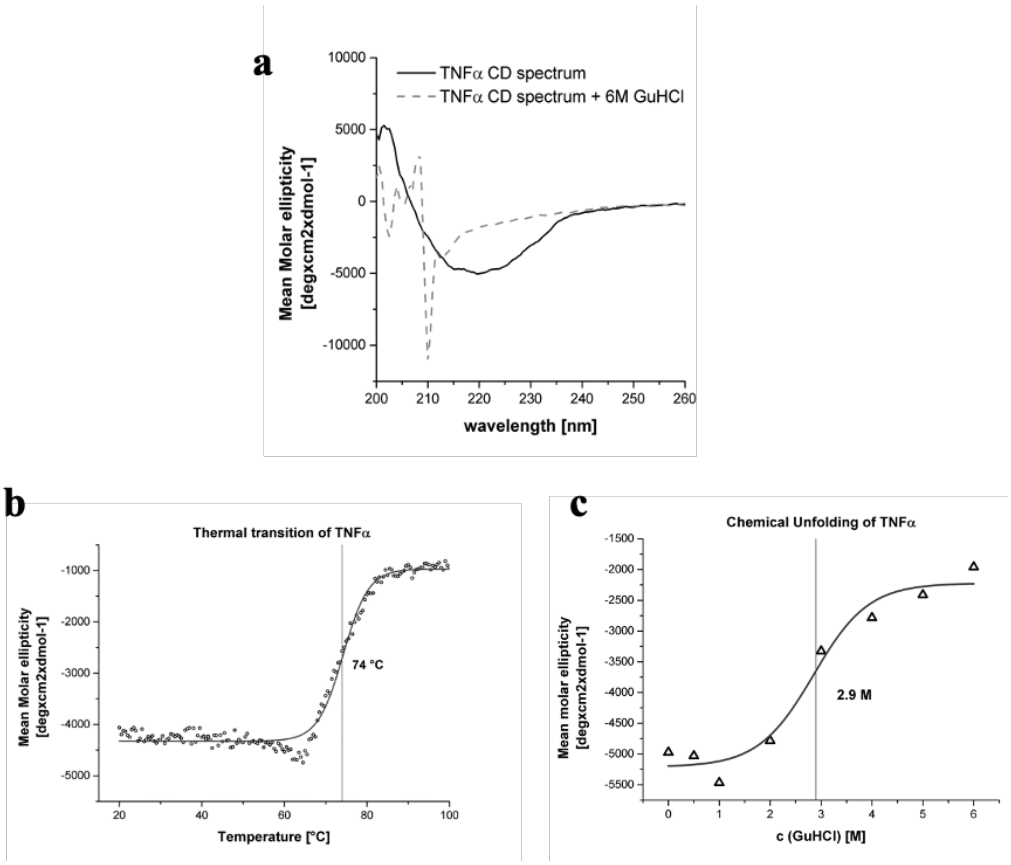

Figure 32: Thermal and chemical stability of TNF. (a) CD spectra before and after chemical unfolding with GuHCl. (b) Thermal unfolding of TNF with a transition point at around 74°C. (c) Chemical unfolding with increasing GuHCL concentrations and a transition point at approx. 3 M denaturant concentration

4.3.4 Effect of urea on TNFα Trimer

The trimeric packing of TNFα is solely based on hydrophobic core and inter-subunit interactions, therefore the effect of increasing urea concentration on the oligomeric state was screened. Size exclusion chromatography of TNFα demonstrates that presence of 2 M urea causes a decrease in elution volume thus an increase in the hydrodynamic radius of the still trimeric protein (Figure 34 (a)). Thermal transition measured by CD spectroscopy in presence of 2 M and 4 M urea respectively clearly shows that while there is still a measurable melting point in presence of 2 M urea, the transition point is no longer detectable in presence of 4 M urea. Additionally, TNFα's melting point decreases from approx. 74°C to 60°C in presence of 2 M urea (Figure 34, (b)).

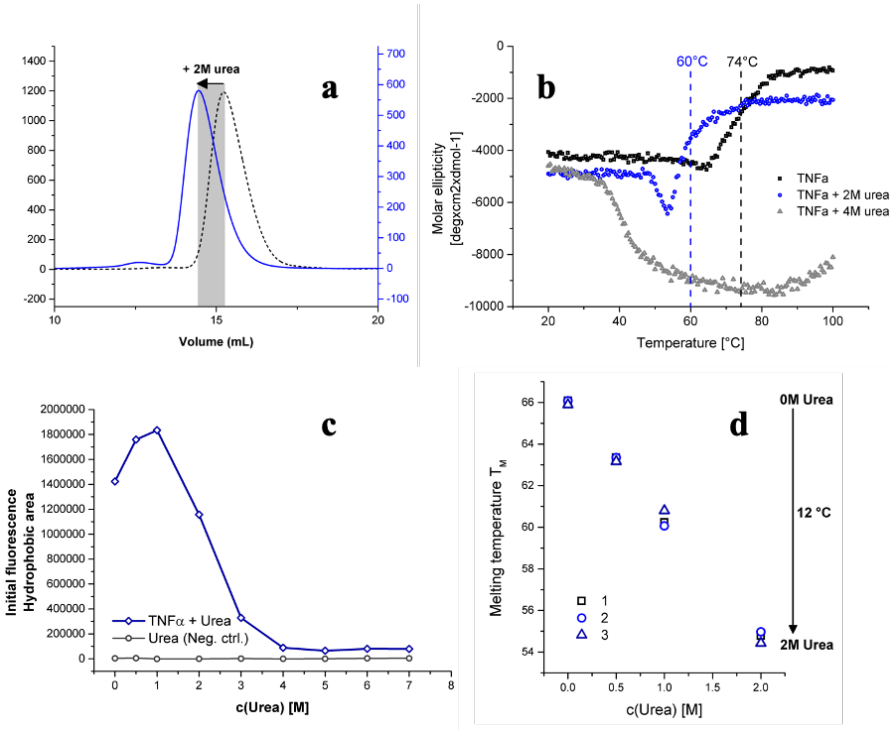

Figure 34: Investigation of the effect of urea on TNFα's trimeric packing. (a) Size exclusion chromatography of TNFα without (dashed lines) compared to in presence of 2M urea (blue). (b) Thermal unfolding without (black) and in presence of 2M urea (blue) and 4M urea (grey). (c) Thermal shift assay (TSA) analysis of the accessible hydrophobic area with increasing urea concentrations. (d) TSA analysis of thermal unfolding between 0 and 2 M urea.

Thermal Shift Assay was performed using increasing urea concentrations from 1 to 7 M, respectively. The initially measured value gives information about the hydrophobic and accessible area which increases until 1.5 M urea suggesting a loosening of the tight packing

(Figure 34, (c)). With further increasing concentrations urea molecules interact with the exposed hydrophobic residues and shields them from SyproOrange detection, since urea itself was shown to not interact with the hydrophobic dye. Also, in the TSA assay a decrease of melting temperature of about 12 °C difference (Figure 34, (d)) was detected which is in nice agreement with the values measured with CD spectroscopy.

2D-Trosy NMR titration experiments confirmed the hypothesis that urea penetrates the hydrophobic core first, loosens the packing of the trimer and finally breaks the proteins 3-dimensional structure at urea concentration of approx. 4 M (Figure 35).

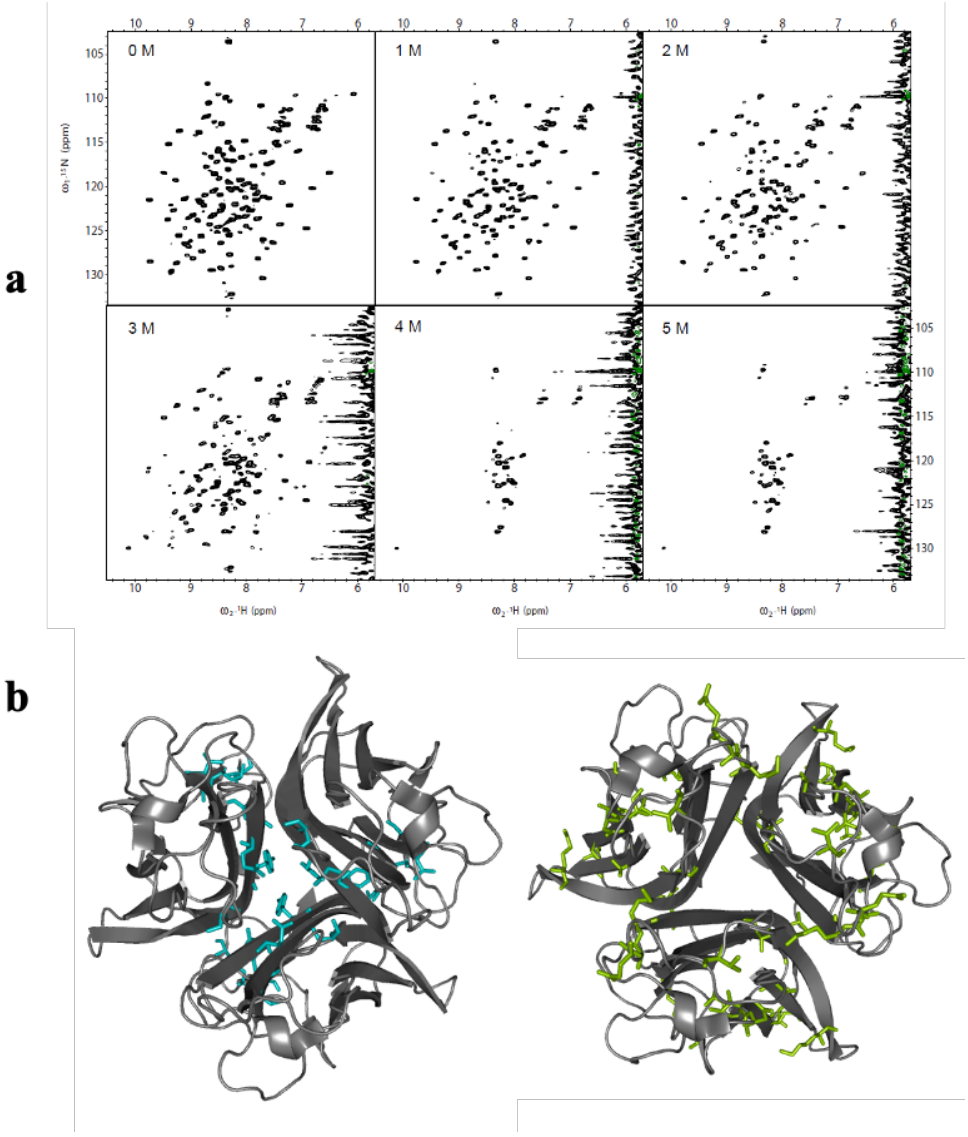

Figure 35: NMR spectroscopic urea titration of TNFα. (a) ^{1}H, ^{15}N-Trosy spectra in presence of 0, 1, 2, 3, 4 and 5 M urea, respectively. The noisy strip at approximately 5.8 ppm derives from urea (b) Representation of the effected amino acids in case of 2M (turquoise) and 4M (green) urea.

4.4 Fragment-based Drug Design

Triple resonance NMR experiments for structure determination using uniformly labelled $^{2}H^{15}N^{13}C$ TNFα were recorded at an 800 MHz spectrometer at 308K. Before completion of the resonance assignment, Hofmann *et al*. published the NMR resonance assignment of soluble TNFα[115], therefore the published NMR resonance assignment was transferred in order to analyze the effects caused by fragment-based compound titrations.

In collaboration with Dr. Grzegorz Popowicz (Helmholtz Zentrum München) preliminary experiments were conducted in terms of future small molecule inhibition of TNFα. The proton spectrum of TNFα was therefore recorded at different irradiation frequencies (Figure 36). An irradiation frequency of 0.459 ppm (off-resonance) was chosen for the following STD experiments.

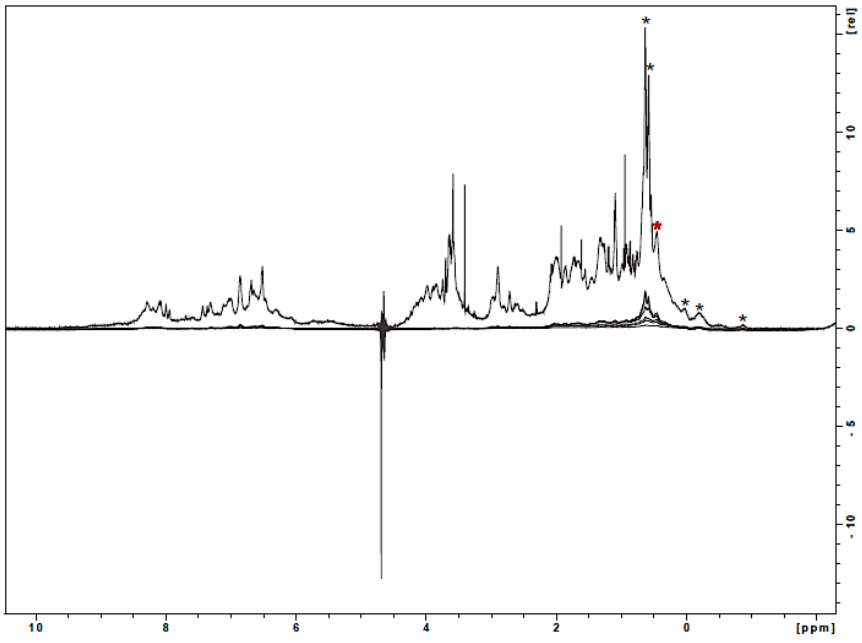

Figure 36: Proton spectrum of unlabeled TNFα recorded at different irradiation frequencies. An irradiation frequency of 0.459 ppm (red asterisk) was chosen for following STD experiments

An overview of the fragment-based STD NMR experimental workflow is depicted in Figure 37. Initial STD experiments were recorded with unlabeled TNFα and 5-compound-mixtures, so-called cocktails, at a 600 MHz spectrometer equipped with a sample changer. 320 of those cocktails, thus 1600 compounds were initially screened. 14 of these cocktails were chosen for

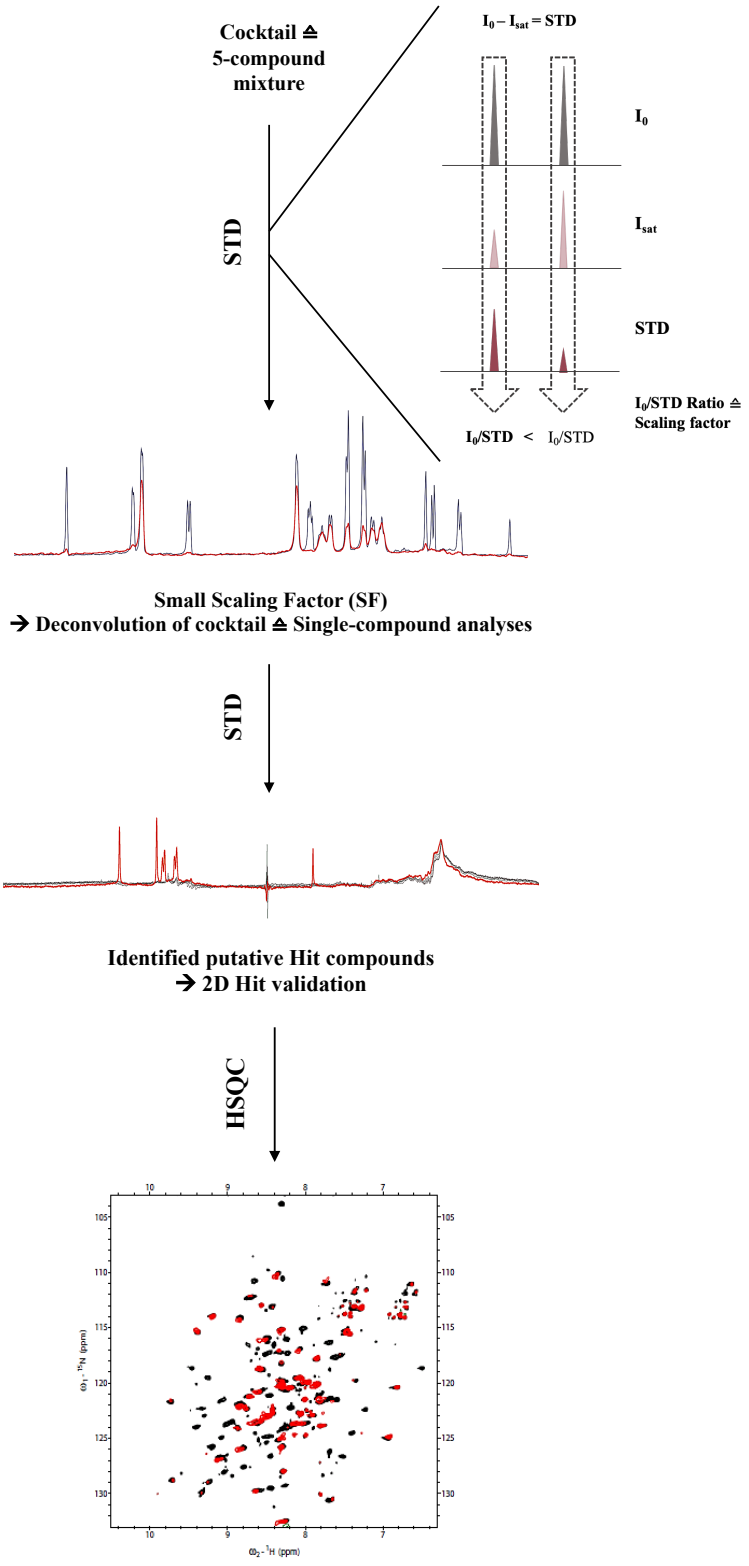

Figure 37: Workflow of NMR-based fragment screening of TNFα. 5-compound-mixtures, so-called cocktails were screened, and cocktails selected that showed a small scaling factor (SF). Deconvolution, thus single-compound screen led to the identification of 17 putative Hit compounds that were further screened in a 2D-HSQC validation

further single compound analysis based on a small scaling factor (SF). This SF is based on the I_0/STD ratio, meaning the ratio between the off-resonance or reference spectrum and the difference spectrum. A signal which experiences a stronger reduction in signal intensity in the

on-resonance spectrum as a consequence of saturation transfer between protein and ligand would consequently lead to a higher intensity upon subtraction of I_0-I_{sat}, thus the ratio of I_0/STD can be used to estimate the STD strength. A small scaling factor (here: SF < 6) is pointing to a putative active molecule within the respective cocktail. The deconvolution, thus the individually screen of the compounds of each promising cocktail led to the identification of 17 active compounds among 70 candidates. Those active Hit compounds were validated using 2D NMR spectroscopy with ^{2}H, ^{15}N-labelled TNFα samples. 300 µM TNFα was therefore mixed with 2 mM respective compound leading to a 1:50 dilution of the compound in DMSO, thus to a 2 % final DMSO concentration. The respective reference HSQC was therefore also recorded with 2% final DMSO concentration. The detailed cocktail and single-compound analyses can be found in the appendix.

4.4.1 Initial compound screen

Compounds #2, #10 and #13 were the first-round compounds to be further tested on their mode of action on TNFα. Initial DLS measurements (Figure 38) of TNFα showed a homogeneous size distribution around 3.5 nm radius. In presence of 1mM respective compound the single size population broadened drastically in addition to an overall slight increase in particle size.

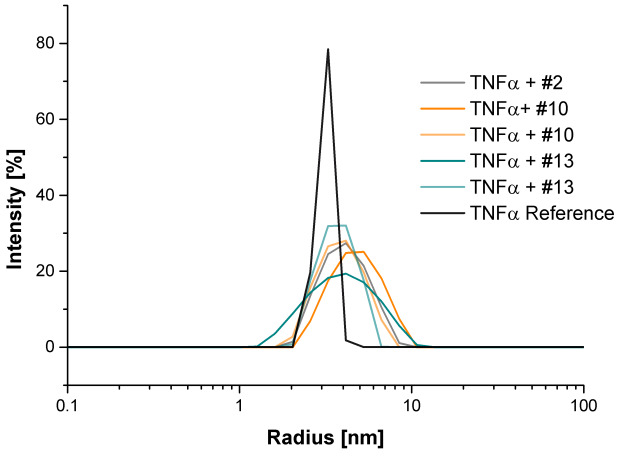

Figure 38: Dynamic light scattering (DLS) of TNFα alone and in presence of excess compound #2, #10 and #13, respectively. Measurements were performed at 37°C.

The observed effect seems to fit well to the hypothesis that the compounds interact with the hydrophobic core thus loosening the tight trimeric packing of TNFα.

Initial screening of structural effects on TNFα included a modified TSA assay to evaluate the accessible hydrophobic area in dependency of compound concentration and furthermore NMR investigation of changes in signal intensity and chemical shift perturbations upon addition of excess compound.

4.4.1.1 Investigation of trimer destabilization using TSA Assay

The Thermal Shift Assay provides useful information regarding the trimeric organization of TNFα since the SyproOrange Dye itself is hydrophobic and therefore reacts with hydrophobic protein areas that are exposed during thermal unfolding. Instead of unfolding, the initial fluorescence values of a compound dilution series were recorded. Loosening of the trimeric packing grants access for the SyproOrange Dye leading to an increase in fluorescence. Among the three first-round-compounds solely #10 showed a pronounced effect in the observed concentration range between 6 µM and 1 mM compound, respectively. The effective concentration of #10 was calculated to be approx. 170 µM (Figure 39, left). Zooming into a lower fluorescence range it seems that #2 also exerts some effect (Figure 39, right) but the

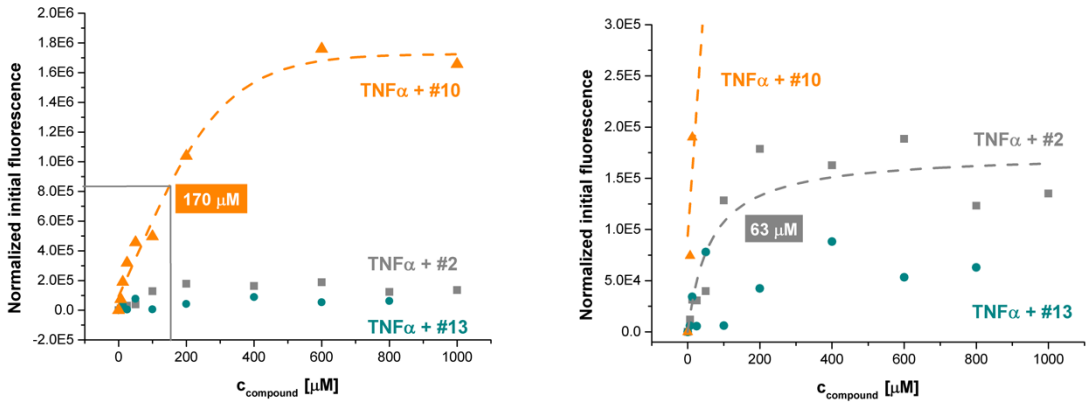

Figure 39: TSA assay of first-round compounds #2, #10 and #13. The initial fluorescence values are plotted against the respective compound concentrations.

determined effective concentration of 63 µM is probably an artifact due to high fluctuations of the measured values. Compound #13 was discarded at this point.

Based on the chemical structure of the three initial compounds a second round of compounds was purchased, namely N1 to N7 which were also tested in the TSA assay (Figure 40). The only compound causing a measurable effect (N1) was one based on the chemical structure of compound #10, although with a slightly higher effective concentration of approx. 190 µM.

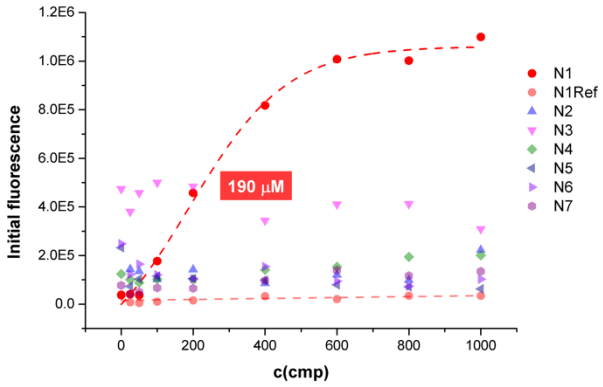

Figure 40: TSA assay of second-round compounds N1 to N7. The initial fluorescence values are plotted against the respective compound concentrations.

Surprisingly, compounds N5 and N6 whose chemical structure show high similarity to compound #10 seemed to have no effect at all. This observation might hint already to a quite specific structure-function-relationship of compound #10.

4.4.1.2 Initial NMR investigation of compound addition

Compounds were added in a 1:100 dilution (100 mM stock concentration in DMSO) to a 300 µL ^{2}H, ^{15}N- labeled TNFα sample of approx. 200 µM leading to a final DMSO concentration of 1% and a respective compound concentration of 1mM. ^{1}H, ^{15}N-TROSY spectra were recorded along with the 1D proton spectra (Figure 41). N4 directly precipitated upon addition. N1 and N2 also showed slight precipitation and the proton spectra made clear that there was obviously no compound left and the recorded 2D TROSY spectra of N1 and N2 perfectly overlay with the TNFα reference. Unfortunately, N1 had shown effects in the TSA assay that could not be confirmed by NMR due to low solubility of this compound. All the other compounds are clearly visible in a frequency range between 7 and 9 ppm.

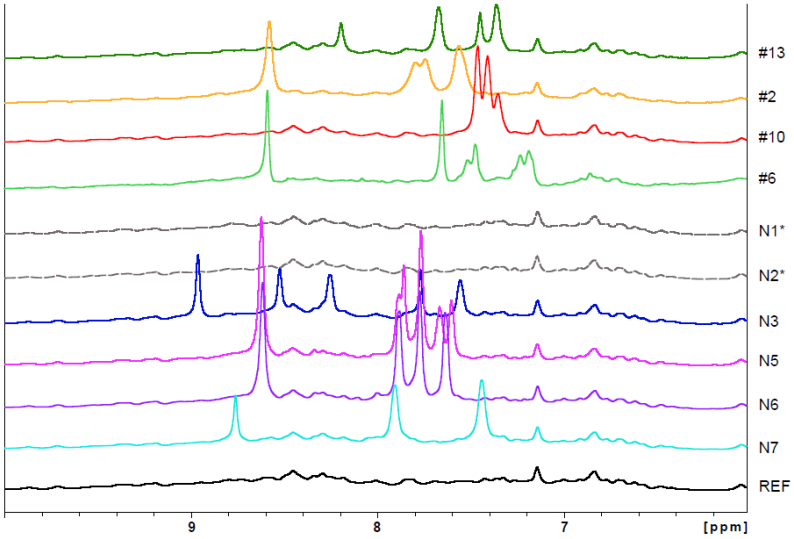

Figure 41: 1D proton spectra of TNF upon addition of excess compound. N1 and N2 precipitated upon addition. The other compounds show clearly visible signals in the 7 to 9 ppm frequency range.

The corresponding ^{1}H, ^{15}N-TROSY spectra are shown in Figure 42 and the results match well with the TSA results. Compound #10 demonstrates drastic signal intensity loss while compound #6 shows a combination of intensity loss, peak splitting and chemical shift perturbations. The reduction in signal intensity is less pronounced in case of compound #2. All second-round compounds that stayed in solution have hardly any effect on the TNFα reference signal distribution or intensity.

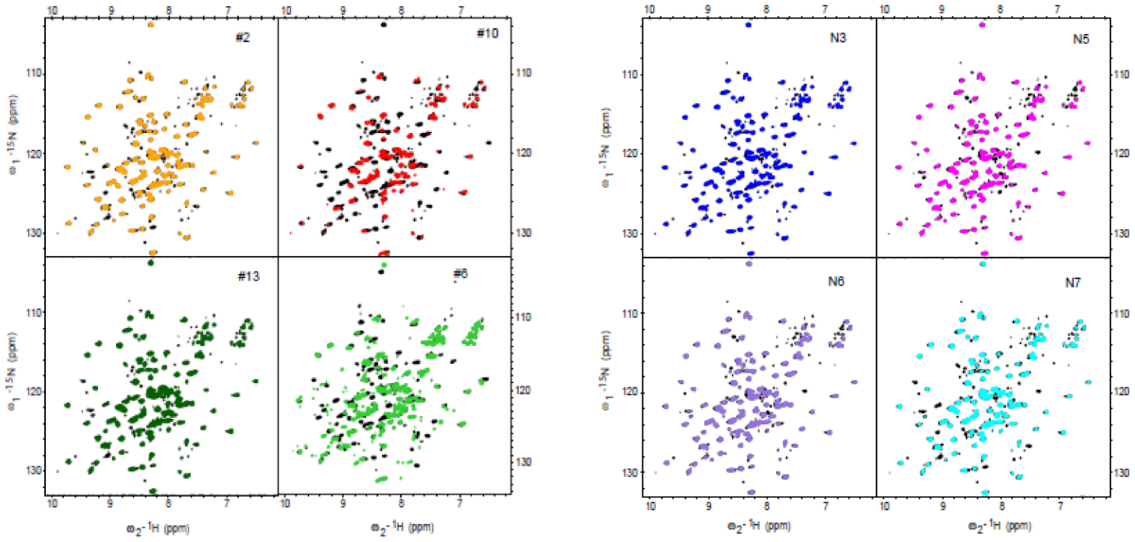

Figure 42: (*Left*) ^{1}H, ^{15}N-TROSY - Screen of first-round compounds #2, #6, #10 and #13. (*Right*) ^{1}H, ^{15}N-TROSY - Screen of second-round compounds N3, N5, N6 and N7

4.4.2 Assay Screen of Lead compounds #2, #6, #10

Compounds #6 and #10 are the most promising candidates which showed effects in the TSA as well as in NMR spectroscopic analysis. CD spectroscopic determination of thermal transitions of TNFα shows a slightly decreased melting temperature in presence of 1 mM compound #6 and #10, respectively (Figure 43). However, the overall decrease of 3-4 °C is not significant suggesting the compounds don't influence the melting of secondary structure.

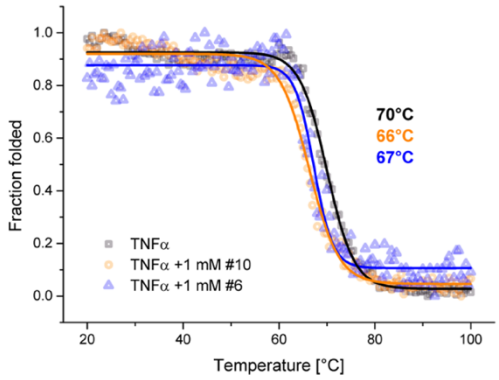

Figure 43: Detection of TNFα thermal melting transition point without (black) and in presence of 1 mM compound #10 (orange and 1mM compound #6 (blue).

4.4.2.1 Cysteine-TNFα (cTNFα) and FRET measurement of subunit exchange

The subunit exchange was measured based on the FRET assay published by van Schie *et al.*[125]. The construct used for cysteine-specific coupling - GB1-THRmut-TNFα – is N-terminally shortened to place the label close to the structured ECD domain. Therefore, this TNFα construct does not suffer from spontaneous N-terminal cleavage and digestion with Thrombin yields the final construct carrying an N-terminal cysteine for coupling to fluorescent dyes, namely 5-IAF and 5-TAMRA. Although reducing agent was present throughout the whole purification, ESI-MS analysis shows the disulfide-linked dimeric protein (Figure 44, top) which is probably one of the reasons for the low labeling degree (approximately 20-40 %) because the cysteine residue is not accessible for the coupling reaction. The final size exclusion chromatography was recorded at 2 different wavelengths to validate the successful coupling, namely 280 nm

detection of aromatic protein residues along with the dye-specific absorption wavelength (Figure 44, bottom).

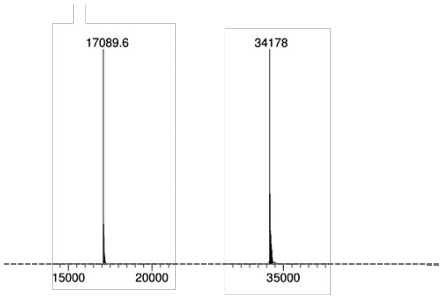

	Calculated mass [Da]	Observed mass [Da]
Monomer	17113.46	17089.6
Dimer	34224.92	34178.0

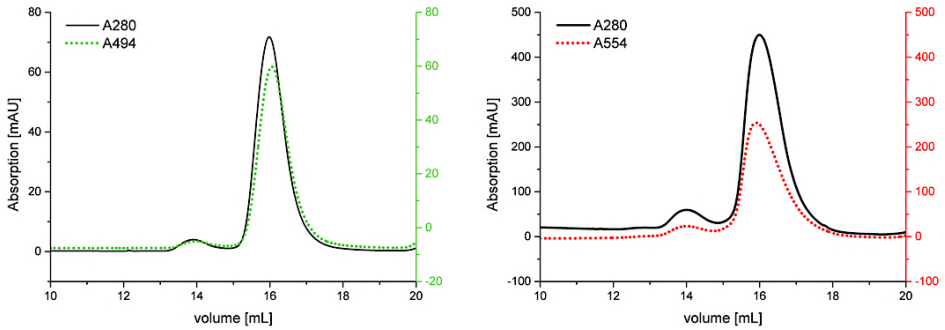

Figure 44: (Top) ESI-MS analysis of cTNFα demonstrates the dimeric, disulfide linked cTNFα even in presence of reducing agent. (Bottom) Size exclusion chromatograms of cTNFα upon cysteine-specific coupling to fluorescent dyes 5-IAF (left, green) and TAMRA (right, red).

The emission and extinction spectra of cTNFα-IAF/-TAMRA were recorded in order to determine the most suitable wavelength for excitation of IAF without co-exciting TAMRA (Figure 45). This wavelength was set at 450 nm. The donor fluorescence (IAF, green) is quenched due to the FRET effect, thus subunit exchange can be tracked by measuring the decrease of the emission fluorescence at 525 nm.

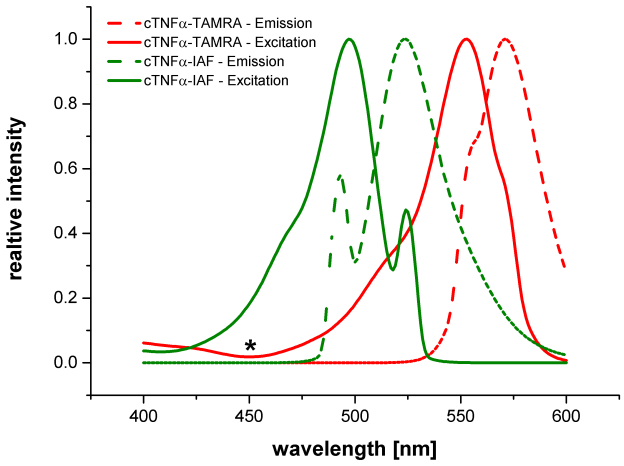

Figure 45: cTNFα FRET pair. cTNFα was coupled to either IAF or TAMRA and the spectra recorded in order to determine the suitable wavelength for excitation of IAF without co-excitation of TAMRA, which was determined to at 450 nm (black asterisk)

The subunit exchange was recorded for 1200 minutes for either the reference pair and upon addition of 10 x molar excess of the respective compound compared to the calculated protein concentration. Compounds #2 and #10 both caused an accelerated exchange rate (Figure 46) suggesting that the compounds destabilize the trimeric assembly and enhance subunit exchange. The effect seen for compound #10 was slightly more pronounced.

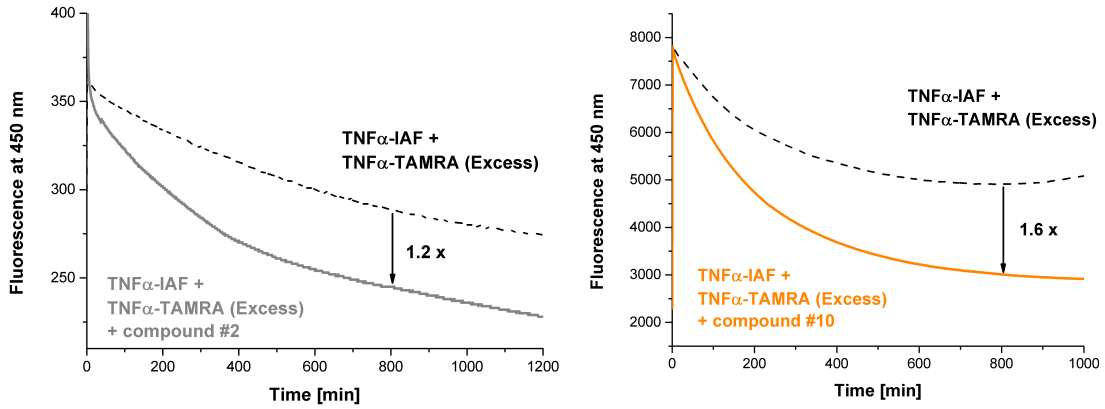

Figure 46: Effect of compound addition to cTNFα subunit exchange measured by FRET. Botch compounds, #2 (grey) and #10 (orange) led to an accelerated subunit exchange which was recorded for approximately 17 hours.

4.4.2.2 NMR Titration of compounds #6 and #10

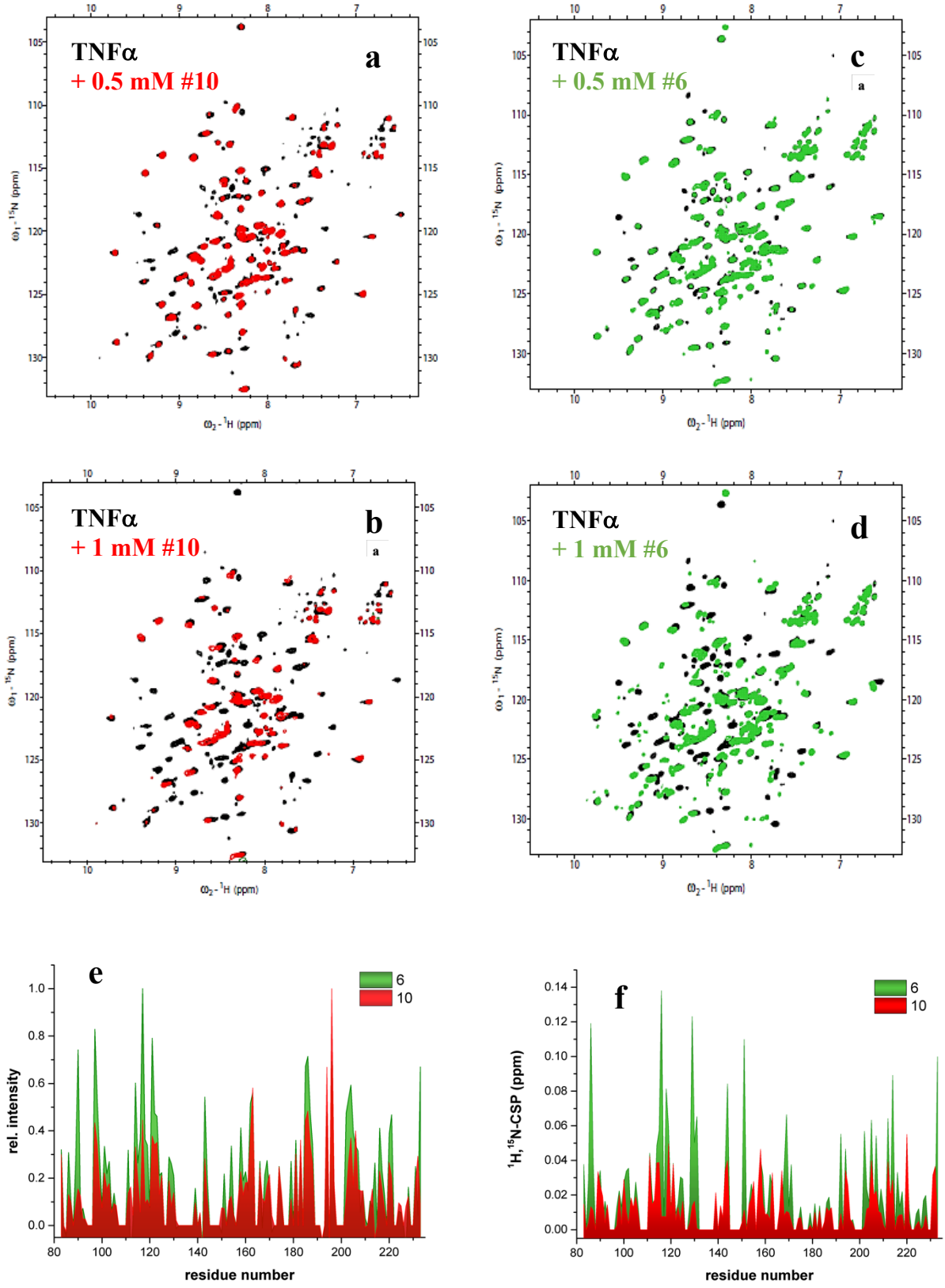

Figure 47: NMR-based titration of TNFα and compounds #6 and #10. (a, b) ^{1}H, ^{15}N-Trosy spectra of TNFα in presence of 0.5 mM and 1 mM compound #10, respectively. (c, d) ^{1}H, ^{15}N-Trosy spectra of TNFα in presence of 0.5 mM and 1 mM compound #6, respectively. (e) relative intensity plot of TNFα signal intensity decrease in presence of 1 mM #6 (green) or 1 mM #10 (red). (f) ^{1}H, ^{15}N-CSP Plot of TNFα signal shift in presence of 1 mM #6 (green) or 1 mM #10 (red).

The most promising fragments, namely #6 and #10, were subjected to an NMR-based titration series (Figure 47). Although structurally similar, the two compounds show drastically different effects with increasing concentrations. Compound #10 leads to a clearly visible intensity decrease or even signal loss by just looking at the spectral overlays. The relative intensity analysis demonstrates that overall reduction in signal intensity is more pronounced for compound #10 compared to compound #6. Although, visualization of the intensity decay (Figure 48) for one selected residue each within the hydrophobic interaction interface shows that both compounds lead to comparable K_D values of 320 µM for compound #10 and 360 µM for compound #6.

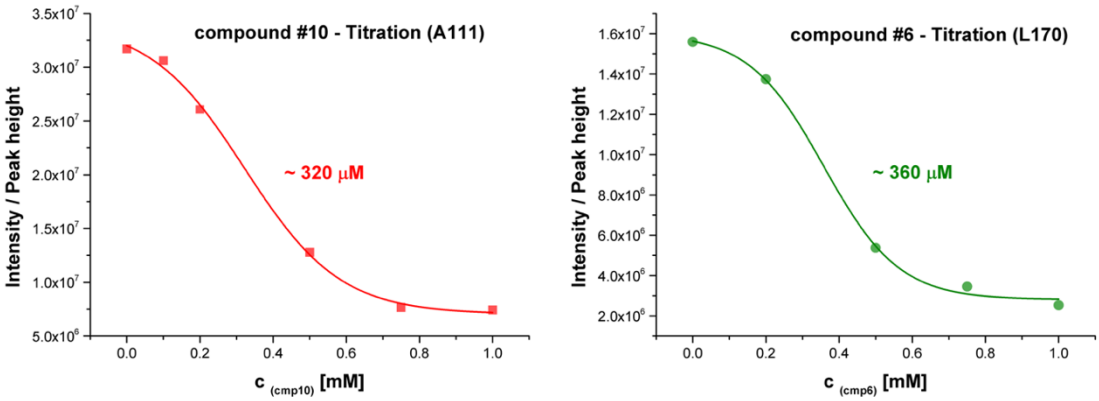

Figure 48: Estimation of an apparent KD values for compounds #10 (left) and #6 (right) for a chosen residue, respectively.

Most interestingly, compound #6 causes pronounced concentration-dependent chemical shift perturbations in the slow exchange regime for most of the signals leading to an observable second set of signals which is shifting towards the second species with further increase of compound concentration as shown here for glycine 116 (Figure 49).

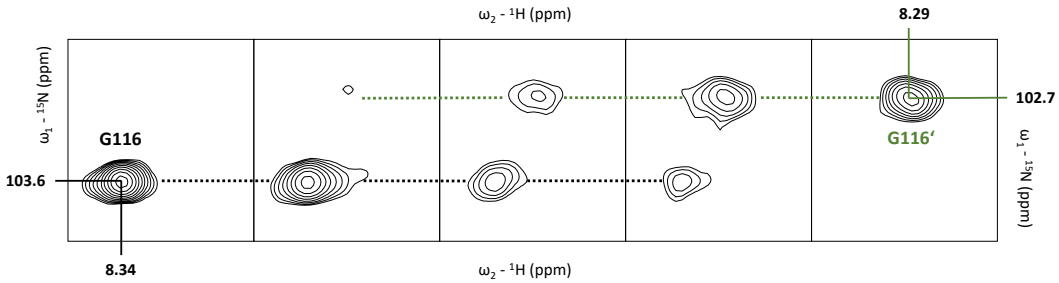

Figure 49: Chemical Shift analysis for compound #6 and glycine 116. Increasing concentrations of compound #6 leads to an upcoming second set of signals starting at an equimolar concentration of 0.2 mM. At a compound concentration of 0.75 mM the second signal is the more dominant one. At 1 mM compound concentration the initial signal is no longer detectable.

Considering the homotrimeric oligomerization state of TNFα and the observed signal intensity loss for residues at the subunit interaction interface, these data might hint to a stepwise loosening of the trimerization interface.

4.5 Biophysical analysis of TNFα-TM

4.5.1 Expression and purification

The expression test of the TNFα transmembrane domain was positive for expression of GB1-TNFα-TM (Figure 50, (a)). Size exclusion of the NiNTA elution fraction displays a nicely shaped peak and the corresponding SDS gel shows GB1-TNFα-TM as smeared bands at around 17 kDa (Figure 50, (b)). Higher molecular weight bands are also clearly visible hinting to a tendency of TNFα-TM to form oligomers. Upon Thrombin digest and removal of the GB1-tag, the TM domain lacks an extinction coefficient, therefore the final size exclusion chromatography was performed with a wavelength detection at 205 and 220 nm (Figure 50, (c)). Different constructs for TNFα-TM were generated within this thesis according to the respective purpose (Figure 50, (d)). Initial extension of a GS-linker was crucial to enable efficient thrombin cleavage. This construct was used for structure determination. Introduction of a C-terminal Sortase A motif was needed for enzymatic coupling and generation of full length TNFα. The construct bearing 23 additional amino acids at the C-terminal end was subjected to crosslinking trials using trifunctional TMEA crosslinker.

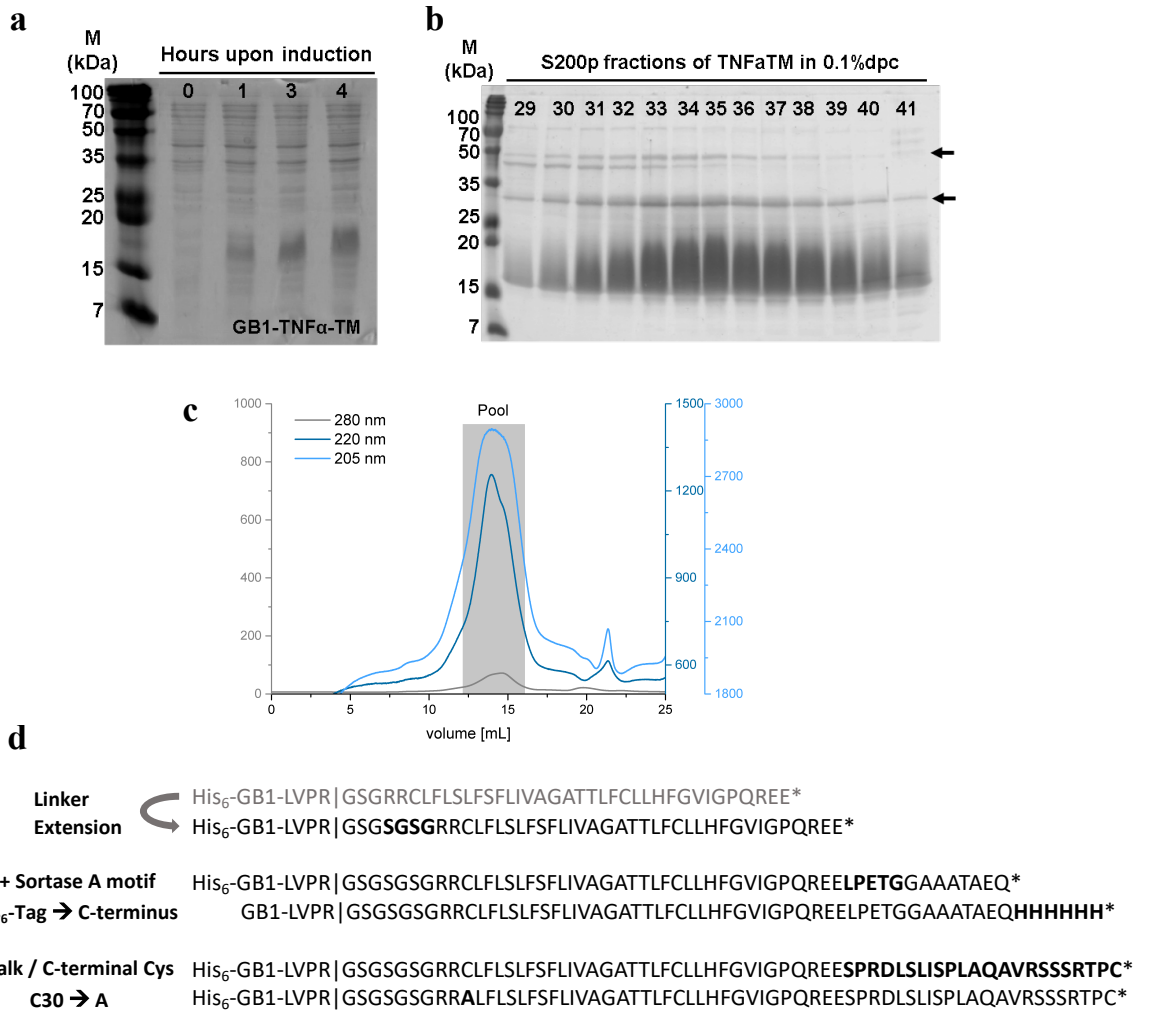

Figure 50: TNFα-TM Expression and purification. (a) Expression test SDS Page shows an intensifying band at around 17 kDa for GB1-TNFα-TM upon induction. (b) SDS Page of S200p size exclusion fractions upon NiNTA purification. Arrows indicate oligomerization of GB1-TNFα-TM. (c) S200a size exclusion chromatogram with multiple wavelength detection and pooled fractions. (d) Constructs of TNFα-TM generated within this thesis. Initial linker extension was necessary for efficient thrombin cleavage. All constructs behaved in a similar way regarding expression yield and purification.

4.5.2 Investigation of TNFα-TM monomer vs. trimer

4.5.2.1 Oligomeric state in MSP1D1ΔH5 nanodiscs

Insertion of TNFα-TM into MSP1D1ΔH5 Nanodiscs was performed at 2 different ratios. The standard ratio of 1:4 (TNFαTM:MSP1D1ΔH5) was used to guarantee an insertion corresponding to the natural oligomeric state since there is an excess of Nanodiscs even if the helix inserts as a monomer. The second ratio used, 3:2 (TNFα-TM:MSP1D1ΔH5), was chosen to force an insertion as a trimer since in theory 3 helices have to be embedded in one Nanodisc

encircled by 2 MSP molecules. Figure 51 shows the SEC profiles for both assemblies after thrombin digest.

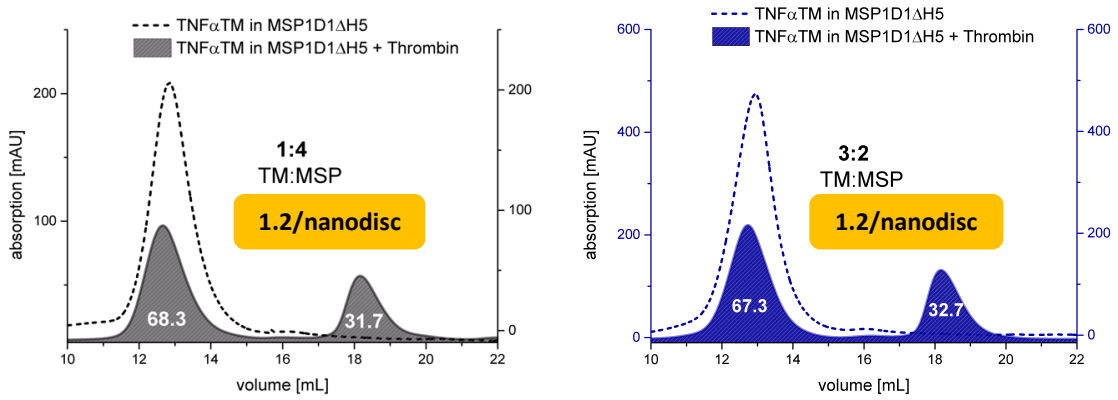

Figure 51: Determination of TNFα-TM oligomeric state in nanodiscs. Nanodisc assembly was performed with a 4:1 excess of MSP protein to TNFα-TM and a ratio of 3:2 (MSP: TNFα-TM) in order to drive insertion of TNFα-TM trimer into one nanodisc. Peak integrals used for calculation are indicated in white below the respective peak. The ratio of number of helices per nanodisc is highlighted with an orange rectangle.

Irrespective of the ratio used for insertion of TNFα-TM into lipid Nanodiscs, the calculations resulted in approx. 1.2 helices/Nanodisc. These results are controversial considering the fact that especially the 3:2 ratio wouldn't allow a monomeric helix to be inserted except 2/3 of TNFα-TM would have been precipitated, but no precipitation was detected. Nevertheless, it seems that the standard ratio of 1:4 promotes an insertion of a monomeric helix suggesting that the TNFα-TM domain does not self-assemble into trimers but that the trimeric state is driven by non-covalent assembly of the TNFα ECD.

4.5.2.2 Mimicking the trimeric state of the transmembrane helix

Investigation of the oligomeric state of TNFα-TM in Nanodiscs confirmed that the transmembrane helix itself does not seem to self-assemble into trimers but that it is rather the trimeric soluble domain that promotes the trimeric state. In order to mimic the trimeric conformation that seems to be driven by homo trimerization of the TNFα soluble domain, the idea was to use a trifunctional crosslinker (TMEA) to chemically crosslink the helices close at the transition to the structured ECD domain. The transmembrane domain construct was therefore extended for the stalk region connecting the ECD and the TM domain. An introduced cysteine residue marks the C-terminus in terms of cysteine-specific crosslinking. Naturally

occurring cysteine 30 was mutated to alanine (C30A) to avoid any unwanted crosslinking reaction. Although EDTA and protease inhibitor cocktail was used throughout the whole purification, ESI-MS analysis of the purified TM construct points out that the stalk region sequence is directed to spontaneous cleavage events (Figure 52). Directly upon purification two additional masses appear which increase drastically upon storage of TNFαTM-C at +4°C (Figure 50). The cleavage pattern was reproducible. The first cleavage site (A|QAV---) was found to be close to the natural ADAM17 cleavage site (---AQA|V---), the second site was six amino acids upstream still within the stalk region. The data indicate that the TNFα stalk region is intrinsically unstable if not protected via o-glycosylation.

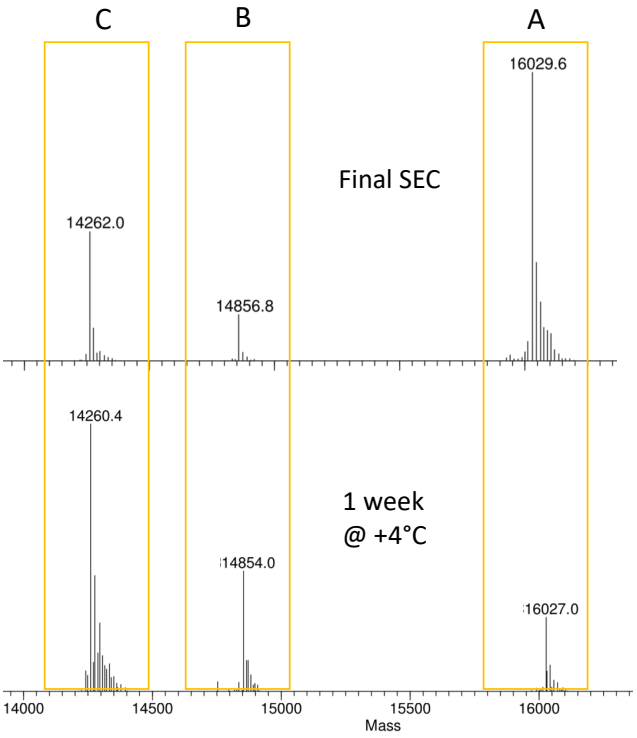

	Sequence	Observed mass [Da]	Calculated mass [Da]
A	His_6-GB1-THR-SGSGSGRRALFLSLFSFLIVAGA TTLFCLLHFGVIGPQREESPRD LSLISPLAQAVRSSSRTPC	16029.6 16027.0	16033.98
B	His_6-GB1-THR-SGSGSGRRALFLSLFSFLIVAGA TTLFCLLHFGVIGPQREESPRD LSLISPLA~~QAVRSSSRTPC~~	14856.8 14854.0	14860.67
C	His_6-GB1-THR-SGSGSGRRALFLSLFSFLIVAGA TTLFCLLHFGVIGPQREESPRD ~~LSLISPLAQAVRSSSRTPC~~	14262.0 14260.4	14265.92

Figure 52: Mass spectrometric analysis of TNFαTM-C construct. Three distinct masses corresponding to (A) the native sequence and (B, C) two cleavage products were detected and cleavage sites were assigned to the stalk region that seems to be intrinsically unstable.

4.6 Production of TNFα-Full length (FL)

4.6.1 Sortase A-mediated protein ligation

Sortase A-mediated ligation was performed similar to the published protocol for Bcl-xl protein[161]. However, the coupling reaction was carried out in a DPC micelle environment rather than starting with a nanodisc-inserted TM helix. TNFαTM was shown to not self-assemble into trimers, therefore, in order to create the native full-length trimer, the idea was to first generate the full-length protein and to insert the trimer into nanodiscs afterwards.

In general, three important factors have to be taken into account:

(i) TNFα ECD has to be purified freshly and subsequently used in the coupling reaction. Optionally, a frozen stock can be thawed prior to reaction.

(ii) TNFα ECD should be saturated with excess TNFαTM-SOR-His_6, since all uncoupled TNFα ECD would engage in mixed trimer assembly.

(iii) Ca^{2+} should be excluded from the reaction conditions to avoid additional metal-catalyzed cleavage of TNFα ECD.

Full-length TNFα (TNFαFL) was successfully ligated which is indicated by the band appearing at around 35 kDa in addition to a decrease in band intensity for TNFα as well as TNFαTM (Figure 53). The importance of using freshly purified TNFα is underlined by comparing the

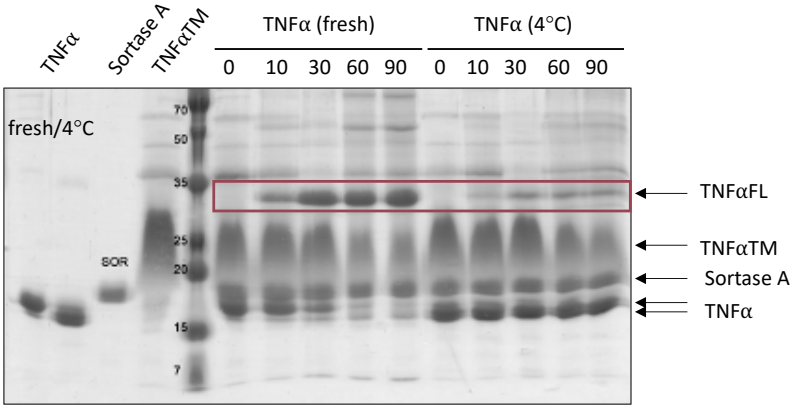

Figure 53: Time course of Sortase A-catalyzed ligation reaction for generation of full-length TNFα. The ligation product TNFα-FL is indicated with a red rectangle.

coupling yield achieved in case of “fresh” and “4°C” protein. Although, TNFα was stored at +4 °C in presence of EDTA, autocatalysis cannot be prevented over a long period time.

After 90 minutes, the reaction mixture was applied to NiNTA affinity chromatography in order to remove His-Tag bearing Sortase A enzyme and excess TNFαTM-SOR-His_6. The flow-through fraction was applied to size exclusion chromatography.

4.6.2 Get3-assisted co-expression of TNFαFL

4.6.2.1 Expression and purification

The ATPase Get3 was identified as a key factor in the posttranslational membrane insertion machinery of tail-anchored proteins by specifically binding to the transmembrane domain and delivering it to the membrane[162,163]. In order to investigate the native full-length protein, Z-tag-TEV-TNFαFL was concomitantly expressed together with MBP-TEV-Get3 inserted in a pT5L/T7 plasmid (kindly provided by Prof. Dr. Blanche Schwappach-Pignataro, University of Göttingen). Figure 54, (a) shows the expression test in *E. coli* BL21 (DE3). The band ~ 80 kDa corresponds to MBP-Get3 fusion while the band at about 42 kDa is the Z-tag-TEV-TNFαFL construct, thus both parts were successfully expressed.

Initial purification by a series of on-column washing steps followed by size exclusion chromatography was not sufficient to yield a pure TNFα-FL protein band (Figure 54, (b, c)). In order to improve the purity, the SEC Pool was transferred back to a NiNTA column and washed extensively. SDS PAGE analysis of a S200a size exclusion chromatography clearly demonstrates that an additional NiNTA caused metal-catalyzed cleavage of the ECD (Figure 54, (d)).

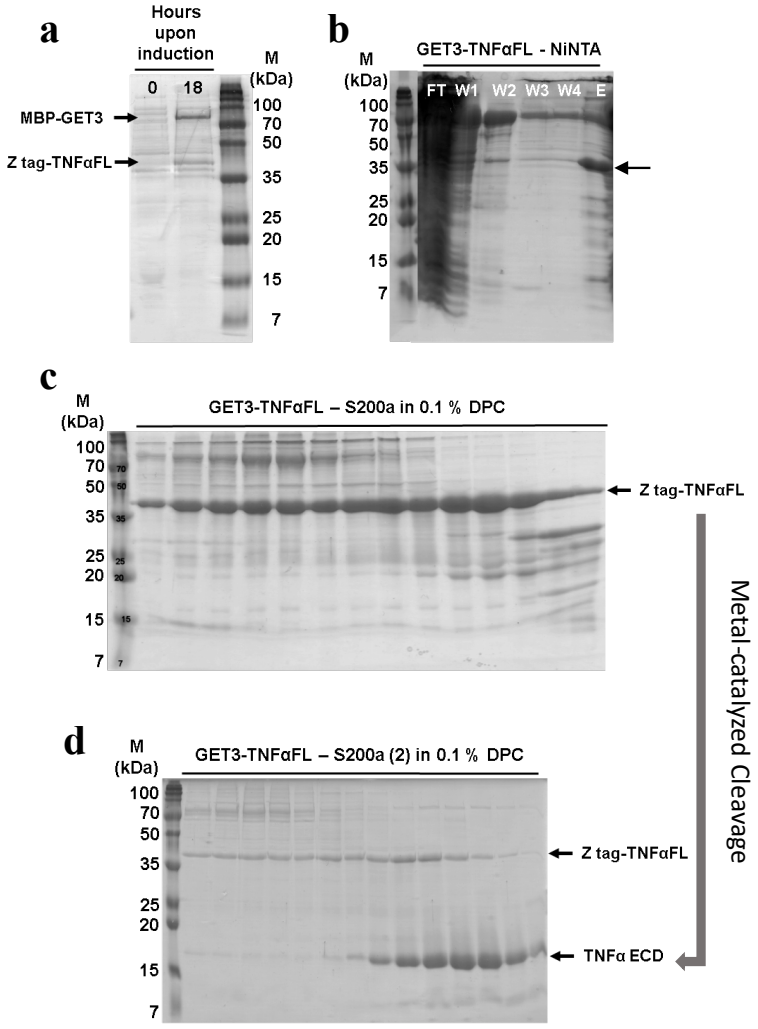

Figure 54: Production of TNFα-FL using Get3 co-expression. (a) Expression test SDS Page indicates successful expression of both fusion proteins, namely MBP-Get3 and Z-tag-TNFα-FL. (b) NiNTA affinity purification of Z-tag- TNFα-FL (black arrow). (c) SDS Page of S200a size exclusion chromatography of NiNTA elution fraction. (d) SDS Page of S200a SEC following an additional NiNTA purification attempt. Metal-catalyzed cleavage leads to appearance of TNFα ECD

5 DISCUSSION

5.1 Inherent substrate flexibility is a feature of γ-secretase substrates

The list of putative γ-secretase substrates includes over 90 reported proteins[164] which seem to have nothing in common except being type I transmembrane proteins and having undergone ectodomain shedding[59,165]. Owing to a lack in sequence homology, the aim of studying TREM2-TM was to expand the scientific knowledge of protein features that define γ-secretase substrates and to link these features to γ-secretase cleavage.

Within this thesis a purification protocol was established for high yield production of wild-type TREM2-TM along with its different charge variants, namely K186A, K186L, K186P and K186N. A comprehensive investigation using solution NMR experiments, CD spectroscopic analysis and a γ-secretase cleavage assay provides insights into intramembrane interaction with signaling partner DAP12, structural and dynamical changes upon charge removal and how γ-secretase selects for its substrates.

TREM2-TM demonstrates an inherent flexibility due to its positively charged lysine residue, which is required for complex formation with DAP12. Without DAP12, the free charge aims for the phospholipid headgroup region causing a short stretch in the TREM2-TM C-terminal region lacking secondary structure and showing increased dynamics. γ-secretase cleavage occurs in this unwound stretch region. By contrast, deletion of the charge (K186A) induces a continuous α-helix which gets cleaved as well but the cleavage site is shifted C-terminally to the end of the rigid α-helix. Based on this observed vertical shift, a piston-like movement of the TREM2-TM helix once it has entered the substrate cavity of γ-secretase seems likely (Figure 55). Recognition of a TM position where C-terminal local unwinding is feasible for γ-secretase determines the cleavage site. Thus, the substrate sampling mechanism of γ-secretase is likely to include screening for local instability and inherent flexibility.

Flexibility induced by lysine 186 in wild-type TREM2-TM is crucial looking at the sequence comparison with γ-secretase substrates APP and Notch-1. The α-helical stretch succeeding the cleavage site is longer in case of TREM2 and required for DAP12 binding. Thus, the unfolded kink region in absence of DAP12 presents the correct cleavage site which is underlined by the fact that K186A gets cleaved 3 amino acids downstream of the wild-type protein. The shorter α-helical stretches in APP and Notch-1 in addition to polar and charged amino acids outside the membrane most likely replace the requirement for an unstructured kink. Interestingly, the three substrates share a polar amino acid in the -2 position to the cleavage site. By contrast to APP (ITL), these polar amino acids are flanked by small amino acids in TREM2 (ASA) and Notch-1 (GCG) facilitating local unfolding by γ-secretase. Instead, APP has a polar threonine

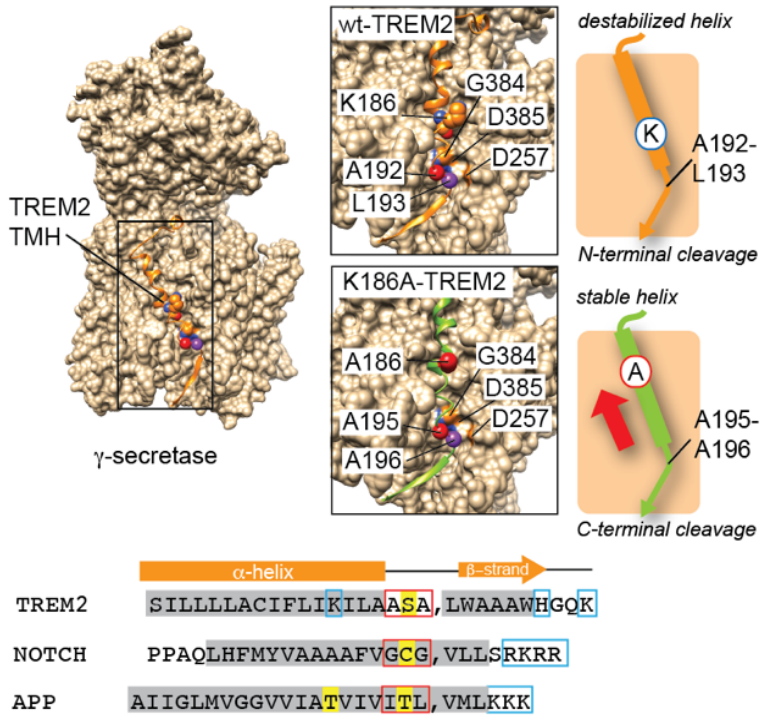

Figure 55: (*Left*) Structural model of the complex of TREM2-TM wild-type and γ-secretase obtained by docking guided by the cryo-EM structure of the γ-secretase-NOTCH complex (Ref [57]). (*Middle and right*) TREM2-TM wild-type in the active site of γ-secretase in a register that would lead to cleavage between residues A192 and L193 (marked by spheres in red and purple), as detected by mass spectrometry. The K186 residue in TREM2 is also shown as well as the catalytically relevant residues in γ-secretase (D385 and D257). In TREM2-TM K186A, the register of the helix moves upwards leading to positioning of A195 and A196 in the active site. The C-terminal end of the helix needs to be unwound by γ-secretase, thus, the intrinsic stability of the helical substrate is a critical determinant of the cleavage position.(*Bottom*) Amino acid sequence comparison of TREM2-TM wild-type with Notch1 and APP. α-helical secondary structure elements in the free form of each protein are labeled by grey boxes. Positively charged residues are marked by blue and polar residues close to the cleavage site (indicated by the comma mark) by yellow boxes. Red boxes indicate the unfolded sequence stretches in the bound state preceding the cleavage site. The secondary structure of the substrate helices (or derived from the structural model for TREM2-TM) in complex with γ-secretase is shown above.

at the same position as the charged lysine in TREM2, which might be involved in further destabilization of the APP helix.

The initial cleavage event at the ε-site probably decreases the energy cost of local helix unwinding by lowering the overall substrate stability therefore facilitating subsequent cleavage events at substrate γ-sites. Studies on TREM2-TM provide scientific evidence regarding substrate sampling by means of inherent flexibility.

5.2 O-glycosylation protects TNFα from metal-catalyzed proteolysis

O-linked glycosylation[166] of secreted or membrane-bound proteins is a post-translationally modification and refers in this specific case to the attachment of glycans to serine or threonine residues. This modification takes place in the cis-Golgi compartment after folding of the protein occurred. O-linked glycosylation is involved in trafficking, enhances solubility and enables cell-to-cell contact. Additionally, it was shown that O-glycosylation in the juxtamembrane region of cell membrane proteins leads to an extension and stabilization of the stem region structure and prevents or downregulates proteolysis, respectively[167].

Increased serum TNFα is related to severe autoimmune diseases and since it was shown that overexpression of TNFα-converting enzyme (TACE) does not lead to aberrant proteolytic activity in vivo[168], a lot of studies focused on the substrate itself. TNFα is post-translationally modified via O-glycosylation at serine 80[104] and loss of this modification enhances metalloprotease-mediated shedding between alanine 76 and valine 77[169]. Recombinantly expressed TNFα within this thesis naturally lacks this O-glycosylation and it was shown that proteolytic cleavage mediated by divalent cations occurs at a distinct site, namely N-terminally of serine 80. The spontaneous cleavage promoting effect of zinc at serine and threonine residues was already demonstrated[170,171]. Zinc is a major trace metal and known to be involved in many biological processes[172]. Here, it was shown that also other divalent ions like Mg^{2+}, Co^{2+}, Ca^{2+},

Ni^{2+} and Cu^{2+} are capable of inducing spontaneous cleavage. Interestingly, zinc only caused partial proteolysis compared to the other metal ions.

Extension of the transmembrane construct of TNFα over the stalk region (Figure 56) showed cleavage as well although the pattern is different but reproducible underlining the importance of protective O-glycosylation in the TNFα stalk region.

GB1-LVPR|GSGGLISPLAQAVRS|SSRTPSDK---
GB1-LVPRGSGSGSGRRALFLSLFSFLIVAGATTLFCLLHFGVIGPQREESPRDLS|LISPLA|QAVRSSSRTPC

Figure 56: Cleavage within the TNFα stalk region as seen for (upper line) TNFα ECD after thrombin cleavage. The peptide bond is specifically cleaved after serine 80. In case of TNFαTM-C (lower line) cleavage occurs at two distinct sites N-terminally of Q75 and L69, respectively. Cleavage sites are indicated with red lines.

To further investigate the mode of O-glycosylation-mediated protection, it might be worth thinking about exploiting strategies to attach the glycan moieties and to study the effects of O-glycosylation on the TNFα stalk region. It was shown that O-glycosylation can be achieved by using *in vivo* co-expression with the truncated and therefore soluble version of human glycosyltransferase GalNAc-T2 in *E. coli*[173]. Alternatively, one might use the published protocol for recombinant expression and refolding from inclusion bodies of full-length GalNAc-T2 to perform the same reaction *in vitro*[174]. Besides enzyme-mediated O-glycosylation, also chemical ligation of glycan moieties to an introduced cysteine residue using a "click thiol-ene coupling" approach might represent a nice way to perform the glycan attachment[175].

5.3 Production of full-length TNFα is not trivial but feasible

Lack of O-glycosylation and consequently metal-catalyzed cleavage was also an issue with respect to the production of full-length protein using either Sortase A-mediated ligation or Get3 co-expression. Both methods yielded full-length TNFα protein but displayed several obstacles that need to be overcome.

Using Sortase A enzyme, production of TNFα-FL was initially hampered by the necessity of adding $CaCl_2$ to guarantee efficient enzyme function. After investigation of metal-catalyzed cleavage within a triple serine motif in the TNFα sequence, this problem could be circumvented by introducing a Ca^{2+} independent Sortase A enzyme. However, omitting calcium drastically reduced the cleavage effect but didn't abolish it. By working under highly optimized conditions it should be possible to reduce the portion of TNFα ECD which undergoes cleavage and consequently co-elutes due to its trimeric nature down to a negligible amount.

Co-Expression with Get3 also yielded full-length TNFα but metal-catalyzed cleavage was detected after loading the protein sample back onto a NiNTA affinity column. It might be possible to circumvent the cleavage by rather continue working with a "dirty" protein sample instead of risking cleavage by repeatedly confronting the sample with divalent ions, here Ni^{2+}.

Another problem which needs to be addressed regarding both approaches is the presence of DPC, especially the drastic increase if concentration steps are required. The transmembrane portion of TNFα is stable in different detergents, e.g. DDM but the purity is much higher if DPC was used throughout the purification protocol. It might be advisable to exchange the detergent prior to Sortase A reaction or after the NiNTA series of washing steps in case of Get3 co-expression to minimize the destructive effect of the harsh DPC detergent on the soluble domain which was determined to drastically increase the helical content of TNFα ECD already

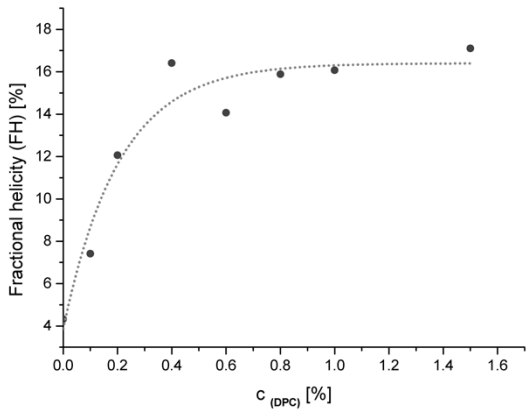

Figure 57: Increase of TNFα ECD helical content due to increasing DPC concentration measured by CD spectroscopy.

within the range of 0 to 0.4 % DPC (Figure 57). It seems crucial to stay close to the CMC of DPC (0.05 %) or slightly above in order to protect the ECD from irreversible damage.

In summary, both methods are suitable to yield full-length TNFα and investigation of membrane-tethered precursor TNFα is still a white spot within the extensive scientific knowledge about TNFα which could be filled by purifying the protein as described here, inserting it into lipid nanodiscs and studying TNFα-FL in a native lipid environment.

5.4 A comprehensive approach for screening and evaluation of TNFα small molecule inhibition was established

Targeting Protein-Protein Interactions (PPI) using small "drug-like" molecules is associated with the term "reaching for the high hanging fruit"[176]. PPI are crucial regulatory events in both physiology and pathology and represent a huge target space for pharmacological intervention. This immense potential for drug development is challenged by two main reasons which are both linked to the nature of a PPI interface. Firstly, the contact surface of two proteins is usually large with a buried area of approximately 1500-3000 Å involving a multitude of polar and hydrophobic interactions[177] which is in strong contrast to the deep cavities of about 300-500 Å that bind small molecules[178]. Secondly, the contact areas are generally flat and therefore limit the binding site to one side of the molecule which is less efficient than contacting more sides in a deep cavity. The identification of "hot spots" at the center of these contact surfaces which show suitable features for small molecule targeting, like hydrophobicity and conformational adaptivity, suggests that some PPI can be targeted by disrupting the interactions mediated by hot spot residues[179,180].

Despite seeking for orthosteric or competitive small molecule inhibitors which directly bind within the interaction interface, pharmaceutical studies nowadays involve method development for identification of allosteric binding sites and discovering small molecules that modulate the activity of proteins by binding to these allosteric sites[181-183].

Fragment-based drug discovery (FBDD)[184] is a powerful method for discovering high-affinity drug candidates demonstrated by numerous success stories[185-187]. FBDD offers several advantages over conventional High-Throughput Screening (HTS) which are mostly based on the smaller size and lower complexity of the fragments. The term "fragment" is commonly used for small molecules with less than 25 heavy atoms and a molecular weight < 250 Da. Therefore, analogs are simpler to synthesize or can even be purchased commercially, a greater chemical space can be covered, and target binding is not restrained by the rest of the molecule. NMR is especially suitable for fragment-based screening because binding events can directly be observed and usually do not suffer from false-positive Hit identification[188].

The objective was the identification of fragments that potently interact with the hydrophobic core of TNFα thereby disturbing the trimeric assembly consequently leading to an allosteric inhibition of protein-protein interaction with its receptor.

Using a STD NMR-based fragment screening approach followed by 2D HSQC validation, 17 compounds were identified to exert an effect on TNFα. Four of them (#2, #6, #10 and #13) showed the most drastic effects and were used to establish screening methods to further evaluate the respective effect. While #13 was discarded, the remaining three demonstrated concentration dependent loosening of the trimer in a FRET-based study of monomeric subunit exchange, in a qPCR-based detection of exposed protein areas using a hydrophobic dye or in NMR-based titration experiments. Interestingly, the two lead compounds #6 and #10 show a similar chemical structure but seem to have different modes of action especially looking at the NMR titration data. A set of second-round compounds that showed structural similarity to the first-round hits were tested and could either not improve existing effects or didn't demonstrate interaction with TNFα at all. This might hint already to a good structure-activity relationship (SAR) of compounds #6 and #10 and further modifications and analyses could pave the way for identification of potent small molecule inhibitors.

To sum up, a solid protocol was established to comparatively investigate the potency and mode of action of compounds on TNFα identified in a fragment-based screening.

REFERENCES

1. Uhlen, M. et al. Proteomics. Tissue-based map of the human proteome. *Science* **347**, 1260419 (2015).
2. Overington, J.P., Al-Lazikani, B. & Hopkins, A.L. How many drug targets are there? *Nat Rev Drug Discov* **5**, 993-6 (2006).
3. Rask-Andersen, M., Almen, M.S. & Schioth, H.B. Trends in the exploitation of novel drug targets. *Nat Rev Drug Discov* **10**, 579-90 (2011).
4. Bill, R.M. et al. Overcoming barriers to membrane protein structure determination. *Nat Biotechnol* **29**, 335-40 (2011).
5. Loll, P.J. Membrane protein structural biology: the high throughput challenge. *J Struct Biol* **142**, 144-53 (2003).
6. Wiener, M.C. A pedestrian guide to membrane protein crystallization. *Methods* **34**, 364-72 (2004).
7. White, S.H. The progress of membrane protein structure determination. *Protein Sci* **13**, 1948-9 (2004).
8. Bai, X.C., McMullan, G. & Scheres, S.H. How cryo-EM is revolutionizing structural biology. *Trends Biochem Sci* **40**, 49-57 (2015).
9. Miao, Y. & Cross, T.A. Solid state NMR and protein-protein interactions in membranes. *Curr Opin Struct Biol* **23**, 919-28 (2013).
10. Almen, M.S., Nordstrom, K.J., Fredriksson, R. & Schioth, H.B. Mapping the human membrane proteome: a majority of the human membrane proteins can be classified according to function and evolutionary origin. *BMC Biol* **7**, 50 (2009).
11. Bormann, B.J., Knowles, W.J. & Marchesi, V.T. Synthetic peptides mimic the assembly of transmembrane glycoproteins. *J Biol Chem* **264**, 4033-7 (1989).
12. MacKenzie, K.R., Prestegard, J.H. & Engelman, D.M. A transmembrane helix dimer: structure and implications. *Science* **276**, 131-3 (1997).
13. Mineev, K.S. et al. Dimeric structure of the transmembrane domain of glycophorin a in lipidic and detergent environments. *Acta Naturae* **3**, 90-8 (2011).
14. Trenker, R., Call, M.E. & Call, M.J. Crystal Structure of the Glycophorin A Transmembrane Dimer in Lipidic Cubic Phase. *J Am Chem Soc* **137**, 15676-9 (2015).
15. Cymer, F., Veerappan, A. & Schneider, D. Transmembrane helix-helix interactions are modulated by the sequence context and by lipid bilayer properties. *Biochim Biophys Acta* **1818**, 963-73 (2012).
16. Lemmon, M.A. et al. Glycophorin A dimerization is driven by specific interactions between transmembrane alpha-helices. *J Biol Chem* **267**, 7683-9 (1992).
17. Teese, M.G. & Langosch, D. Role of GxxxG Motifs in Transmembrane Domain Interactions. *Biochemistry* **54**, 5125-35 (2015).
18. Call, M.E., Wucherpfennig, K.W. & Chou, J.J. The structural basis for intramembrane assembly of an activating immunoreceptor complex. *Nat Immunol* **11**, 1023-9 (2010).
19. Russ, W.P. & Engelman, D.M. The GxxxG motif: a framework for transmembrane helix-helix association. *J Mol Biol* **296**, 911-9 (2000).
20. Dawson, J.P., Weinger, J.S. & Engelman, D.M. Motifs of serine and threonine can drive association of transmembrane helices. *J Mol Biol* **316**, 799-805 (2002).
21. Ridder, A., Skupjen, P., Unterreitmeier, S. & Langosch, D. Tryptophan supports interaction of transmembrane helices. *J Mol Biol* **354**, 894-902 (2005).
22. Unterreitmeier, S. et al. Phenylalanine promotes interaction of transmembrane domains via GxxxG motifs. *J Mol Biol* **374**, 705-18 (2007).
23. Herrmann, J.R. et al. Complex patterns of histidine, hydroxylated amino acids and the GxxxG motif mediate high-affinity transmembrane domain interactions. *J Mol Biol* **385**, 912-23 (2009).

24. Choma, C., Gratkowski, H., Lear, J.D. & DeGrado, W.F. Asparagine-mediated self-association of a model transmembrane helix. *Nat Struct Biol* **7**, 161-6 (2000).
25. Gratkowski, H., Lear, J.D. & DeGrado, W.F. Polar side chains drive the association of model transmembrane peptides. *Proc Natl Acad Sci U S A* **98**, 880-5 (2001).
26. Petros, A.M., Olejniczak, E.T. & Fesik, S.W. Structural biology of the Bcl-2 family of proteins. *Biochim Biophys Acta* **1644**, 83-94 (2004).
27. Eck, M.J. & Sprang, S.R. The structure of tumor necrosis factor-alpha at 2.6 A resolution. Implications for receptor binding. *J Biol Chem* **264**, 17595-605 (1989).
28. Garrett, T.P. et al. Crystal structure of a truncated epidermal growth factor receptor extracellular domain bound to transforming growth factor alpha. *Cell* **110**, 763-73 (2002).
29. Jura, N. et al. Mechanism for activation of the EGF receptor catalytic domain by the juxtamembrane segment. *Cell* **137**, 1293-307 (2009).
30. Sako, Y., Minoghchi, S. & Yanagida, T. Single-molecule imaging of EGFR signalling on the surface of living cells. *Nat Cell Biol* **2**, 168-72 (2000).
31. Moriki, T., Maruyama, H. & Maruyama, I.N. Activation of preformed EGF receptor dimers by ligand-induced rotation of the transmembrane domain. *J Mol Biol* **311**, 1011-26 (2001).
32. Arkhipov, A. et al. Architecture and membrane interactions of the EGF receptor. *Cell* **152**, 557-69 (2013).
33. Bargmann, C.I., Hung, M.C. & Weinberg, R.A. Multiple independent activations of the neu oncogene by a point mutation altering the transmembrane domain of p185. *Cell* **45**, 649-57 (1986).
34. Fleishman, S.J., Schlessinger, J. & Ben-Tal, N. A putative molecular-activation switch in the transmembrane domain of erbB2. *Proc Natl Acad Sci U S A* **99**, 15937-40 (2002).
35. Bell, C.A. et al. Rotational coupling of the transmembrane and kinase domains of the Neu receptor tyrosine kinase. *Mol Biol Cell* **11**, 3589-99 (2000).
36. Arkhipov, A., Shan, Y., Kim, E.T., Dror, R.O. & Shaw, D.E. Her2 activation mechanism reflects evolutionary preservation of asymmetric ectodomain dimers in the human EGFR family. *Elife* **2**, e00708 (2013).
37. Beevers, A.J. et al. Effects of the oncogenic V(664)E mutation on membrane insertion, structure, and sequence-dependent interactions of the Neu transmembrane domain in micelles and model membranes: an integrated biophysical and simulation study. *Biochemistry* **51**, 2558-68 (2012).
38. Siddig, A. et al. HER-2/neu Ile655Val polymorphism and the risk of breast cancer. *Ann N Y Acad Sci* **1138**, 84-94 (2008).
39. Meyers, G.A., Orlow, S.J., Munro, I.R., Przylepa, K.A. & Jabs, E.W. Fibroblast growth factor receptor 3 (FGFR3) transmembrane mutation in Crouzon syndrome with acanthosis nigricans. *Nat Genet* **11**, 462-4 (1995).
40. Eggers, S.D., Keswani, S.C., Melli, G. & Cornblath, D.R. Clinical and genetic description of a family with Charcot-Marie-Tooth disease type 1B from a transmembrane MPZ mutation. *Muscle Nerve* **29**, 867-9 (2004).
41. Bennasroune, A. et al. Transmembrane peptides as inhibitors of ErbB receptor signaling. *Mol Biol Cell* **15**, 3464-74 (2004).
42. Yin, H. et al. Computational design of peptides that target transmembrane helices. *Science* **315**, 1817-22 (2007).
43. Hebert, T.E. et al. A peptide derived from a beta2-adrenergic receptor transmembrane domain inhibits both receptor dimerization and activation. *J Biol Chem* **271**, 16384-92 (1996).
44. Li, Y.M. et al. Photoactivated gamma-secretase inhibitors directed to the active site covalently label presenilin 1. *Nature* **405**, 689-94 (2000).

45. Esler, W.P. et al. Transition-state analogue inhibitors of gamma-secretase bind directly to presenilin-1. *Nat Cell Biol* **2**, 428-34 (2000).
46. Seiffert, D. et al. Presenilin-1 and -2 are molecular targets for gamma-secretase inhibitors. *J Biol Chem* **275**, 34086-91 (2000).
47. Edbauer, D. et al. Reconstitution of gamma-secretase activity. *Nat Cell Biol* **5**, 486-8 (2003).
48. Sato, T. et al. Active gamma-secretase complexes contain only one of each component. *J Biol Chem* **282**, 33985-93 (2007).
49. Osenkowski, P. et al. Cryoelectron microscopy structure of purified gamma-secretase at 12 A resolution. *J Mol Biol* **385**, 642-52 (2009).
50. Esch, F.S. et al. Cleavage of amyloid beta peptide during constitutive processing of its precursor. *Science* **248**, 1122-4 (1990).
51. Vassar, R. et al. Beta-secretase cleavage of Alzheimer's amyloid precursor protein by the transmembrane aspartic protease BACE. *Science* **286**, 735-41 (1999).
52. Golde, T.E., Estus, S., Younkin, L.H., Selkoe, D.J. & Younkin, S.G. Processing of the amyloid protein precursor to potentially amyloidogenic derivatives. *Science* **255**, 728-30 (1992).
53. Hardy, J.A. & Higgins, G.A. Alzheimer's disease: the amyloid cascade hypothesis. *Science* **256**, 184-5 (1992).
54. Suzuki, N. et al. An increased percentage of long amyloid beta protein secreted by familial amyloid beta protein precursor (beta APP717) mutants. *Science* **264**, 1336-40 (1994).
55. Takami, M. et al. gamma-Secretase: successive tripeptide and tetrapeptide release from the transmembrane domain of beta-carboxyl terminal fragment. *J Neurosci* **29**, 13042-52 (2009).
56. Fluhrer, R. et al. A gamma-secretase-like intramembrane cleavage of TNFalpha by the GxGD aspartyl protease SPPL2b. *Nat Cell Biol* **8**, 894-6 (2006).
57. Yang, G. et al. Structural basis of Notch recognition by human gamma-secretase. *Nature* **565**, 192-197 (2019).
58. Zhou, R. et al. Recognition of the amyloid precursor protein by human gamma-secretase. *Science* **363**(2019).
59. Beel, A.J. & Sanders, C.R. Substrate specificity of gamma-secretase and other intramembrane proteases. *Cell Mol Life Sci* **65**, 1311-34 (2008).
60. Colonna, M. TREMs in the immune system and beyond. *Nat Rev Immunol* **3**, 445-53 (2003).
61. Bouchon, A., Dietrich, J. & Colonna, M. Cutting edge: inflammatory responses can be triggered by TREM-1, a novel receptor expressed on neutrophils and monocytes. *J Immunol* **164**, 4991-5 (2000).
62. Kober, D.L. et al. Neurodegenerative disease mutations in TREM2 reveal a functional surface and distinct loss-of-function mechanisms. *Elife* **5**(2016).
63. Sudom, A. et al. Molecular basis for the loss-of-function effects of the Alzheimer's disease-associated R47H variant of the immune receptor TREM2. *J Biol Chem* **293**, 12634-12646 (2018).
64. Hamerman, J.A. et al. Cutting edge: inhibition of TLR and FcR responses in macrophages by triggering receptor expressed on myeloid cells (TREM)-2 and DAP12. *J Immunol* **177**, 2051-5 (2006).
65. Lanier, L.L., Corliss, B.C., Wu, J., Leong, C. & Phillips, J.H. Immunoreceptor DAP12 bearing a tyrosine-based activation motif is involved in activating NK cells. *Nature* **391**, 703-7 (1998).

66. Mason, L.H., Willette-Brown, J., Taylor, L.S. & McVicar, D.W. Regulation of Ly49D/DAP12 signal transduction by Src-family kinases and CD45. *J Immunol* **176**, 6615-23 (2006).
67. Colonna, M. & Wang, Y. TREM2 variants: new keys to decipher Alzheimer disease pathogenesis. *Nat Rev Neurosci* **17**, 201-7 (2016).
68. Colonna, M. DAP12 signaling: from immune cells to bone modeling and brain myelination. *J Clin Invest* **111**, 313-4 (2003).
69. Daws, M.R. et al. Pattern recognition by TREM-2: binding of anionic ligands. *J Immunol* **171**, 594-9 (2003).
70. Wang, Y. et al. TREM2 lipid sensing sustains the microglial response in an Alzheimer's disease model. *Cell* **160**, 1061-71 (2015).
71. Atagi, Y. et al. Apolipoprotein E Is a Ligand for Triggering Receptor Expressed on Myeloid Cells 2 (TREM2). *J Biol Chem* **290**, 26043-50 (2015).
72. Bailey, C.C., DeVaux, L.B. & Farzan, M. The Triggering Receptor Expressed on Myeloid Cells 2 Binds Apolipoprotein E. *J Biol Chem* **290**, 26033-42 (2015).
73. Yeh, F.L., Wang, Y., Tom, I., Gonzalez, L.C. & Sheng, M. TREM2 Binds to Apolipoproteins, Including APOE and CLU/APOJ, and Thereby Facilitates Uptake of Amyloid-Beta by Microglia. *Neuron* **91**, 328-40 (2016).
74. Jendresen, C., Arskog, V., Daws, M.R. & Nilsson, L.N. The Alzheimer's disease risk factors apolipoprotein E and TREM2 are linked in a receptor signaling pathway. *J Neuroinflammation* **14**, 59 (2017).
75. Zhao, Y. et al. TREM2 Is a Receptor for beta-Amyloid that Mediates Microglial Function. *Neuron* **97**, 1023-1031 e7 (2018).
76. Zhong, L. et al. Amyloid-beta modulates microglial responses by binding to the triggering receptor expressed on myeloid cells 2 (TREM2). *Mol Neurodegener* **13**, 15 (2018).
77. Lammich, S. et al. Constitutive and regulated alpha-secretase cleavage of Alzheimer's amyloid precursor protein by a disintegrin metalloprotease. *Proc Natl Acad Sci U S A* **96**, 3922-7 (1999).
78. Wunderlich, P. et al. Sequential proteolytic processing of the triggering receptor expressed on myeloid cells-2 (TREM2) protein by ectodomain shedding and gamma-secretase-dependent intramembranous cleavage. *J Biol Chem* **288**, 33027-36 (2013).
79. Kleinberger, G. et al. TREM2 mutations implicated in neurodegeneration impair cell surface transport and phagocytosis. *Sci Transl Med* **6**, 243ra86 (2014).
80. Schlepckow, K. et al. An Alzheimer-associated TREM2 variant occurs at the ADAM cleavage site and affects shedding and phagocytic function. *EMBO Mol Med* **9**, 1356-1365 (2017).
81. Thornton, P. et al. TREM2 shedding by cleavage at the H157-S158 bond is accelerated for the Alzheimer's disease-associated H157Y variant. *EMBO Mol Med* **9**, 1366-1378 (2017).
82. Lichtenthaler, S.F., Haass, C. & Steiner, H. Regulated intramembrane proteolysis--lessons from amyloid precursor protein processing. *J Neurochem* **117**, 779-96 (2011).
83. Zhang, Y.W. et al. Presenilin/gamma-secretase-dependent processing of beta-amyloid precursor protein regulates EGF receptor expression. *Proc Natl Acad Sci U S A* **104**, 10613-8 (2007).
84. Schroeter, E.H., Kisslinger, J.A. & Kopan, R. Notch-1 signalling requires ligand-induced proteolytic release of intracellular domain. *Nature* **393**, 382-6 (1998).
85. Jiang, T. et al. A rare coding variant in TREM2 increases risk for Alzheimer's disease in Han Chinese. *Neurobiol Aging* **42**, 217 e1-3 (2016).
86. Jonsson, T. et al. Variant of TREM2 associated with the risk of Alzheimer's disease. *N Engl J Med* **368**, 107-16 (2013).

87. Jonsson, T. & Stefansson, K. TREM2 and neurodegenerative disease. *N Engl J Med* **369**, 1568-9 (2013).
88. Paloneva, J. et al. Mutations in two genes encoding different subunits of a receptor signaling complex result in an identical disease phenotype. *Am J Hum Genet* **71**, 656-62 (2002).
89. Sirkis, D.W., Aparicio, R.E. & Schekman, R. Neurodegeneration-associated mutant TREM2 proteins abortively cycle between the ER and ER-Golgi intermediate compartment. *Mol Biol Cell* **28**, 2723-2733 (2017).
90. Chen, C., Bonifacino, J.S., Yuan, L.C. & Klausner, R.D. Selective degradation of T cell antigen receptor chains retained in a pre-Golgi compartment. *J Cell Biol* **107**, 2149-61 (1988).
91. Bonifacino, J.S., Suzuki, C.K., Lippincott-Schwartz, J., Weissman, A.M. & Klausner, R.D. Pre-Golgi degradation of newly synthesized T-cell antigen receptor chains: intrinsic sensitivity and the role of subunit assembly. *J Cell Biol* **109**, 73-83 (1989).
92. Bonifacino, J.S., Cosson, P. & Klausner, R.D. Colocalized transmembrane determinants for ER degradation and subunit assembly explain the intracellular fate of TCR chains. *Cell* **63**, 503-13 (1990).
93. Bonifacino, J.S., Cosson, P., Shah, N. & Klausner, R.D. Role of potentially charged transmembrane residues in targeting proteins for retention and degradation within the endoplasmic reticulum. *EMBO J* **10**, 2783-93 (1991).
94. Wileman, T., Carson, G.R., Concino, M., Ahmed, A. & Terhorst, C. The gamma and epsilon subunits of the CD3 complex inhibit pre-Golgi degradation of newly synthesized T cell antigen receptors. *J Cell Biol* **110**, 973-86 (1990).
95. Wilson, M.J., Lindquist, J.A. & Trowsdale, J. DAP12 and KAP10 (DAP10)-novel transmembrane adapter proteins of the CD3zeta family. *Immunol Res* **22**, 21-42 (2000).
96. Garrity, D., Call, M.E., Feng, J. & Wucherpfennig, K.W. The activating NKG2D receptor assembles in the membrane with two signaling dimers into a hexameric structure. *Proc Natl Acad Sci U S A* **102**, 7641-6 (2005).
97. Call, M.E. et al. The structure of the zetazeta transmembrane dimer reveals features essential for its assembly with the T cell receptor. *Cell* **127**, 355-68 (2006).
98. Call, M.E. & Wucherpfennig, K.W. Molecular mechanisms for the assembly of the T cell receptor-CD3 complex. *Mol Immunol* **40**, 1295-305 (2004).
99. Lanier, L.L. DAP10- and DAP12-associated receptors in innate immunity. *Immunol Rev* **227**, 150-60 (2009).
100. Call, M.E. & Chou, J.J. A view into the blind spot: solution NMR provides new insights into signal transduction across the lipid bilayer. *Structure* **18**, 1559-69 (2010).
101. Pennica, D. et al. Human tumour necrosis factor: precursor structure, expression and homology to lymphotoxin. *Nature* **312**, 724-9 (1984).
102. Pocsik, E., Mihalik, R., Ali-Osman, F. & Aggarwal, B.B. Cell density-dependent regulation of cell surface expression of two types of human tumor necrosis factor receptors and its effect on cellular response. *J Cell Biochem* **54**, 453-64 (1994).
103. Stevenson, F.T., Bursten, S.L., Locksley, R.M. & Lovett, D.H. Myristyl acylation of the tumor necrosis factor alpha precursor on specific lysine residues. *J Exp Med* **176**, 1053-62 (1992).
104. Takakura-Yamamoto, R., Yamamoto, S., Fukuda, S. & Kurimoto, M. O-glycosylated species of natural human tumor-necrosis factor-alpha. *Eur J Biochem* **235**, 431-7 (1996).
105. Moss, M.L. et al. Cloning of a disintegrin metalloproteinase that processes precursor tumour-necrosis factor-alpha. *Nature* **385**, 733-6 (1997).

106. Friedmann, E. et al. SPPL2a and SPPL2b promote intramembrane proteolysis of TNFalpha in activated dendritic cells to trigger IL-12 production. *Nat Cell Biol* **8**, 843-8 (2006).
107. Vandenabeele, P., Declercq, W., Beyaert, R. & Fiers, W. Two tumour necrosis factor receptors: structure and function. *Trends Cell Biol* **5**, 392-9 (1995).
108. Wallach, D. et al. Soluble and cell surface receptors for tumor necrosis factor. *Agents Actions Suppl* **35**, 51-7 (1991).
109. Grell, M. et al. The transmembrane form of tumor necrosis factor is the prime activating ligand of the 80 kDa tumor necrosis factor receptor. *Cell* **83**, 793-802 (1995).
110. Moudgil, K.D. & Choubey, D. Cytokines in autoimmunity: role in induction, regulation, and treatment. *J Interferon Cytokine Res* **31**, 695-703 (2011).
111. Sticherling, M. Psoriasis and autoimmunity. *Autoimmun Rev* **15**, 1167-1170 (2016).
112. Ellis, J.S. & Braley-Mullen, H. Mechanisms by Which B Cells and Regulatory T Cells Influence Development of Murine Organ-Specific Autoimmune Diseases. *J Clin Med* **6**(2017).
113. Meier, F.M., Frerix, M., Hermann, W. & Muller-Ladner, U. Current immunotherapy in rheumatoid arthritis. *Immunotherapy* **5**, 955-74 (2013).
114. He, M.M. et al. Small-molecule inhibition of TNF-alpha. *Science* **310**, 1022-5 (2005).
115. Hofmann, D., Salmon, L. & Wider, G. Activity of Tumor Necrosis Factor α Is Modulated by Dynamic Conformational Rearrangements. *Journal of the American Chemical Society* **140**, 167-175 (2018).
116. Alexiou, P. et al. Rationally designed less toxic SPD-304 analogs and preliminary evaluation of their TNF inhibitory effects. *Arch Pharm (Weinheim)* **347**, 798-805 (2014).
117. Luzi, S. et al. Subunit disassembly and inhibition of TNFalpha by a semi-synthetic bicyclic peptide. *Protein Eng Des Sel* **28**, 45-52 (2015).
118. O'Connell, J. et al. Small molecules that inhibit TNF signalling by stabilising an asymmetric form of the trimer. *Nat Commun* **10**, 5795 (2019).
119. Horiuchi, T., Mitoma, H., Harashima, S., Tsukamoto, H. & Shimoda, T. Transmembrane TNF-alpha: structure, function and interaction with anti-TNF agents. *Rheumatology (Oxford)* **49**, 1215-28 (2010).
120. Okubo, Y., Mera, T., Wang, L. & Faustman, D.L. Homogeneous expansion of human T-regulatory cells via tumor necrosis factor receptor 2. *Sci Rep* **3**, 3153 (2013).
121. McCann, F.E. et al. Selective tumor necrosis factor receptor I blockade is antiinflammatory and reveals immunoregulatory role of tumor necrosis factor receptor II in collagen-induced arthritis. *Arthritis Rheumatol* **66**, 2728-38 (2014).
122. Unger, T., Jacobovitch, Y., Dantes, A., Bernheim, R. & Peleg, Y. Applications of the Restriction Free (RF) cloning procedure for molecular manipulations and protein expression. *J Struct Biol* **172**, 34-44 (2010).
123. Liu, D., Xu, R., Dutta, K. & Cowburn, D. N-terminal cysteinyl proteins can be prepared using thrombin cleavage. *FEBS Lett* **582**, 1163-7 (2008).
124. Morrisett, J.D., David, J.S., Pownall, H.J. & Gotto, A.M., Jr. Interaction of an apolipoprotein (apoLP-alanine) with phosphatidylcholine. *Biochemistry* **12**, 1290-9 (1973).
125. van Schie, K.A. et al. Therapeutic TNF Inhibitors can Differentially Stabilize Trimeric TNF by Inhibiting Monomer Exchange. *Sci Rep* **6**, 32747 (2016).
126. Hagn, F., Etzkorn, M., Raschle, T. & Wagner, G. Optimized phospholipid bilayer nanodiscs facilitate high-resolution structure determination of membrane proteins. *J Am Chem Soc* **135**, 1919-25 (2013).

127. Denisov, I.G., Grinkova, Y.V., Lazarides, A.A. & Sligar, S.G. Directed self-assembly of monodisperse phospholipid bilayer Nanodiscs with controlled size. *J Am Chem Soc* **126**, 3477-87 (2004).
128. Hausler, E. et al. Quantifying the insertion of membrane proteins into lipid bilayer nanodiscs using a fusion protein strategy. *Biochim Biophys Acta Biomembr* **1862**, 183190 (2020).
129. Hirakawa, H., Ishikawa, S. & Nagamune, T. Ca2+ -independent sortase-A exhibits high selective protein ligation activity in the cytoplasm of Escherichia coli. *Biotechnol J* **10**, 1487-92 (2015).
130. Dorr, B.M., Ham, H.O., An, C., Chaikof, E.L. & Liu, D.R. Reprogramming the specificity of sortase enzymes. *Proc Natl Acad Sci U S A* **111**, 13343-8 (2014).
131. Fleck, D. et al. Proteolytic Processing of Neuregulin 1 Type III by Three Intramembrane-cleaving Proteases. *J Biol Chem* **291**, 318-33 (2016).
132. Sastre, M. et al. Presenilin-dependent gamma-secretase processing of beta-amyloid precursor protein at a site corresponding to the S3 cleavage of Notch. *EMBO Rep* **2**, 835-41 (2001).
133. Fukumori, A. & Steiner, H. Substrate recruitment of gamma-secretase and mechanism of clinical presenilin mutations revealed by photoaffinity mapping. *EMBO J* **35**, 1628-43 (2016).
134. Jo, S., Kim, T., Iyer, V.G. & Im, W. CHARMM-GUI: a web-based graphical user interface for CHARMM. *Journal of computational chemistry* **29**, 1859-65 (2008).
135. Phillips, J.C. et al. Scalable molecular dynamics with NAMD. *Journal of computational chemistry* **26**, 1781-802 (2005).
136. Darden, T., York, D. & Pedersen, L. Particle mesh Ewald: An N-log(N) method for Ewald sums in large systems. *J Chem Phys* **98**, 10089-100894 (1993).
137. Humphrey, W., Dalke, A. & Schulten, K. VMD: visual molecular dynamics. *J Mol Graph* **14**, 33-8, 27-8 (1996).
138. Lee, W., Tonelli, M. & Markley, J.L. NMRFAM-SPARKY: enhanced software for biomolecular NMR spectroscopy. *Bioinformatics* **31**, 1325-7 (2015).
139. Pervushin, K., Riek, R., Wider, G. & Wuthrich, K. Attenuated T2 relaxation by mutual cancellation of dipole-dipole coupling and chemical shift anisotropy indicates an avenue to NMR structures of very large biological macromolecules in solution. *Proc Natl Acad Sci U S A* **94**, 12366-71 (1997).
140. Wuthrich, K., Wider, G., Wagner, G. & Braun, W. Sequential resonance assignments as a basis for determination of spatial protein structures by high resolution proton nuclear magnetic resonance. *J Mol Biol* **155**, 311-9 (1982).
141. Salzmann, M., Pervushin, K., Wider, G., Senn, H. & Wuthrich, K. TROSY in triple-resonance experiments: new perspectives for sequential NMR assignment of large proteins. *Proceedings of the National Academy of Sciences of the United States of America* **95**, 13585-90 (1998).
142. Hyberts, S.G., Arthanari, H. & Wagner, G. Applications of non-uniform sampling and processing. *Topics in current chemistry* **316**, 125-48 (2012).
143. Hyberts, S.G., Takeuchi, K. & Wagner, G. Poisson-gap sampling and forward maximum entropy reconstruction for enhancing the resolution and sensitivity of protein NMR data. *Journal of the American Chemical Society* **132**, 2145-7 (2010).
144. Hyberts, S.G., Milbradt, A.G., Wagner, A.B., Arthanari, H. & Wagner, G. Application of iterative soft thresholding for fast reconstruction of NMR data non-uniformly sampled with multidimensional Poisson Gap scheduling. *Journal of biomolecular NMR* **52**, 315-27 (2012).
145. Delaglio, F. et al. NMRPipe: a multidimensional spectral processing system based on UNIX pipes. *Journal of biomolecular NMR* **6**, 277-93 (1995).

146. Shen, Y., Delaglio, F., Cornilescu, G. & Bax, A. TALOS+: a hybrid method for predicting protein backbone torsion angles from NMR chemical shifts. *Journal of biomolecular NMR* **44**, 213-23 (2009).
147. Schwieters, C.D., Kuszewski, J.J., Tjandra, N. & Clore, G.M. The Xplor-NIH NMR molecular structure determination package. *Journal of magnetic resonance* **160**, 65-73 (2003).
148. Lovell, S.C. et al. Structure validation by Calpha geometry: phi,psi and Cbeta deviation. *Proteins* **50**, 437-50 (2003).
149. Wand, A.J. Dynamic activation of protein function: a view emerging from NMR spectroscopy. *Nat Struct Biol* **8**, 926-31 (2001).
150. Kay, L.E., Torchia, D.A. & Bax, A. Backbone dynamics of proteins as studied by 15N inverse detected heteronuclear NMR spectroscopy: application to staphylococcal nuclease. *Biochemistry* **28**, 8972-9 (1989).
151. Wagner, G. The importance of being floppy. *Nat Struct Biol* **2**, 255-7 (1995).
152. Bieri, M., d'Auvergne, E.J. & Gooley, P.R. relaxGUI: a new software for fast and simple NMR relaxation data analysis and calculation of ps-ns and mus motion of proteins. *J Biomol NMR* **50**, 147-55 (2011).
153. d'Auvergne, E.J. & Gooley, P.R. Optimisation of NMR dynamic models II. A new methodology for the dual optimisation of the model-free parameters and the Brownian rotational diffusion tensor. *J Biomol NMR* **40**, 121-33 (2008).
154. d'Auvergne, E.J. & Gooley, P.R. Optimisation of NMR dynamic models I. Minimisation algorithms and their performance within the model-free and Brownian rotational diffusion spaces. *J Biomol NMR* **40**, 107-19 (2008).
155. Mayer, M. & Meyer, B. Characterization of Ligand Binding by Saturation Transfer Difference NMR Spectroscopy. *Angew Chem Int Ed Engl* **38**, 1784-1788 (1999).
156. van Zundert, G.C.P. et al. The HADDOCK2.2 Web Server: User-Friendly Integrative Modeling of Biomolecular Complexes. *J Mol Biol* **428**, 720-725 (2016).
157. Pettersen, E.F. et al. UCSF Chimera--a visualization system for exploratory research and analysis. *J Comput Chem* **25**, 1605-12 (2004).
158. Cordes, F.S., Bright, J.N. & Sansom, M.S. Proline-induced distortions of transmembrane helices. *J Mol Biol* **323**, 951-60 (2002).
159. Langelaan, D.N., Wieczorek, M., Blouin, C. & Rainey, J.K. Improved helix and kink characterization in membrane proteins allows evaluation of kink sequence predictors. *J Chem Inf Model* **50**, 2213-20 (2010).
160. Shearman, M.S. et al. L-685,458, an aspartyl protease transition state mimic, is a potent inhibitor of amyloid beta-protein precursor gamma-secretase activity. *Biochemistry* **39**, 8698-704 (2000).
161. Raltchev, K., Pipercevic, J. & Hagn, F. Production and Structural Analysis of Membrane-Anchored Proteins in Phospholipid Nanodiscs. *Chemistry* **24**, 5493-5499 (2018).
162. Stefanovic, S. & Hegde, R.S. Identification of a targeting factor for posttranslational membrane protein insertion into the ER. *Cell* **128**, 1147-59 (2007).
163. Favaloro, V., Spasic, M., Schwappach, B. & Dobberstein, B. Distinct targeting pathways for the membrane insertion of tail-anchored (TA) proteins. *J Cell Sci* **121**, 1832-40 (2008).
164. Haapasalo, A. & Kovacs, D.M. The many substrates of presenilin/gamma-secretase. *J Alzheimers Dis* **25**, 3-28 (2011).
165. Lleo, A. Activity of gamma-secretase on substrates other than APP. *Curr Top Med Chem* **8**, 9-16 (2008).
166. Van den Steen, P., Rudd, P.M., Dwek, R.A. & Opdenakker, G. Concepts and principles of O-linked glycosylation. *Crit Rev Biochem Mol Biol* **33**, 151-208 (1998).

167. Varki, A. Biological roles of oligosaccharides: all of the theories are correct. *Glycobiology* **3**, 97-130 (1993).
168. Yoda, M. et al. Systemic overexpression of TNFalpha-converting enzyme does not lead to enhanced shedding activity in vivo. *PLoS One* **8**, e54412 (2013).
169. Goth, C.K. et al. A systematic study of modulation of ADAM-mediated ectodomain shedding by site-specific O-glycosylation. *Proc Natl Acad Sci U S A* **112**, 14623-8 (2015).
170. Yashiro, M. et al. Metal-ion-assisted hydrolysis of dipeptides involving a serine residue in a neutral aqueous solution. *Org Biomol Chem* **1**, 629-32 (2003).
171. Lyons, B., Kwan, A.H. & Truscott, R.J. Spontaneous cleavage of proteins at serine and threonine is facilitated by zinc. *Aging Cell* **15**, 237-44 (2016).
172. Laity, J.H., Lee, B.M. & Wright, P.E. Zinc finger proteins: new insights into structural and functional diversity. *Curr Opin Struct Biol* **11**, 39-46 (2001).
173. Mueller, P. et al. High level in vivo mucin-type glycosylation in Escherichia coli. *Microb Cell Fact* **17**, 168 (2018).
174. Ramakrishnan, B., Boeggeman, E. & Qasba, P.K. Novel method for in vitro O-glycosylation of proteins: application for bioconjugation. *Bioconjug Chem* **18**, 1912-8 (2007).
175. Dondoni, A., Massi, A., Nanni, P. & Roda, A. A new ligation strategy for peptide and protein glycosylation: photoinduced thiol-ene coupling. *Chemistry* **15**, 11444-9 (2009).
176. Wells, J.A. & McClendon, C.L. Reaching for high-hanging fruit in drug discovery at protein-protein interfaces. *Nature* **450**, 1001-9 (2007).
177. Hwang, H., Vreven, T., Janin, J. & Weng, Z. Protein-protein docking benchmark version 4.0. *Proteins* **78**, 3111-4 (2010).
178. Fuller, J.C., Burgoyne, N.J. & Jackson, R.M. Predicting druggable binding sites at the protein-protein interface. *Drug Discov Today* **14**, 155-61 (2009).
179. Clackson, T. & Wells, J.A. A hot spot of binding energy in a hormone-receptor interface. *Science* **267**, 383-6 (1995).
180. Arkin, M.R. & Wells, J.A. Small-molecule inhibitors of protein-protein interactions: progressing towards the dream. *Nat Rev Drug Discov* **3**, 301-17 (2004).
181. Hansen, S.K. et al. Allosteric inhibition of PTP1B activity by selective modification of a non-active site cysteine residue. *Biochemistry* **44**, 7704-12 (2005).
182. Hansen, K.B. et al. Structure, function, and allosteric modulation of NMDA receptors. *J Gen Physiol* **150**, 1081-1105 (2018).
183. Trinh, P.N.H., May, L.T., Leach, K. & Gregory, K.J. Biased agonism and allosteric modulation of metabotropic glutamate receptor 5. *Clin Sci (Lond)* **132**, 2323-2338 (2018).
184. Erlanson, D.A., Fesik, S.W., Hubbard, R.E., Jahnke, W. & Jhoti, H. Twenty years on: the impact of fragments on drug discovery. *Nat Rev Drug Discov* **15**, 605-619 (2016).
185. Hajduk, P.J. & Greer, J. A decade of fragment-based drug design: strategic advances and lessons learned. *Nat Rev Drug Discov* **6**, 211-9 (2007).
186. Chessari, G. & Woodhead, A.J. From fragment to clinical candidate--a historical perspective. *Drug Discov Today* **14**, 668-75 (2009).
187. Murray, C.W. & Blundell, T.L. Structural biology in fragment-based drug design. *Curr Opin Struct Biol* **20**, 497-507 (2010).
188. Wu, B. et al. HTS by NMR of combinatorial libraries: a fragment-based approach to ligand discovery. *Chem Biol* **20**, 19-33 (2013).
189. Laskowski, R.A., Rullmannn, J.A., MacArthur, M.W., Kaptein, R. & Thornton, J.M. AQUA and PROCHECK-NMR: programs for checking the quality of protein structures solved by NMR. *J Biomol NMR* **8**, 477-86 (1996).

APPENDIX

Protein constructs with respective amino acid sequence

His_6-GB1-THR-**TNFα_69-233** (TNFα ECD)

MSYYHHHHHHDYDIPTTAMEYKLILNGKTLKGETTTEAVDAATAEKVFKQYANDN
GVDGEWTYDDATKTFTVTEIPTTLVPRGSGGLISPLAQAVRSSSRTPSDKPVAHVVAN
PQAEGQLQWLNRRANALLANGVELRDNQLVVPSEGLYLIYSQVLFKGQGCPSTHVL
LTHTISRIAVSYQTKVNLLSAIKSPCQRETPEGAEAKPWYEPIYLGGVFQLEKGDRLSA
EINRPDYLDFAESGQVYFGIIAL*

His_6-GB1-THRmut-**TNFα_80-233** (cTNFα)

MSYYHHHHHHDYDIPTTAMEYKLILNGKTLKGETTTEAVDAATAEKVFKQYANDN
GVDGEWTYDDATKTFTVTEIPTTLVPRCSSRTPSDKPVAHVVANPQAEGQLQWLNR
RANALLANGVELRDNQLVVPSEGLYLIYSQVLFKGQGCPSTHVLLTHTISRIAVSYQT
KVNLLSAIKSPCQRETPEGAEAKPWYEPIYLGGVFQLEKGDRLSAEINRPDYLDFAES
GQVYFGIIAL*

His_6-GB1-THR-**TNFα-TM_28-62** (TNFα-TM)

MSYYHHHHHHDYDIPTTAMEYKLILNGKTLKGETTTEAVDAATAEKVFKQYANDN
GVDGEWTYDDATKTFTVTEIPTTLVPRGSGSGSGRRCLFLSLFSFLIVAGATTLFCLLH
FGVIGPQREE*

His_6-GB1-THR-**TNFα-TM_28-84 + Cys** (TNFαTM-C)

MSYYHHHHHHDYDIPTTAMEYKLILNGKTLKGETTTEAVDAATAEKVFKQYANDN
GVDGEWTYDDATKTFTVTEIPTTLVPRGSGSGSGRRCLFLSLFSFLIVAGATTLFCLLH
FGVIGPQREESPRDLSLISPLAQAVRSSSRTP**C***

GB1-THR-**TNFα-TM_28-62-SOR**-His_6 (TNFαTM-SOR)

MEYKLILNGKTLKGETTTEAVDAATAEKVFKQYANDNGVDGEWTYDDATKTFTVT
EIPTTLVPRGSGSGSGRRCLFLSLFSFLIVAGATTLFCLLHFGVIGPQREELPETGGAAA
TAEQHHHHHH*

GB1-THR-**TREM2_19-141**-His_6 (TREM2_19-141)

MEYKLILNGKTLKGETTTEAVDAATAEKVFKQYANDNGVDGEWTYDDATKTFTVT
EIPTTLVPRGSGGSSHNTTVFQGVAGQSLQVSCPYDSMKHWGRRKAWCRQLGEKGP
CQRVVSTHNLWLLSFLRRWNGSTAITDDTLGGTLTITLRNLQPHDAGLYQCQSLHGS
EADTLRKVLVEVLADPLDHRDAGDLEHHHHHH*

TREM2_19-131 (TREM2 ECD)

MHNTTVFQGVAGQSLQVSCPYDSMKHWGRRKAWCRQLGEKGPCQRVVSTHNLWL
LSFLRRWNGSTAITDDTLGGTLTITLRNLQPHDAGLYQCQSLHGSEADTLRKVLVEV
LAD*

GB1-THR-**TREM2-SOR**-His_6 (TREM2-SOR)

MEYKLILNGKTLKGETTTEAVDAATAEKVFKQYANDNGVDGEWTYDDATKTFTVT
EIPTTLVPRGSGGSSHNTTVFQGVAGQSLQVSCPYDSMKHWGRRKAWCRQLGEKGP
CQRVVSTHNLWLLSFLRRWNGSTAITDDTLGGTLTITLRNLQPHDAGLYQCQSLHGS
EADTLRKVLVEVLADPLDHRDAGDLPETGGAAATAEHHHHHH*

His_6-GB1-THR-**TREM2-TM** (TREM2-TM WT)

MSYYHHHHHHDYDIPTTAMEYKLILNGKTLKGETTTEAVDAATAEKVFKQYANDN
GVDGEWTYDDATKTFTVTEIPTTLVPRGSGRSLLEGEIPFPPTSILLLLACIFLIKILAAS
ALWAAAWHGQKPGTH*

His_6-GB1-THR-**TREM2-TM_K186A** (K186A)

MSYYHHHHHHDYDIPTTAMEYKLILNGKTLKGETTTEAVDAATAEKVFKQYANDN
GVDGEWTYDDATKTFTVTEIPTTLVPRGSGRSLLEGEIPFPPTSILLLLACIFLI**A**ILAAS
ALWAAAWHGQKPGTH*

His_6-GB1-THR-**TREM2-TM_K186L** (K186L)

MSYYHHHHHHDYDIPTTAMEYKLILNGKTLKGETTTEAVDAATAEKVFKQYANDN
GVDGEWTYDDATKTFTVTEIPTTLVPRGSGRSLLEGEIPFPPTSILLLLACIFLI**L**ILAAS
ALWAAAWHGQKPGTH*

His_6-GB1-THR-**TREM2-TM_K186P** (K186P)

MSYYHHHHHHDYDIPTTAMEYKLILNGKTLKGETTTEAVDAATAEKVFKQYANDN
GVDGEWTYDDATKTFTVTEIPTTLVPRGSGRSLLEGEIPFPPTSILLLLACIFLI**P**ILAAS
ALWAAAWHGQKPGTH*

His_6-GB1-THR-**TREM2-TM_K186N** (K186N)

MSYYHHHHHHDYDIPTTAMEYKLILNGKTLKGETTTEAVDAATAEKVFKQYANDN
GVDGEWTYDDATKTFTVTEIPTTLVPRGSGRSLLEGEIPFPPTSILLLLACIFLI**N**ILAAS
ALWAAAWHGQKPGTH*

His_6-GB1-**DAP12-TM_22-70_C33S** (DAP12-TM)

MSYYHHHHHHDYDIPTTAMEYKLILNGKTLKGETTTEAVDAATAEKVFKQYANDN
GVDGEWTYDDATKTFTVTEIPTTLVPRGLRPVQAQAQSD**S**SCSTVSPGVLAGIVMGD
LVLTVLIALAVYFLGRLVPR

STD NMR Screening for Hit identification

Cocktail (5-compound mixture) Screening

Table 19: Cocktail STD Screen and determination of Scaling factor

Cocktail	Scaling Factor	Cocktail	Scaling Factor	Cocktail	Scaling Factor	Cocktail	Scaling Factor
1	11.3	81	-	161	-	241	-
2	16.4	82	23.4	162	12.3	242	9.6
3	13.6	83	-	163	15.6	**243**	**4.2**
4	-	84	-	**164**	**4.5**	244	-
5	-	85	-	**165**	**4.3**	245	10.8
6	9.3	86	-	166	16.0	246	-
7	-	87	13.2	167	8.9	247	-
8	10.0	88	-	168	13.7	248	-
9	13.02	89	18.0	169	-	249	11.5
10	17.79	90	-	170	8.9	250	17.0
11	9.4	91	-	171	-	**251**	**4.7**
12	-	92	-	172	-	252	-
13	-	93	25.8	173	12.6	253	-
14	-	94	-	174	17.0	254	-
15	-	95	-	175	15.1	255	18.1
16	25.7	96	-	176	14.6	256	15.0
17	18.6	97	-	177	8.9	257	-
18	20.4	98	-	178	-	258	16.1
19	9.2	99	-	179	-	259	12.7
20	20.2	100	10.3	180	6.5	260	-
21	-	101	10.2	**181**	**3.8**	261	-
22	-	102	19.8	182	-	262	-
23	-	103	-	183	-	263	-
24	-	104	-	184	-	264	-
25	-	105	20.4	185	-	265	-
26	10.2	106	7.9	186	-	266	-
27	14.5	**107**	**3.6**	187	-	267	-
28	18.0	108	31.2	188	-	268	8.8
29	21.4	109	14.3	189	-	270	-
30	-	110	20.4	190	-	271	14.5
31	-	111	19.2	191	18.9	272	-
32	-	112	9.3	192	11.5	273	8.8
33	-	113	20.0	193	9.3	274	-
34	18.5	114	-	194	-	275	-
35	-	115	9.3	195	-	276	-
36	-	**116**	**5.5**	196	-	277	-
37	19.2	**117**	**4.3**	197	12.0	278	-
38	28.2	118	-	198	7.2	279	10.9
39	-	119	7.5	199	-	280	-
40	38.1	120	-	200	10.8	281	-
41	24.3	121	8.0	201	13.8	282	-
42	**4.6**	122	10.5	202	21.6	283	-

43	15.7	123	-	203	11.9	283	-
44	10.2	124	-	204	-	284	-
45	17.6	125	-	205	-	285	-
46	-	126	-	206	-	286	-
47	13.1	127	13.3	207	-	287	-
48	-	128	-	208	-	288	-
49	16.3	129	15.2	209	16.1	289	-
50	9.5	130	12.9	210	22.3	290	-
51	13.7	**131**	**3.8**	211	10.5	291	-
52	-	132	12.8	212	-	292	-
53	-	**133**	**5.6**	213	-	293	-
54	-	134	6.6	214	-	294	-
55	-	135	20.0	215	-	295	-
56	-	136	-	216	-	296	-
57	13.3	137	-	217	-	297	-
58	-	**138**	**5.8**	218	9.7	298	-
59	**4.4**	139	-	219	16.1	299	-
60	-	140	13.0	220	-	300	-
61	-	141	15.7	221	21.6	301	-
62	18.1	142	6.7	222	-	302	-
63	-	143	18.9	223	-	303	-
64	13.9	144	-	224	-	304	-
65	23.8	145	8.4	225	-	305	-
66	12.5	146	6.9	226	16.7	306	-
67	12.8	147	8.0	227	-	307	-
68	-	148	-	228	-	308	-
69	-	149	-	229	19.8	309	-
70	24.8	150	17.5	230	-	310	-
71	-	151	-	231	-	311	-
72	-	152	6.5	232	-	312	-
72	-	153	-	233	18.7	313	-
74	-	154	-	**234**	**3.7**	314	-
75	28.1	155	-	235	10.9	315	-
76	-	156	-	236	10.1	316	-
77	-	157	-	237	20.1	317	-
78	13.4	158	-	238	-	318	-
79	-	159	-	239	17.4	319	-
80	7.7	160	13.4	240	-	320	-

Single-compound Screen

Table 20: Single-compound STD Screen pipetting scheme

	No.	Plate	Position	Cocktail	New Position
1	AC39877R	3	H4		A1
2	SB01342R	4	A2		A2
3	SB01963R	4	B2	42	A3
4	**SEW00783**	4	G2		A4
5	SEW00891	4	H2		A5
6	SEW03999	4	D3		A6
7	**MAY00293**	7	B3		A7
8	**MAY00296**	7	D3	59	A8
9	MO00450R	7	H3		A9
10	MO08070R	7	C4		A10
11	SPB05355	7	A6		A11
12	TL01023R	7	D6		A12
13	CD09766R	7	A7	107	B1
14	SB01105R	7	A8		B2
15	**GK01295R**	7	G8		B3
16	AC39931R	7	B1		B4
17	CC74109R	8	B5		B5
18	CD10514R	8	B6	116	B6
19	JFD04065	8	E6		B7
20	**RH01216R**	8	E7		B8
21	**AC42616R**	7	G1		B9
22	**SEW02076**	8	F7		B10
23	BTB07343	8	H7	117	B11
24	CD07933R	8	B8		B12
25	CD09866R	8	C8		C1
26	AC39848R	8	E9		C2
27	AC10867R	10	C5		C3
28	**AC12212R**	10	B6	131	C4
29	AC12572R	10	F6		C5
30	**AC13091R**	10	A7		C6
31	AC10269R	8	A1		C7
32	AC15236R	8	B1		C8
33	BTB09242	8	C1	133	C9
34	SB01146R	9	A2		C10
35	**CC40823R**	9	D2		C11
36	CC18301R	9	H2		C12
37	**SEW05178**	9	G3		D1
38	SB01835R	9	D4	138	D2
39	KM09206R	9	H4		D3
40	**KM08693R**	9	C5		D4
41	**AC13399R**	10	E7		D5
42	**AC13217R**	14	H4	164	D6
43	**AC27604R**	14	C5		D7
44	AC11374R	14	F5		D8
45	CC07116R	14	B8		D9

46	AC13458R	10	F7	165	D10
47	CC01416R	14	D8		D11
48	GK01351R	14	G8		D12
49	**BTB10554**	14	A9		E1
50	JFD01576	14	F9		E2
51	AC34205R	11	D5	181	E3
52	**RDR03964**	15	A7		E4
53	RH00054R	15	B7		E5
54	RH00264R	15	C7		E6
55	RH01844R	15	D7		E7
56	AC39962R	14	G2	234	E8
57	AC39836R	14	A3		E9
58	AC36949R	14	D3		E10
59	AC10460R	14	E3		E11
60	AC16035R	14	F3		E12
61	BTB09974	14	E7	243	F1
62	KM01033R	18	E4		F2
63	KM06670R	18	F4		F3
64	SB01187R	18	H4		F4
65	SB01188R	18	A5		F5
66	JFD01174	15	E5	251	F6
67	JFD03925	15	B6		F7
68	KM03760R	15	E6		F8
69	KM06409R	15	F6		F9
70	S10539R3	15	H7		F10

Structural statistics of TREM2-TM in DPC micelles

Table 21: Structural statistics of TREM2-TM in DPC micelles[a]

	TREM2-TM		
	wt	**K186A**	**DAP12 complex**
Structural Information			
Number of NOEs restraints	64	58	69
Number of hydrogen bond restraints	19	24	24
Number of dihedral angle restraints (TALOS+ [146])	68	64	66
Backbone rmsd for entire transmembrane helical region (aa 173-198) (Å) [b]	2.0 ± 0.6	0.6 ± 0.2	0.7 ± 0.4
Backbone rmsd for first α-helix (aa 173-189) (Å)	0.2 ± 0.1	0.3 ± 0.1	0.4 ± 0.2
Ramachandran Map Analysis [c]			
Most favored regions	97.3 %	100 %	81.1 %
Additionally allowed regions	0 %	0 %	13.5 %
Generously allowed regions	2.7%	0 %	5.4 %
Disallowed regions	0 %	0 %	0.0 %
Deviation from Restraints and Idealized Geometry			
Distance restraints (Å)	0.030 ± 0.003	0.023 ± 0.002	0.022 ± 0.001
Dihedral angle restraints (deg)	0.066 ± 0.033	0.24 ± 0.02	0.33 ± 0.018
Bonds (Å)	0.0022 ± 0.0001	0.0029 ± 0.0003	0.0029 ± 0.0001
Angles (deg)	0.576 ± 0.002	0.698 ± 0.007	0.679 ± 0.004
Impropers (deg)	1.1 ± 0.1	1.7 ± 0.2	2.1 ± 0.1

[a] Analysis of the 20 lowest-energy structures
[b] rmsd values are calculated relative to a non-minimized average structure of each ensemble
[c] Ramachandran analysis with PROCHECK-NMR [189] was performed on the lowest-energy structure

ACKNOWLEDGEMENT

I would like to thank my supervisor Professor Dr. Franz Hagn for his trust in my project work and for all the scientific discussions we had. I am grateful for the high degree of freedom and independence which gave me the possibility to try new approaches and methods, deal with failures and to finally succeed.

Thanks to all current and former colleagues - Kai, Inguna, Melina, Kolio, David, Lisa, Laura & KK – it was a nice ride together! And always remember the recipe for success: 50/50/50!

To my thesis committee members Prof. Dr. Christian Haass and Prof. Dr. Dierk Niessing. I always enjoyed our meetings and appreciated your suggestions and support a lot. I couldn't imagine a nicer atmosphere for my meetings as the one you created!

To my co-authors Dr. Kai Schlepckow, Bettina Brunner, Prof. Dr. Harald Steiner and Prof. Dr. Christian Haass for the tireless dedication to our publication!

To all the students who accompanied me along the way: Maxi, Sarah, Gereon und especially my sunshine Mareike!

Finally, I want to express my deepest gratitude to all the people who supported me on my journey to become a PhD, above all to my parents and their unshakable believe that I can accomplish everything as long as I keep my course!

Thank you

STATUTORY DECLARATION

Anhang I

Eidesstattliche Erklärung

Ich erkläre an Eides statt, dass ich die bei der promotionsführenden Einrichtung
Technische Universität München

der TUM zur Promotionsprüfung vorgelegte Arbeit mit dem Titel:
Structural and biophysical studies on human disease-related single-pass transmembrane proteins TNFa and TREM2

in Fakultät für Chemie – Professur für Strukturelle Membranbiochemie
Fakultät, Institut, Lehrstuhl, Klinik, Krankenhaus, Abteilung

unter der Anleitung und Betreuung durch: Prof. Dr. Franz Hagn ohne sonstige Hilfe erstellt und bei der Abfassung nur die gemäß § 6 Ab. 6 und 7 Satz 2 angebotenen Hilfsmittel benutzt habe.

☒ Ich habe keine Organisation eingeschaltet, die gegen Entgelt Betreuerinnen und Betreuer für die Anfertigung von Dissertationen sucht, oder die mir obliegenden Pflichten hinsichtlich der Prüfungsleistungen für mich ganz oder teilweise erledigt.

☒ Ich habe die Dissertation in dieser oder ähnlicher Form in keinem anderen Prüfungsverfahren als Prüfungsleistung vorgelegt.

☐ Die vollständige Dissertation wurde in englischer Sprache veröffentlicht. Die promotionsführende Einrichtung
Technische Universität München - Fakultät für Chemie

hat der Veröffentlichung zugestimmt.

☒ Ich habe den angestrebten Doktorgrad noch nicht erworben und bin nicht in einem früheren Promotionsverfahren für den angestrebten Doktorgrad endgültig gescheitert.

☐ Ich habe bereits am _____ bei der Fakultät für _____

_____

der Hochschule _____

unter Vorlage einer Dissertation mit dem Thema _____

_____

die Zulassung zur Promotion beantragt mit dem Ergebnis: _____

_____

Die öffentlich zugängliche Promotionsordnung der TUM ist mir bekannt, insbesondere habe ich die Bedeutung von § 28 (Nichtigkeit der Promotion) und § 29 (Entzug des Doktorgrades) zur Kenntnis genommen. Ich bin mir der Konsequenzen einer falschen Eidesstattlichen Erklärung bewusst.

Mit der Aufnahme meiner personenbezogenen Daten in die Alumni-Datei bei der TUM bin ich

☒ einverstanden, ☐ nicht einverstanden.

Ort, Datum, Unterschrift